Geological Quarterly, 2025, 69, 11
DOI: https://doi.org/10.7306/gq.1784

The geology and mineralization of the Sar-e-Yazd Cu (Mo) porphyry deposit in the Saveh-Naein-Jiroft magmatic belt (SNJMB), Iran

Fayeq HASHEMI[1], Mohammadreza HOSSEINZADEH[1], Mohssen MOAYYED[1] and Hamid HARATI[2]

[1] University of Tabriz, Department of Earth Sciences, Faculty of Natural Sciences, Tabriz, Iran; ORCID: 0009-0005-8069-6531 [F.H.], 0000-0002-6319-5840 [M.H.], 0000-0002-7600-7482 [M.M.]

[2] Payame Noor University, Department of Earth Sciences, Tehran, Iran; ORCID: 0000-0003-0543-5233

Hashemi, F., Hosseinzadeh, M., Moayyed, M., Harati, H., 2025. The geology and mineralization of the Sar-e-Yazd Cu (Mo) porphyry deposit in the Saveh-Naein-Jiroft magmatic belt (SNJMB), Iran. Geological Quarterly, 69, 11; https://doi.org/10.7306/gq.1784

Associate Editor: Jacek Szczepański

The Sar-e-Yazd Cu (Mo) deposit is located in the Naein-Jiroft magmatic belt or Kerman belt. It is in the southern part of the Cenozoic Saveh-Nain-Jiroft magmatic belt of Iran. This deposit is spatially associated with Oligocene shallow porphyritic porphyries intruded into dacite porphyry to porphyritic quartzdiorite and middle Eocene volcanoclastic rocks. Hypogene ore minerals include chalcopyrite, magnetite, pyrrhotite, molybdenite, bornite and pyrite occurring as veinlets and disseminations mostly in the both intrusive rocks. Hydrothermal alteration from inside to outside is marked by potassic, carbonate alteration, an extensive phyllic assemblage and irregular zones of propylitic (actinolite, epidote and chlorite sub-zone) and clay assemblages with no consistent zoning patterns. The study of faults in the area reveals that, in general, they align with the pre-existing joints in the structure of the Sani Abad syncline. These faults are attributed to ancient fractures within the right-lateral shear system between the Anar and Dehshir right-striking faults. Three sets of faults are recognized in the eastern Mehriz area (Sar-e-Yazd region): 1– longitudinal direction joints (or tension faults), along with early intrusions and the first group of dykes with WNW–ESE extension, are attributed to old T_2 fractures in the shear system. However, the second group of later dykes, often intruded in a N–S direction, is attributed to tensile fractures in the T_1 shear system, 2 – cross direction joints (or expansion faults) and 3 – diagonal direction joints (or shear faults; the late intrusive, branches of the epithermal Cu-Fe and the Pb-Zn apophyse intruding aligned with these faults direction. The veins shows two main trends: a- tension split is related to T_1 and tensile fractures (epithermal Cu-Fe veins) and b- the pennant vein pattern is related to R/R' diagonal fractures. Fractures with the NW–SE trend (R), which are mostly filled by iron oxides, are younger and don't have an effective role in mineralization and it seems that the fractures with the R' shear system have been effective in the placement of intrusive. The total average of the highest metallic mineralization is enriched in supergene zone at each boreholes (BH): BH_{01}, BH_{03}, BH_{04} and BH_{23}. Cu: 3881 ppm, Mo: 43.7 ppm, Pb: 13390 ppm, Zn: 18250 ppm and Ag: 6.7 ppm in the 25 to 58 m depth. Fluid inclusion studies indicate a wide range of homogenization temperatures in the veinlets and phyllic porphyritic quartzdiorite alteration, ranging from 136°C to 542°C, with salinities of 4–62 wt.% NaCl equivalent. The coexistence of vapour-rich inclusions (F3 type) with high salinity and liquid-rich inclusions (F2 type) with similar Th values provides strong evidence for boiling. Parts of the copper content in the solution could be deposited as a result of boiling processes as chalcopyrite which was the major mineral at the Sar-e-Yazd deposit (similar to porphyry copper deposits). The analysis of borehole samples indicates a moderate correlation between Cu and Mo, suggesting porphyry Cu (Mo) deposits in Sar-e-Yazd. Cu also shows a strong correlation with Pb, Zn, and Ag, which are key indicator elements of these deposits. Finally based on the distribution and zoning of the main metal ores, the porphyry mineralization of Sar-e-Yazd shows a significant resemblance to the Cu-Mo mineralization in the Mineral Park deposit in Arizona.

Key words: fluid inclusion, ore mineralization, geochemistry, Sar-e-Yazd, Cu (Mo) Porphyry, Saveh-Nain-Jiroft magmatic belt, Iran.

INTRODUCTION

Cu porphyry deposits are significant sources of copper, formed from hydrothermal fluids originating from a large magma chamber several kilometres below the Earth's surface (Sillitoe, 2010). These deposits are characterized by disseminated copper minerals within a large volume of rock, often associated with porphyritic intrusive rocks (Cox, 1986). The formation process involves multiple stages of hydrothermal alteration, creating a core of disseminated ore minerals surrounded by successive envelopes of altered rock (Shanks III et al., 2012). Porphyry copper systems are mainly developed at convergent plate margins, including continental margin and island-arc settings (Sillitoe, 2010), where subduction of oceanic crust is related to arc-type magmatism that generates most of the hydrous, oxidized upper crustal granitoids genetically related to ores. In these magmatic arcs, deformation can be very complex, and porphyry copper deposits can form in a variety of tectonic settings (Richards, 2009). They are economically important due to their large size and the relatively low copper concentrations required for profitable ex-

* Corresponding author, e-mail: mr-hosseinzadeh@tabrizu.ac.ir

Received: March 12, 2024; accepted: March23, 2025; first published online: June 13, 2025

traction (Singer, 1995). In addition to copper, these deposits often contain valuable by-products like Mo, Au, and Ag. In this work, we present data on the main geological features of the Sar-e-Yazd Cu (Mo) deposit. Considering that no detailed and comprehensive study has been done, the authors intend to discuss ore formation conditions using a multidisciplinary approach. This includes fieldwork, logging drill cores, microscopic inspections, and geochronology to conduct a more detailed investigation into the geology, hydrothermal alteration, fluid inclusion study, geochemistry and the relationship of mineralization with fault structures. The Sar-e-Yazd Cu (Mo) deposit is characterized by porphyry-style mineralization and is located within the Naein-Jiroft magmatic belt (NJMB) or Kerman copper belt (KB) in the southern part of the Cenozoic Saveh-Naein-Jiroft magmatic belt (SNJMB) of Iran (Fig. 1). Iran's significant porphyry copper belts can be categorized into three magmatic belts (Karimpour et al., 2021): 1 – Saveh-Naein-Jiroft magmatic belt (SNJMB): this belt is a significant geological formation that has been proposed as a replacement for the previously recognized Uromieh-Dokhtar magmatic belt, particularly noted for its predominance of Miocene age igneous rocks (Karimpour et al., 2021), 2 – Lut block: this belt dates from the Eocene to Oligocene, and 3 – Qaradagh or Arasbaran Belt: this belt is also significant (Fig. 1). These deposits are associated with Tertiary granitoids. The Saveh-Nain-Jiroft magmatic belt extends from Saveh to Jiroft with a NW–SE trend and hosts the most significant porphyry copper deposits in Iran. Notable deposits between Saveh and Naein include Dalli, Kahang, Darreh Zereshk, and Ali Abad, have been identified as originating from the early to middle Miocene. However, the most important and largest porphyry copper deposits in Iran are concentrated between Naein and Jiroft, an area also known as the Kerman copper porphyry belt. The granitoids and volcanic rocks in this zone range from the Paleocene to Pleistocene and are related to the Neo-Tethyan subduction zone (Agard et al., 2005, 2011; Omrani et al. 2008; Sarjoughian and Kananian, 2017). The porphyry deposits in this section are mostly Oligocene-Miocene in age (Shafiei, 2010; Aghazadeh et al., 2015). The Naein-Jiroft or Kerman copper belt is one of Iran's most promising copper zones. Over 200 deposits and signs of copper minerals have been identified in this belt (Ghorbani, 2013). To date, 20 known copper deposits with evidence of porphyry have been discovered in that region (Ghorbani, 2013). Sarcheshmeh, the largest porphyry copper mine in Iran, is located in this section. The Sar- e-Yazd Cu (Mo) deposit is situated 4 km south of Sar- e-Yazd village, 5 km east of Mehriz, and 24 km south of Yazd (Fig. 1). In the report on the completion of exploration activities at Sar-e-Yazd, focusing on the Mehriz mining area and geological mapping, Moayyed (2019) provides a comprehensive overview of the undertaken exploration activities. The report outlines the methodologies employed in geological mapping, including field surveys and sampling techniques, which were utilized to assess the mineral potential of the region. The maximum depth of boreholes in the Sar-e-Yazd porphyry deposit is 776 m. Mineralization at Sar-e-Yazd occurs mainly in porphyritic granodiorite and dacite porphyry to porphyritic quartzdiorite rocks. The zoning pattern and distribution of alteration assemblages and fluid inclusion studies make the Sar-e-Yazd Cu (Mo) deposit similar to other known porphyry systems in the NJMB or Kerman copper belt (KB), including the world-class Sarcheshmeh (Waterman and Hamilton, 1975), Meiduk (Alirezaei et al., 2013), and Daraloo (Alimohammadi et al., 2015). However, the age of the Sar-e-Yazd porphyry deposit (Oligocene), based on geological mapping (Moayyed, 2019) is distinctly older than the middle to late Miocene reported for most porphyry Cu deposits south of the Sar-e-Yazd Cu (Mo) deposit (Sarcheshmeh and Meiduk). A similar Oligocene age has been recently reported for the Bondar-e-Hanza porphyry (Mohebi, 2015) and Takht-e-Gonbad copper deposit (Hosseini et al., 2017) in the NJMB or Kerman copper belt. These two deposits and the Sar-e-Yazd deposit occur towards the southern margin of the KB and imply a discrete episode of copper mineralization, likely before collision.

GEOLOGICAL SETTING

REGIONAL GEOLOGY

As mentioned above, the Sar-e-Yazd Cu (Mo) deposit, located to the east of Mehriz, is situated within the Yazd block of Central Iran, and is influenced by the Cenozoic magmatism of the Naein-Jiroft Magmatic Belt (NJMB) in the Zagros Orogenic Belt. Based on Alavi (1994) the southeastern Zagros Orogenic Belt in Iran consists of three parallel tectonic subdivisions, from north-east to south-west: 1 – Urumieh-Dokhtar Magmatic Assemblage (ADMA); 2 – Sanandaj-Sirjan Zone (SSZ); 3 – Zagros Fold-Thrust Belt (ZFTB). The Urumieh-Dokhtar Magmatic belt is an ensialic intrusive-extrusive complex, constructed by subduction of the Neo-Tethyan oceanic lithosphere underneath the Iranian terranes in a continental island arc setting (Berberian et al. 1982; Shahabpour, 2007). However, as is shown in Figure 1 based on new research by Karimpour et al (2021), due to the evidence of lack of magmatism between Saveh to the extent of Takab and absence of air magnet anomaly the name of UDMA was changed to Saveh-Nain-Jiroft magmatic belt (SNJMB) and magmatism of Urumieh to Takab is a continuation of the western Alborz magmatic belt (AMB). As depicted in Figure 1, Sar-e-Yazd porphyry Cu (Mo) deposit is an unknown porphyry copper deposit of Iran, located in the Saveh-Naein-Jiroft magmatic belt (SNJMB). The main magmatic activities of the SNJMB are related to the Tertiary period. The magmatic activities started from the Paleocene and continued until the end of the Pleistocene (Alavi, 2007; Chiu et al., 2013; Hosseini et al., 2017; Fazeli et al., 2017). These igneous rocks include both intrusive and volcanic units.

During the middle Eocene period, igneous activities peaked and were followed by extensive volcanic activity, which is visible throughout the belts (Alavi, 2007). Based on the characteristics of magmatism and mineralization, SNJMB can be divided into two distinct belts: 1 – Saveh-Naein Magmatic Belt (SNMB), which mainly consists of non-adakitic barren I-type magnetic granitoids, 2 – Naein-Jiroft Magmatic Belt (NjMB) which hosts porphyry copper deposits. The Miocene granitoids of this belt are magnetite series and I-type adakite. Geochemically, adakitic volcanic rocks are similar to the fertile adakitic granitoids of NJMB, but these units lack any mineralization.

LOCAL GEOLOGY

The oldest observed rock units in the southwest of Mehriz are part of the Jurassic Shemshak formation and the Shir-Kuh granite batholith, as noted by Nabavi in 1972. The Shemshak formation is primarily characterized by a sequence of sedimentary rocks that offer insights into the geological history and palaeoenvironment of the Jurassic period. This formation plays a crucial role in understanding the stratigraphic evolution in the region. On the other hand, the Shir-Kuh granite batholith exemplifies igneous activity from the same era, indicating significant geological processes such as volcanic activity and tectonic movements that contributed to the region's current geological framework. The Jurassic Shemshak formation exhibits significant geological characteristics due to its interaction with the

Fig. 1. Paleogene magmatism is the most voluminous magmatic episode in Iran and includes the Saveh-Naein-Jiroft magmatic belt (SNJMB), Lut magmatic belt (LMB) and Alborz magmatic belt (AMB)

The location of the Sar-e-Yazd porphyry Cu (Mo) deposit in the Naein-Jiroft magmatic belt (NJMB) or Kerman porphyry belt (KB) a part of Saveh-Naein-Jiroft magmatic belt is between the Sanandaj-Sirjan zone (SSZ) and the Central Iranian zone (CIM), NJMB or Kerman porphyry copper belt is located between two important faults of Dehshir or Naein-Baft and Nayband (NBF). The Dehshir and Anar faults limit the studied area from the east and west

Shir-Kuh granite batholith. This granite batholith, which intruded into the surrounding sedimentary rocks, has led to contact metamorphism in the Shemshak formation. In the southwest of Mehriz, the early Cretaceous formation is observed to unconformably overlie the Shir-Kuh granite batholith, indicating a significant geological relationship between these two formations. This unconformity suggests a period of erosion or non-deposition that occurred between the formation of the granite batholith and the deposition of the Cretaceous sediments. The Cretaceous sedimentary series in this region is divided into three distinct parts: the lower Sangestan formation, the middle Taft formation, and the upper Darreh-Zanjir formation. The Sangestan formation is a significant geological formation characterized primarily by its clastic sediments, which include various types of rock fragments such as conglomerate, sandstone, shale, siltstone, and oolitic limestone. In the area, a thick sequence of Sangestan sediments is exposed, resting unconformably on the Jurassic Shir-Kuh granite or the contact metamorphic Shemshak formation. The Taft formation includes organic matter-rich shale, siltstone, limestone and dolomite. The Darreh-Zanjir formation comprises of shale, chert-bearing bedded limestone and marl rocks, overlies concordantly on the Taft forma-

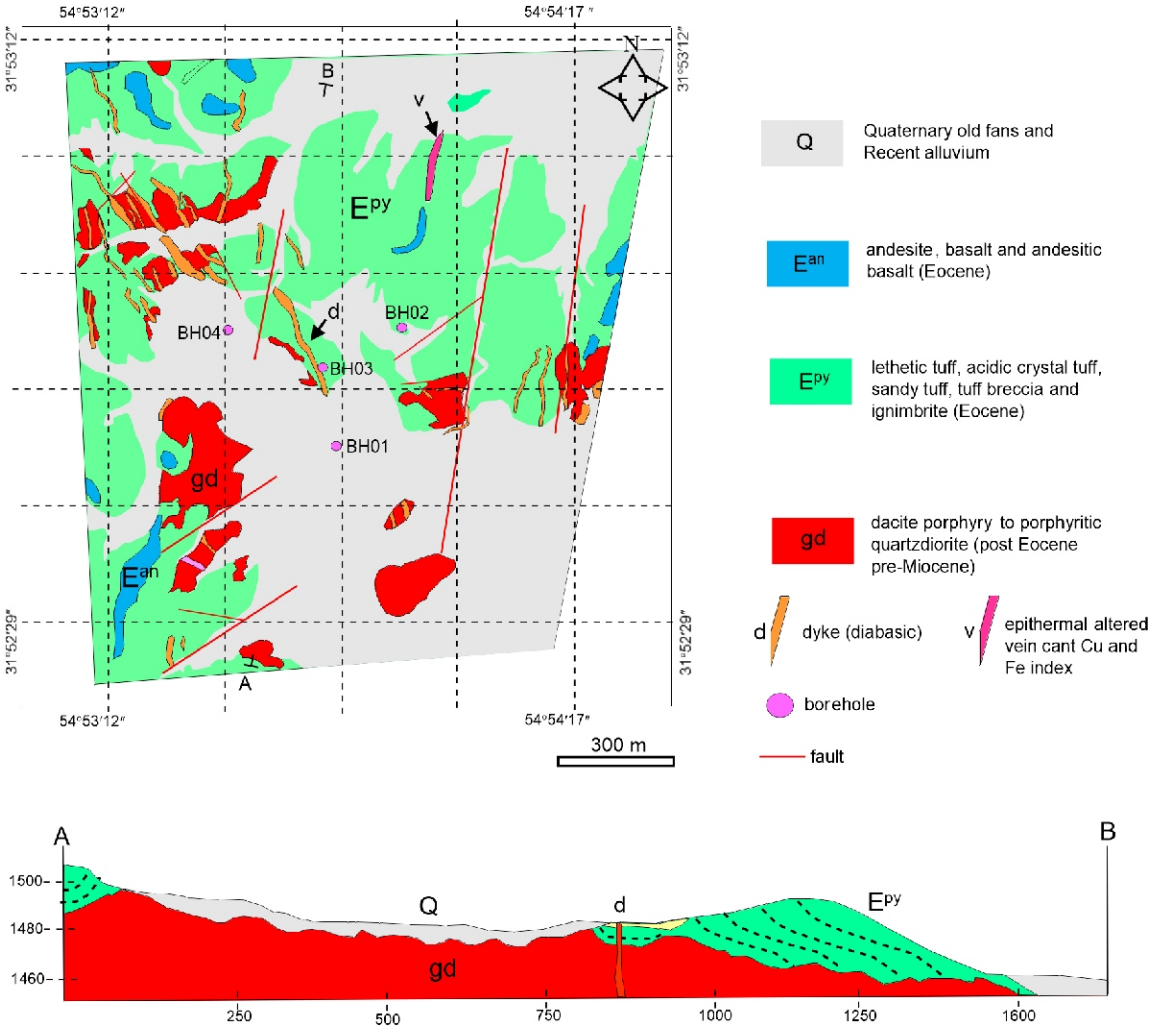

Fig. 2. Simplified geological map of the Sar-e-Yazd area and cross section (A–B) in N–S direction (redrawn and modified after Moayyed, 2019)

The locations of the Sar-e-Yazd Cu (Mo) deposit is shown in the central part of the map and is indicated by some boreholes

tion. In the eastern part of Mehriz (Sar-e-Yazd area), the outcrops are primarily composed of Cenozoic volcanic and volcanoclastic sequences. These Cenozoic rocks are intruded by a shallow dacite porphyry to porphyritic quartzdiorite and porphyritic granodiorite in the Sar-e-Yazd area (Figs. 1 and 2). The Cenozoic in the Nain-Jiroft Magmatic Belt (NjMB) is divided into two important volcanic and plutonic parts. The Naein-Jiroft Magmatic Belt (NJMB) region is generally characterized by volcanic activity during the Upper Cretaceous and Eocene periods, and plutonic activity during the Eocene-Oligocene and Middle Miocene periods. These geological events coincide with the Pyrenean and Styrian orogenic phases, which are considered to have stimulated preheated areas due to prior volcanic activity (Stocklin, 1968). The most considerable Cenozoic rock units in the Mehriz area are the Kerman conglomerate and the Eocene volcano-volcanogenic sequence. Regionally, volcanic rocks sequence consists of andesite, basalt and andesitic basalt as well as volcanoclastic rocks (lethetic tuff, acidic crystal tuff, sandy tuff, tuff breccia, and ignimbrite), the age of which is Eocene (Moayyed, 2019; Fig. 2). Also based on the field studies of the current research, in the central area, in the periphery of the Cu (Mo) Sar-e-Yazd deposit outcrops are mainly of Tertiary age. Outcrops consist of Eocene volcanics and volcanoclastics as well as Oligo-Miocene dacite porphyry to porphyritic quartzdiorite and late diabasic dyke, which cut across earlier rocks. Volcanoclastic rocks consist of stratified green carbonate tuff, lithic andesitic tuff, argillic crystalline tuff, and stratified red silty calcareous tuff Volcanics are quartz andesite porphyry that form the summit of the peaks. The emplacement of intrusive rocks and the formation of dykes within geological units have significantly influenced their structural dynamics and mineral composition. As these intrusive formations penetrate existing rock units, they create new pathways and voids, facilitating changes in mineralization processes. In particular, the mineralized silica veins within these units have expanded due to the increased heat and pressure associated with the intrusions (Figs. 2 and 3). Subsequently, later, hidden porphyritic granodiorite intruded inside this earlier suite, becoming visible in depth of borehole, and is the main agent of mineralization in the Sar-e-Yazd area (Harati and Moayyed, 2020; Fig. 3).

CHARACTERISTICS OF REGIONAL FAULT STRUCTURES IN THE SAR-E-YAZD AREA

The studied area is significantly influenced by two right- lateral strike-slip faults: Anar (160/85 N) and Dehshir (150/85 N), which define its north-east and south-west boundaries. These faults play a crucial role in shaping the geological dynamics of the region, leading to the formation of a right-rotating shear system (Fig. 4A). The Sani Abad syncline has been created in the

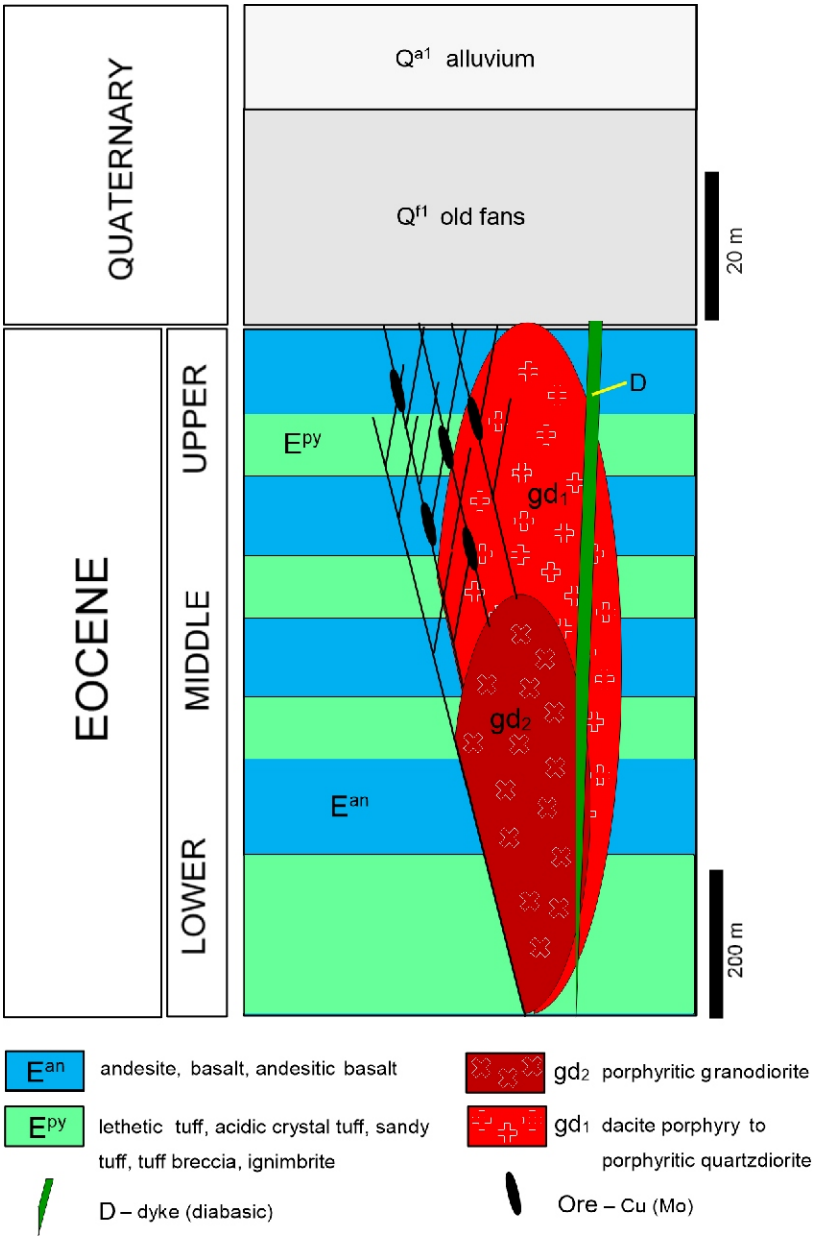

Fig. 3. Composite schematic stratigraphic columns showing the geologic context of different parts of the Sar-e-Yazd Cu (Mo) deposit (based on logging of drilling core)

Simplified geology from surface to ~0.8 km below surface. Scale is approximate. Age of lithology units based on Figure 2; drawn of these columns is based on the Moayyed, (2019) petrography in the Sar-e-Yazd area)

north-west direction with axial line 130 N in this shear system. The study of faults in the Sar-e-Yazd area demonstrates a significant correlation with the pre-existing joints found within the Sani Abad syncline structure. Geological investigations reveal that the faults observed in this region align with the ancient joint patterns, suggesting that the tectonic history of the area has played a crucial role in shaping its current geological framework. The consistency of these faults with the older joints indicates a complex interplay between past geological events and more recent fault activity. This relationship provides valuable insights into the structural evolution of the Sar-e-Yazd area and enhances our understanding of regional tectonics. Recent studies have identified three significant faults in the eastern Mehriz area, specifically in the Sar-e-Yazd region, through a combination of satellite imagery and field observations. These faults include: 1 – Longitudinal Joints: these release or tension faults are oriented in the 130/90 N direction. They represent the primary tensile stress direction, indicating the presence of extensional tectonic forces in the region, 2 – Cross Joints: also known as expansion faults, these joints are oriented in the 45/90 N direction. They accommodate extensional strain and facilitate the expansion of the rock mass in response to tectonic stress and 3 – Diagonal Joints: these include oblique, double, or shear faults with orientations of 160/80 N and 20/80 N (as illustrated in Fig. 4B). They form due to shear stress, resulting in complex fault interactions that accommodate both horizontal

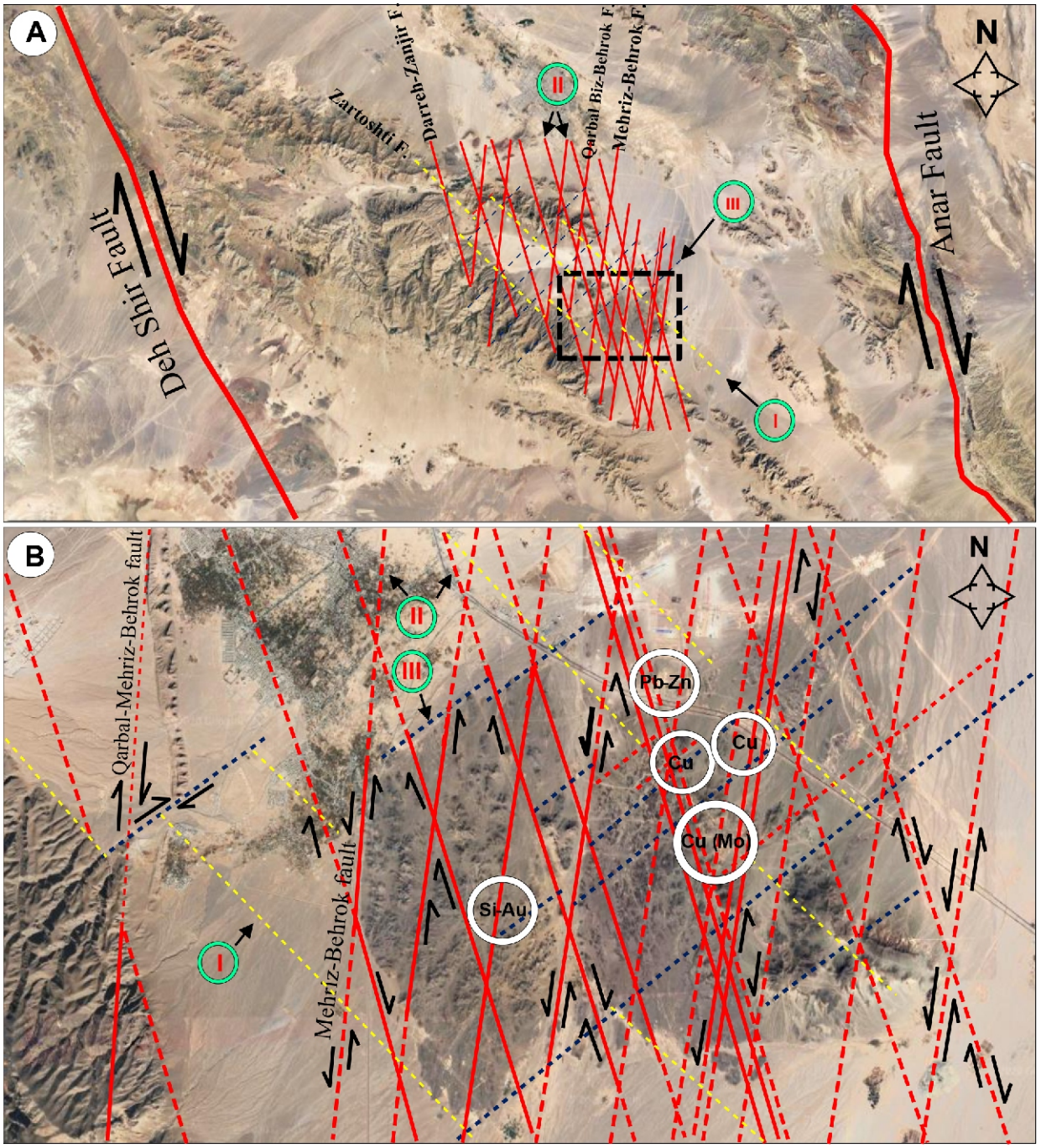

Fig. 4. Satellite images showing the location of the Sar-e-Yazd deposit and the major faults of the area relative to the Mehriz area

I – longitudinal faults (WNW), II – diagonal faults (NNW and NNE), III – cross faults (NE)

and vertical displacements. Figure 4B highlights the structural patterns that demonstrate the interplay between the tectonic settings, the ancient syn-folding fractures (faults) within the Sani-Abad syncline and later region's shear system formation. Additionally, it illustrates the relationship between these syn-folding fractures and the emplacement of dikes, hydrothermal veins, and porphyry copper deposits. The significant ancient fractures and the region's shear system formation are pivotal in understanding geological processes, particularly in the intrusion of igneous bodies, the emplacement of dykes, and the formation of mineralization veins. In the Sar-e-Yazd area which of syn-folding fractures include different type of intrusion, dykes and veins that: I – longitudinal fracture or fault (parallel to the Zartoshti fault): the early dacite porphyry to porphyritic quartzdiorite intrusions and the first group of diabasic dykes often intrude into longitudinal fractures resulting from folding.

II – the diagonal fracture or fault (parallel to the Qarbal-Biz-Behrok and Mehriz-Behrok faults and diagonally with the Darreh Zanjir fault): the late porphyritic granodiorite intrusion of intrusive, branches of the epithermal Cu-Fe vein and the Pb-Zn apophyse intruded parallel to these faults. Finally III – cross faults that align parallel to the fault valleys on the southwestern

side of the Sani-Abad anticline have significantly impacted the geological landscape, particularly in the displacement of Eocene volcanic rocks. These faults play a crucial role in the structural changes of the region's rock formations. The uplift and subsidence of rock formations in the Sar-e-Yazd area are significantly influenced by the movements and displacements of these faults (Fig. 4). It is worth mentioning that there are two groups of dykes in the region, each exhibiting distinct orientations due to variations in the shear system formation: first group of dykes as mentioned above with WNW extension are attributed to old T_2 fractures by Storti et al. (2006); shear system, but the second group of later diabasic dykes are often intruded with N–S direction that they are attributed to tensile fractures in the T_1 shear system. However the pattern of veins is directly related to the regional stress, so the study of veins in the region, reveals two main trends: (1) tension splits associated with T_1 and tensile fractures, which play a crucial role in the mineralization system of the region, and (2) the pennant vein pattern, which is linked to R/R' diagonal fractures. Fractures with a NNW trend (R), mostly filled with iron oxides, are younger and do not play a significant role in mineralization. In contrast, fractures aligned with the NNE (north-northeast) trend of the R' shear system have been instrumental in geological processes related to the emplacement of intrusive rocks in the region. This aligns with Saric's (1973) theory on the emplacement of porphyritic intrusions. According to studies conducted on geological formations, the delayed intrusion of intrusive rocks has notably increased at the tension centres located between diagonal faults. This phenomenon has led to the development of a horst and graben structure in these areas. The Eocene sequence has experienced significant geological changes due to the interaction of compressive and tensile forces within the region. The operation of faults, which primarily occur in a compressive-tensile manner, has played a crucial role in shaping the structural integrity of the Eocene rock formations.

LITHOLOGIES

Geological maps and lithological information obtained from logging drilling cores play a crucial role in characterizing the geology of the Sar-e-Yazd area. The outcrops in this region predominantly belong to the Eocene epoch, comprising andesite interlayered with tuff. During the Oligo-Miocene period, dacite porphyry, porphyritic quartzdiorite, and porphyritic granodiorite intrusions, along with subsequent diabasic dykes, penetrated the Eocene volcanic and volcanoclastic rocks. Together, these formations define the general geological framework of the region (Harati and Moayyed, 2020).

VOLCANOCLASTIC ROCKS

The volcanoclastic rocks in the Sar-e-Yazd area are composed of four predominant types of tuff: stratified green carbonate tuff, lithic andesitic tuff, argillic crystalline tuff, and stratified red silty calcareous tuff (Figs. 5 and 6). The Intrusion of intrusives within these units has altered the surrounding rocks, leading to the expansion of ore-bearing silica veins.

Stratified green carbonate tuff is a distinctive geological formation characterized by its composition, which includes granular and semi-rounded quartz grains, along with fragments of primary minerals. The primary minerals within this tuff are predominantly fine and disseminated plagioclase that have undergone alteration to calcite, sericite, and clay minerals. Ferromagnesian minerals have altered to amphibole, pyroxene, and, ultimately, garnet to epidote. These components generally occur as pyroclastic grains welded together by tuff. Additionally, some calcite is present in the matrix. The abundance of granular quartz, calcite, sericite, epidote, and plagioclase fragments, along with the alteration of ferromagnesian minerals to epidote, indicates that the sample belongs to a calcite-sericite field. The green colour is mainly due to the presence of epidote (Figs. 5A, B and 6A).

Breccia siliceous andesitic tuff is a type of volcanic rock distinguished by its unique mineral composition and textural features. This tuff primarily consists of fine-grained plagioclase that has undergone alteration to form sericite, a process that enhances its stability and texture. Additionally, the rock contains quartz, present as fine-grained and disseminated crystals, which contribute to its overall resilience and structural integrity. It also includes small fragments separated from the primary large porphyry andesite lithic. This composition indicates that it is indeed a breccia siliceous andesitic tuff (Figs. 5A and 6B).

Argillic crystalline tuff is a distinctive geological material characterized by its rich composition of clay minerals, sericite, epidote, and quartz. These constituents predominantly appear in the form of microcrystals and disseminated grains. These components are welded together by tuff in a massive shape, showing a fine ash vitric tuff texture. The hand sample has a green colour and a shelly fracture (Figs. 5B and 6C).

Stratified red silty carbonate tuff is a unique geological formation, notable for its pale-red colouration and distinctly thinner layers compared to other rock types. Under microscopic examination, this tuff is composed of primary quartz grains with varied shapes, disseminated oxidized pyrite, calcite, and fragmented pieces of primary altered minerals. The matrix comprises calcite and some sericite, which result from the alteration of primary minerals into carbonate cement. The oxidation of pyrite to iron oxides imparts a red-brown hue to the sample (as depicted in Fig. 6D). Small laminations can be seen throughout the sample. Based on the texture and mineralogy, the sample is a stratified red silty calcareous tuff in the mineralization region of the Sar-e-Yazd deposit, indicated by the presence of primary granular quartz minerals with various shapes, abundant calcite, fine laminae, fused texture, and traces of primary minerals (plagioclase; Figs. 5C and 6D).

VOLCANIC ROCKS

Based on Harati and Moayyed (2020), volcanic rocks consist of lavas with basaltic, andesitic and basaltic-andesitic compositions, which are placed obliquely on the set of volcanoclastic rocks mentioned above (Fig. 5D and E):

Basalt is a widely occurring type of volcanic rock, distinguished by its dark green to black colouration, a characteristic attributed to its mineral composition. The primary mineral constituents of basalt include plagioclase, clinopyroxene, and olivine. While plagioclase and clinopyroxene crystals remain unaltered, olivine phenocrysts exhibit alterations to anthophyllite, carbonate, and occasionally iddingsite. Additionally, chlorite and carbonate are observable in the rock matrix. The texture of basalt is microlithic porphyritic, and it has undergone weak propylitic alteration (refer to Fig. 5E).

Andesite. Andesitic rocks are characterized by a greenish grey colour and their main minerals are plagioclase and amphibole. Accessory minerals include zircon, apatite and opaque minerals. The plagioclase phenocrysts have slightly altered to sericite and the amphibole phenocrysts have also been transformed into carbonate, chlorite and iron oxides. Accumulations of secondary quartz, chlorite and carbonate can be seen in the rock matrix. Their texture is microlithic porphyritic and they have undergone weak to moderate propylitic-sericite alteration (Figs. 5E and 6E).

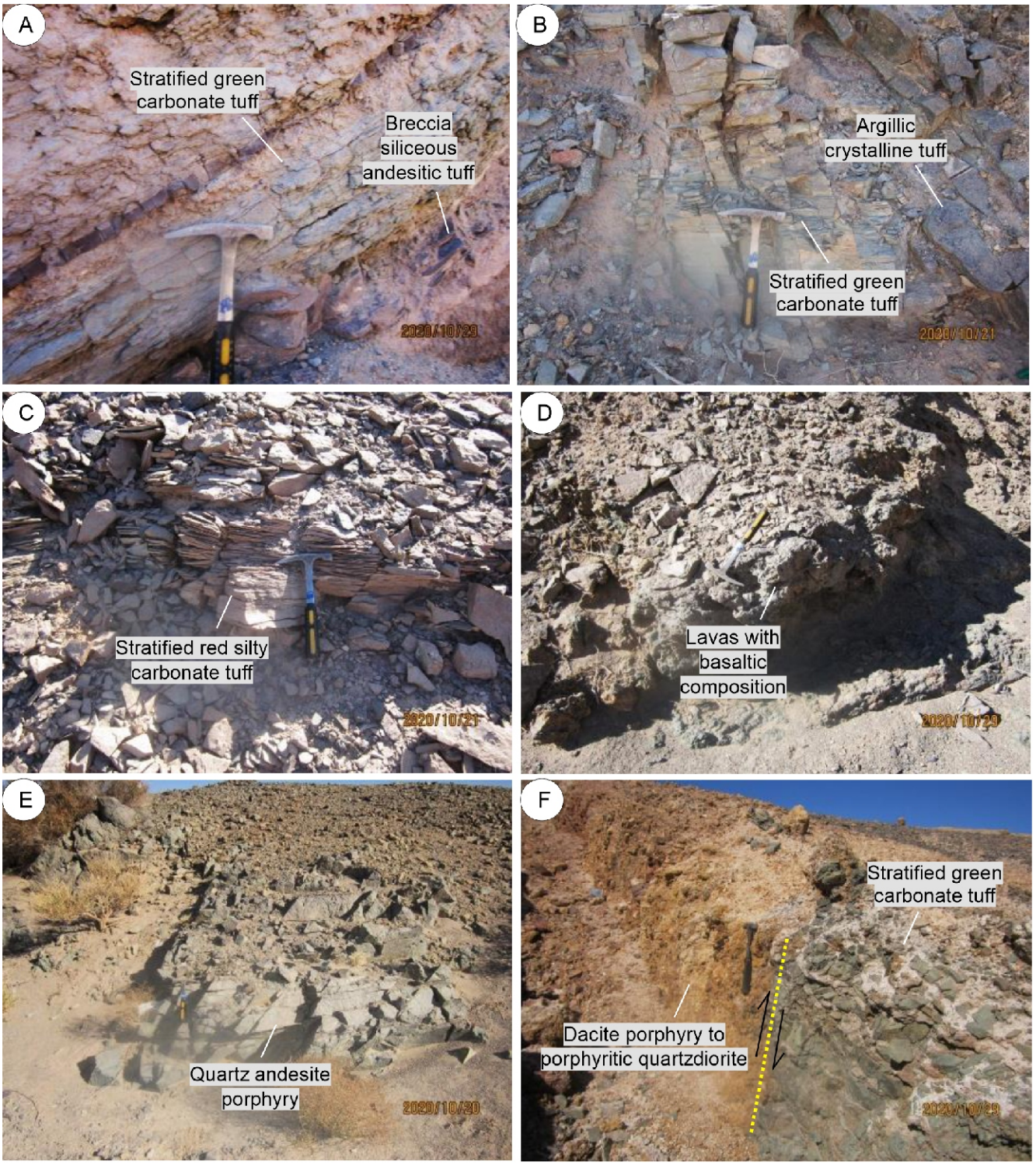

Fig. 5. Field photographs of the studied volcanoclastic, volcanic and intrusive rocks in the Sar-e-Yazd Cu (Mo) porphyry deposit

A–**C** – volcanoclastic tuff: A – outcrop of stratified green carbonate tuff, breccia siliceous andesitic tuff, B – argillic crystalline tuff, C – stratified red silty carbonate tuff composed of altered glass shards, plagioclase, and opaques; **D**, **E** – the volcanic rocks: D – lavas with basaltic composition, E – an outcrop of quartz andesite porphyry; **F** – subvolcanic dacite porphyry to porphyritic quartzdiorite. Geological hammer used for scale is 50 cm long

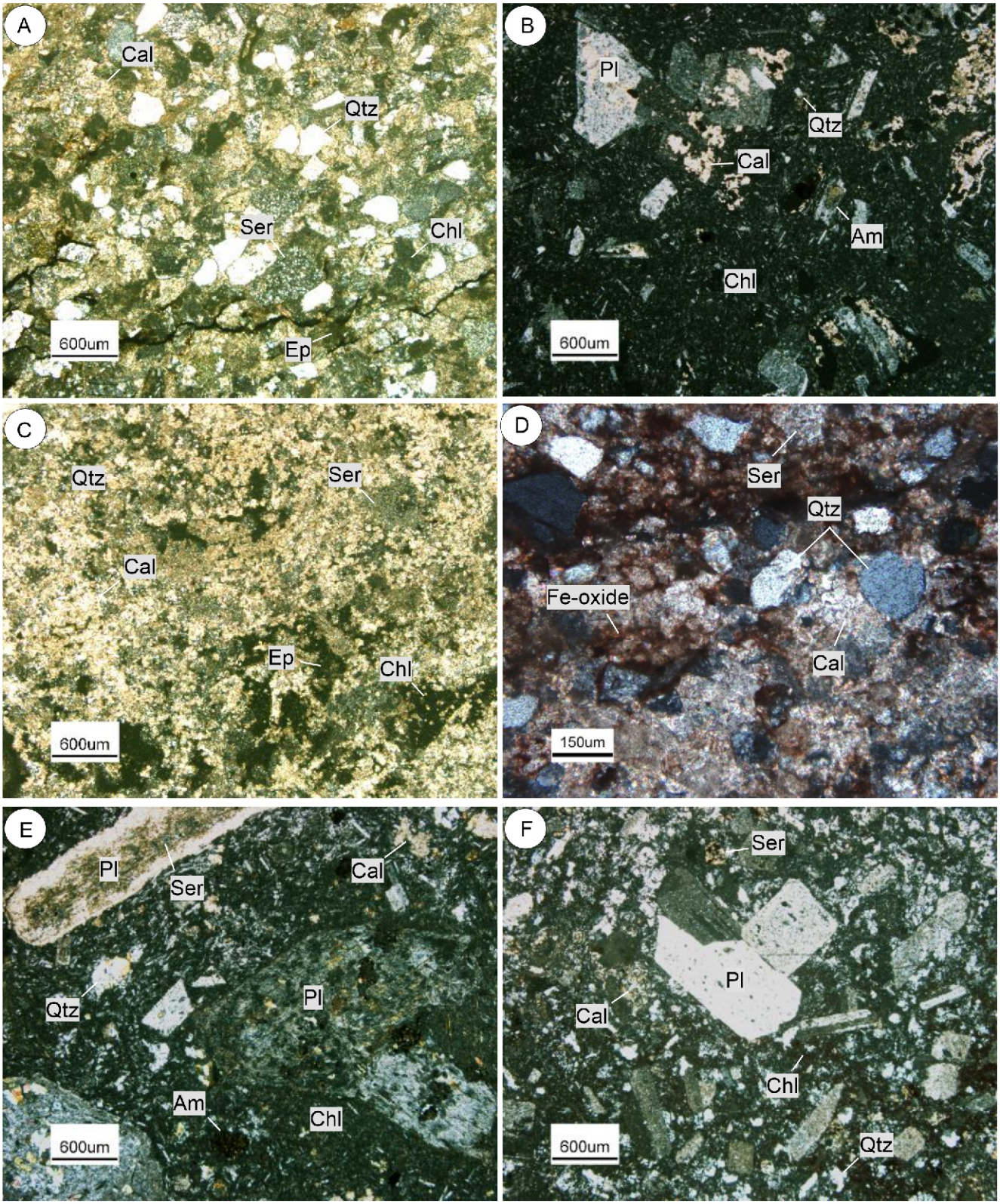

Fig. 6. Microphotographs of the studied volcanoclastic, volcanic and intrusive rocks in the Sar-e-Yazd Cu (Mo) porphyry disposit

Thin section photomicrographs of: **A –** stratified green carbonate tuff; **B** – breccia silliceoes andesitic tuff; **C** – fine ash vitric tuff texture in the argillic crystalline tuff; **D** – laminated texture according to the layering of tuff material in different sizes, part of the rock contained scattered quartz, sericite and Fe-oxide; **E** – quartz andesite porphyry; **F** – dacite porphyry to porphyritic quartzdiorite. Mineral abbreviations after Whitney and Evans (2010) used are: primary minerals: Pl – plagioclase, Am – amphibole and secondary minerals: Qtz – quartz, Ser – sericite, Chl – chlorite, Cal – calcite, Ep – epidote

Basaltic-andesite. Basaltic-andesitic rocks represent an intermediate composition between the two previously discussed groups. Their primary mineral components include plagioclase, clinopyroxene, and amphibole, accompanied by minor minerals such as zircon, apatite, and opaque minerals. Notably, plagioclase phenocrysts in these rocks frequently undergo alteration to carbonate and sericite, while clinopyroxene phenocrysts are replaced by chlorite, carbonate, and iron oxides. Similarly, amphibole crystals are transformed into carbonate and iron oxides. Additionally, these rocks often contain xenoliths of internal igneous rocks exhibiting a microgranular texture. These microgranular xenoliths, with a microdioritic composition, are interpreted as host rocks entrapped during the ascent of magma from the Earth's interior to the surface. The texture of basaltic-andesitic rocks is described as hyalomicrolytic porphyritic, and they typically experience weak to moderate propylitic alteration, as well as minor sericitic alteration.

INTRUSIVE ROCKS

Surface investigations revealed a notable geological feature: a porphyritic intrusion exhibiting compositional variation from dacite porphyry to porphyritic quartzdiorite, as shown in Figure 5F. Within this intrusion, coarse-grained and characteristic plagioclase were observed in a microlithic matrix composed of finely altered plagioclase, sericite, and quartz. The mentioned plagioclases had been completely altered into clay minerals. Granular quartz, characterized by medium-sized crystals and occasionally exhibiting an alugoidal texture, is extensively disseminated and aggregated within the matrix. Additionally, sericite, which forms as a result of the alteration of primary minerals, is also prevalent (Figs. 5F and 6F). Also the presence of large plagioclase crystals with a porphyritic texture in a microlithic context, along with abundant quartz and sparse ferromagnesian minerals (such as amphibole and pyroxene), suggests that this sample represents dacite porphyry to porphyritic quartzdiorite in the studied area (Fig. 6F). However, recent exploratory excavations have uncovered a significant geological feature beneath the initial layers. At deeper levels, an additional intrusion characterized by porphyritic granodiorite has been identified. Finally intrudes of polymetallic and epithermal veins into the old porphyritic intrusive and volcanoclastic rocks. The phenomenon of subsurface intrusion of intrusives, particularly those that lack surface outcrops, exhibits fascinating geological characteristics. It is hypothesized that branches of porphyritic granodiorite intruded into and intersected the pre-existing dacite porphyry, resulting in the formation of what is now identified as porphyritic quartzdiorite. This interaction underscores a complex history of magmatic activity, wherein younger intrusion of intrusives penetrated older geological structures, significantly altering the local geology. The Group 2 dykes, recognized for their mineralized content, are likely products of these dynamic magmatic processes. The intrusive of porphyritic granodiorite has been observed in some boreholes (BH_{23}, BH_{24}, and BH_{25}) and at great depths (more than 400 m; Harati and Moayyed, 2020). These two porphyritic intrusion of intrusive in the BH_{24} had a clear boundary and xenoliths with microdiorite composition were observed inside the porphyritic quartzdiorite. Polymetallic veins, distinguished by their rich deposits of multiple metals, are commonly observed on the periphery of the Sar-e-Yazd porphyry system and have historically been the focus of extensive mining activities. These veins frequently exhibit mineralization composed of iron, lead, zinc, and copper. Additionally, studies of diabasic dykes in the region highlight their significant interactions with the surrounding volcanoclastic rocks and intrusive formations. These dykes, which intrude into the volcanic material along a WNW–ESE orientation, often result in the formation of alteration halos along their margins. Such alteration processes are attributed to hydrothermal activity, driven by the heat and mineral exchange occurring between the dykes and the surrounding rocks.

HYDROTHERMAL ALTERATIONHYDROTHERMAL ALTERATION

Alteration and mineralization were analysed through detailed studies of the mineralogy and petrography ofdrilling core and outcrop samples collected from various locations and host rocks within the Sar-e-Yazd Cu (Mo) porphyry deposit. Hydrothermal alteration, a significant geological process affecting magmatic and adjacent volcanoclastic rocks, can be predominantly categorized into three main stages: (1) an early-stage potassic or K-silicate alteration core forms at the centre of the system during the initial evolution of the porphyry deposit, (2) a peripheral halo of propylitic alteration surrounding the potassic zone develops, and (3) late-stage alterations occur, characterized by sericitic (phyllic) and clay alterations (Fig. 7). No particular patterns are ascribed to the distribution of the hydrothermal alteration, which is mostly spatially associated with the porphyritic granodiorite and dacite porphyry to porphyritic quartzdiorite and regional structures. However, the alteration zoning observed in drill core samples demonstrates a systematic distribution, distinguished by distinct zones arranged sequentially from the core outward: potassic, propylitic (actinolite, epidote and chlorite sub-zone; as Holliday and Cooke, 2007 classification), sericitic or phyllic and clay alteration (have cores of silicic and advanced argillic alteration surrounded by advanced argillic, argillic, and propylitic alteration assemblages). The boundaries between these alteration zones are highly irregular, presenting challenges for detailed mapping.

EARLY-STAGE

POTASSIC ALTERATION

At the Sar-e-Yazd Cu (Mo) porphyry deposit, potassic alteration is closely associated with porphyritic granodiorite intrusions. This alteration is typically localized and spatially restricted. The subsequent overprinting by sericitic alteration further confines the spatial extent of the potassic alteration. Potassic alteration forms during the early stages of the porphyry system's evolution and is enveloped by a propylitic alteration halo. Drill core samples indicate that this alteration predominantly occurs at depth, particularly at intervals of 250–270 m and 685 m. Notably, it is not exposed at the surface. Potassic alteration is characterized by K-feldspar, biotite, and sericite minerals (Damian, 2003), and formed near the mineralized zone. The potassic alteration zone in the Sar-e-Yazd was identified by secondary biotite, plagioclase, and quartz with porphyritic texture (Fig. 7A and B). As well as the traces and signs of potassic alteration at great depths in the samples obtained from borehole 26 (at 685 m) showed that biotite was neoformed and turned into chlorite and epidote.

PROPYLITIC ALTERATION

In the studied area, the propylitic halo extends laterally for ~1 km from the potassic core, forming a distinctive green halo observable in the outermost regions. This halo is notably extensive, affecting not only the porphyritic granodiorite but also the dacite porphyry and the porphyritic quartzdiorite, as confirmed

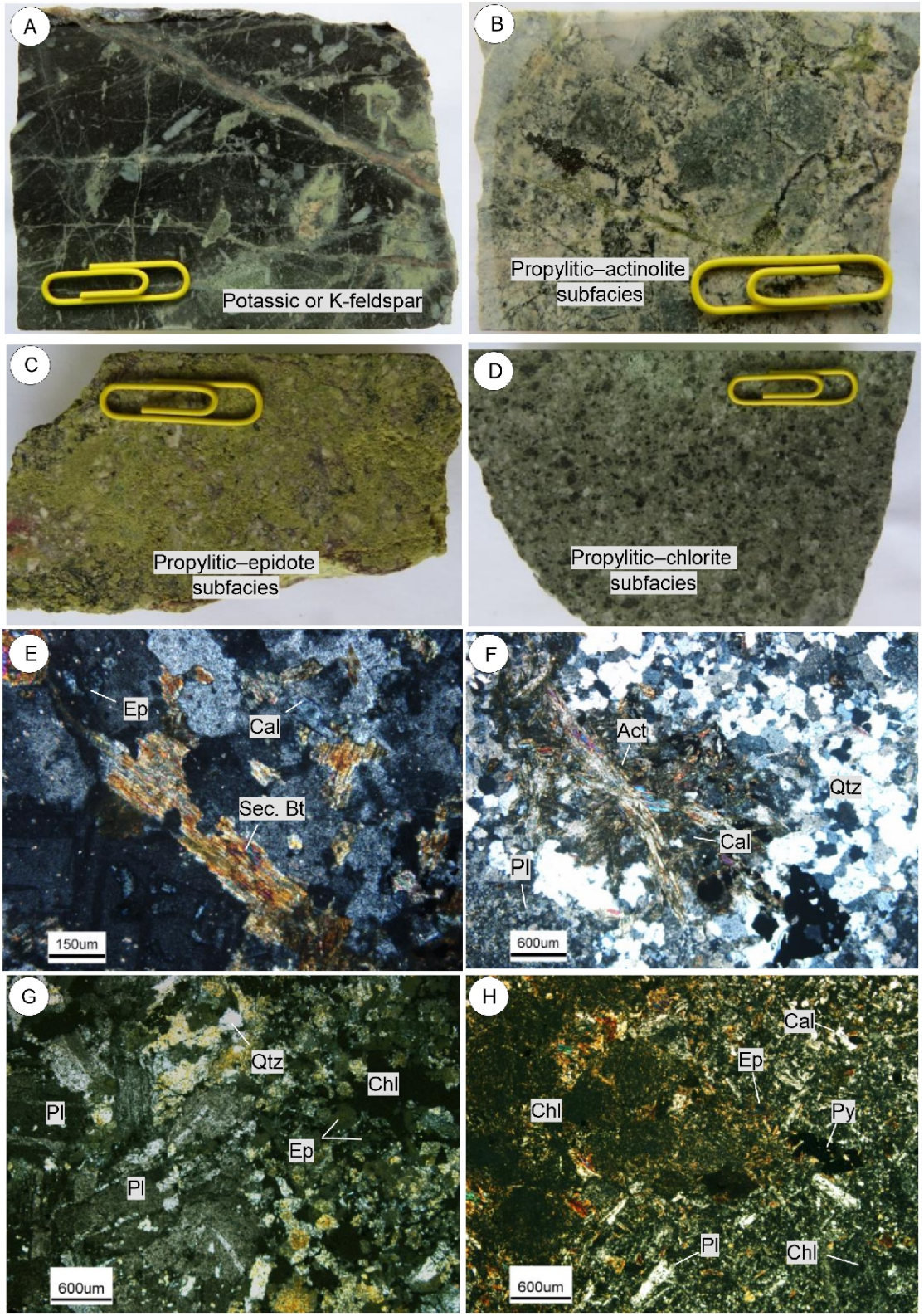

Fig. 7. Photographs (A–D) and photomicrographs (E–H) texture, minerals and hydrothermal alterations related to early stage of porphyry Sar-e-Yazd Cu (Mo) deposit

A – slab of potassic alteration; plagioclase and secondary biotite dispersed in K-feldspar and quartz groundmass and three propylitic hydrothermal alteration subfacies [actinolite (**B**), epidote (**C**), and chlorite zones (**D**)] that occurred around the potassic-altered rocks. Photomicrographs of minerals of the hydrothermal alterations (polarized light); **E** – hydrothermal secondary biotite (Sec. Bt), quartz and altered plagioclase (Pl) from an A-type veinlet of the potassic alteration in a dacite porphyry to porphyritic quartzdiorite drill core sample; three sub-zone propylitic hydrothermal alteration (F, G and H) in the dacite porphyry to porphyritic quartzdiorite; **F** – actinolite sub-zone: act-epi-chl-py-ab-cb, **G** – epidote sub-zone: epi-chl-py-ab-cb±hm and **H –** chlorite sub-zone: chl-py-ab-cb. Abbreviations after Whitney and Evans (2010): primary minerals: Pl – plagioclase, Py – pyrite and secondary minerals: Sec. Bt – secondary biotite, Ac – actinolite, Qtz – quartz, Chl – chlorite, Cal – calcite, Ep – epidote

by analyses of drill core logs. The characteristic hydrothermal minerals are divided into three subzones (Fig. 7C, D and E): 1 – inner, high-temperature actinolite subfacies (actinolite-epidote-chlorite-calcite-pyrite-magnetite-hematite-chalcopyrite); 2 – moderate-temperature epidote subfacies (epidote-chlorite-calcite-pyrite-hematite-chalcopyrite); and 3 – outer, low-temperature chlorite subfacies (chlorite-calcite-pyrite-prehnite-zeolites). This alteration occurs at high temperature and the presence of chlorite and epidote indicates temperature condition ranging from 220 to 340°C (Lagat, 2009). Mapping propylitic assemblages can therefore provide a useful vector toward the central, high-temperature mineralized and potassic altered core of a porphyry deposit.

CARBONATE ALTERATION

Carbonate alteration, classified as a subtype of propylitic alteration associated with sulphide minerals, is prominently observed at the Sar-e-Yazd deposit. This alteration, characterized by calcite as the dominant mineral, occurs locally in two main forms: as scattered patches of calcite + pyrite ± quartz ± chalcopyrite and as sulphide-bearing calcite veinlets within the granodiorite bodies and volcanoclastic rocks. Evidence from cross-cutting relationships (Fig. 9C) indicates that carbonate alteration developed during the later stages of the hydrothermal system's evolution.

LATE-STAGE CLAY ALTERATION

The Sar-e-Yazd porphyry Cu (Mo) deposit displays a range of late-stage alteration assemblages, prominently including phyllic, argillic, and advanced argillic alterations. The phyllic alteration is characterized by quartz, sericite, pyrite, and chalcopyrite, whereas the argillic alteration comprises quartz, kaolinite, illite, and pyrite. In comparison, the advanced argillic alteration is defined by the presence of quartz, alunite, kaolinite, and pyrite. These clay-rich assemblages are typically fault-controlled, exhibit upward-flaring geometries, and overprint the earlier potassic and propylitic alteration assemblages (Fig. 8).

PHYLLIC ALTERATION

Sericite and quartz mineral assemblage indicate phyllic alteration, formed by the complete replacement of the plagioclase by sericite and of the mafic minerals by quartz (Damian, 2003). Phyllic alteration implies low pH (acidic) conditions (Lagat, 2009). Phyllic alteration often includes networks of stockwork fractures (Sinclair, 2007). These alteration may be subdivided into two different types (Sillitoe, 2010): an uncommon, early variety that is greenish to greenish-grey in colour and a later, far more common and widespread, white variety.

In the Sar-e-Yazd porphyry deposit, just the white variety phyllic or sericitic alteration affects both the magmatic and volcanoclastic rocks. In the dacite porphyry to porphyritic quartzdiorite, it overprints the potassic and propylitic alteration and locally results in the complete replacement of plagioclase. Sericite forms acicular to prismatic aggregates, which are accompanied by disseminations and veins of quartz and pyrite (Fig. 8A). The K-feldspar replacement by sericite is generally controlled by the distribution of micro-fractures. In these cases, only the relic crystal habit of K-feldspar remains, forming vugs of different sizes (Fig. 8A and F). In this alteration, quartz and sericite expand around the veins and replace all primary silicate minerals. Plagioclase altered to sericite and mafic minerals (amphibole and biotite) changing to chlorite.

ARGILLIC AND ADVANCED ARGILLIC ALTERATION

Argillic alteration is characterized by the formation of the clay minerals such as illite, kaolinite, muscovite, and montmorillonite (Damian, 2003), and is a low-temperature episode (Lagat, 2009). In the near-surface environment (<1 km below the palaeosurface), lateral flow of acidic fluids along permeable horizons produce thick, extensive domains of clay alteration that are referred to as lithocaps (Sillitoe, 1995, 2010; Chang et al., 2011). Lithocaps are typically characterized by cores of silicic and advanced argillic alteration, surrounded by advanced argillic, argillic, and propylitic alteration assemblages. At the Sar-e-Yazd porphyry deposit, geological studies have identified significant mineralogical alterations, particularly in feldspar, to a depth of 47 m in borehole 26 (BH_{26}). In this area, feldspar shows localized alteration to clay, and the entire rock has been transformed into an assemblage comprising hematite, clay minerals, and quartz. Kaolinite, a prominent phyllosilicate mineral with a layered structure and a composition primarily of aluminum silicate, is frequently observed alongside illite. These minerals are typically found at depths of 30 to 50 m below the surface. In regions affected by steep fractures, kaolinite and illite are often overprinted by silicic-argillic alteration, which is dominated by silica and argillaceous materials (Fig. 8B, C and G). Advanced argillic alteration has been identified at a depth of 684 m, featuring K-alunite, which constitutes less than 10% of the entire advanced argillic zone, along with aluminum-phosphate-sulphate minerals such as kaolinite (Fig. 8D and H). At the surface, advanced argillic alteration is characterized by residual quartz, commonly referred to as "vuggy quartz" (Fig. 8E). This style of alteration is typically buff or gray in colour, serving as a visual indicator of the geochemical processes involved. It is frequently accompanied by the presence of late-stage dickite, a clay mineral closely associated with hydrothermal systems, which occurs within fractures in the rock. In general, the shallow alteration represents a supergene zone over the deposit. Siliceous ledges occur within the quartz- kaolinite zone at shallow depths, generally in the dacite porphyry to porphyritic quartzdiorite (Fig. 8B). The surface exposures (Fig. 8E) and information from above 770-m elevation suggest that the siliceous ledges are preferentially developed around the periphery of the Sar-e-Yazd porphyry deposit, particularly top of dacite porphyry to porphyritic quartzdiorite on the surface. However, it is suspected that ledge development simply penetrated more deeply around the system margins, thereby leading to earlier erosional removal of the ledges that once capped the central parts of the system.

ORE MINERALIZATION

The Sar-e-Yazd Cu (Mo) deposit exhibits significant ore mineralization within a porphyry system characterized by a diverse geological setting. This mineralization is primarily hosted by dacite porphyry and porphyritic quartzdiorite, as well as volcanoclastic rocks that are present at the surface. Additionally, the underlying geology includes porphyritic granodiorite (>400 m), which plays a critical role in the overall mineralization process (Fig. 9). At the surface, the metallic mineralization is almost totally oxidized. The oxidation zone has a maximum depth of 40 to 50 m. The hypogene mineralization at the surface is restricted to the dacite porphyry to porphyritic quartzdiorite, and in the drill core samples, it is well exposed below the oxidized zone to an unknown depth. Volcanic rocks and shallowly emplaced porphyry systems (<1 km depth) are typically poorly mineral-

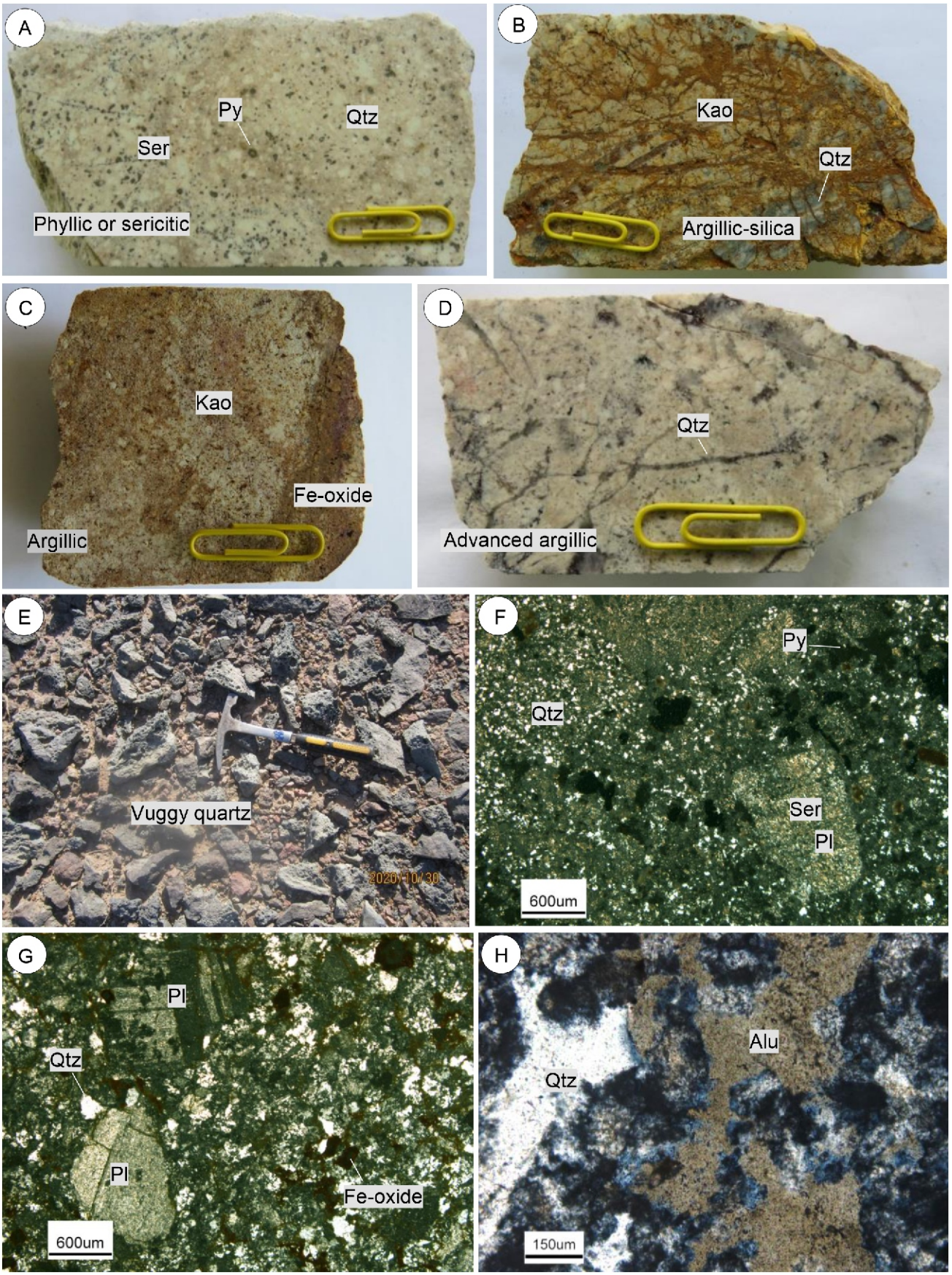

Fig. 8. Slab and photomicrograph of minerals and late-stage hydrothermal alterations of Sar-e-Yazd porphyry deposit

A – phyllic alteration; quartz, sericite and pyrite are the major constituents of this hydrothermal alteration; **B, C** – slab of argillic and silica alteration; **D** – slab of advanced argillic alteration; **E** – dacite vuggy residual quartz/silicification top of the dacite porphyry to porphyritic quartzdiorite. Photomicrograph (cross polarized light) of **F** – phyllic alteration (quartz-sericite-pyrite); **G** – argillic and silica alteration; **H** – Quartz and tabular alunite (Alu + Qtz) in the advanced argillic alteration. Abbreviations after Whitney and Evans (2010): primary minerals: Pl – plagioclase, Py – pyrite and secondary minerals: Alu – alunite, Qtz – quartz, Ser – sericite, Kao – kaolinite, Fe-oxide – hydroxide

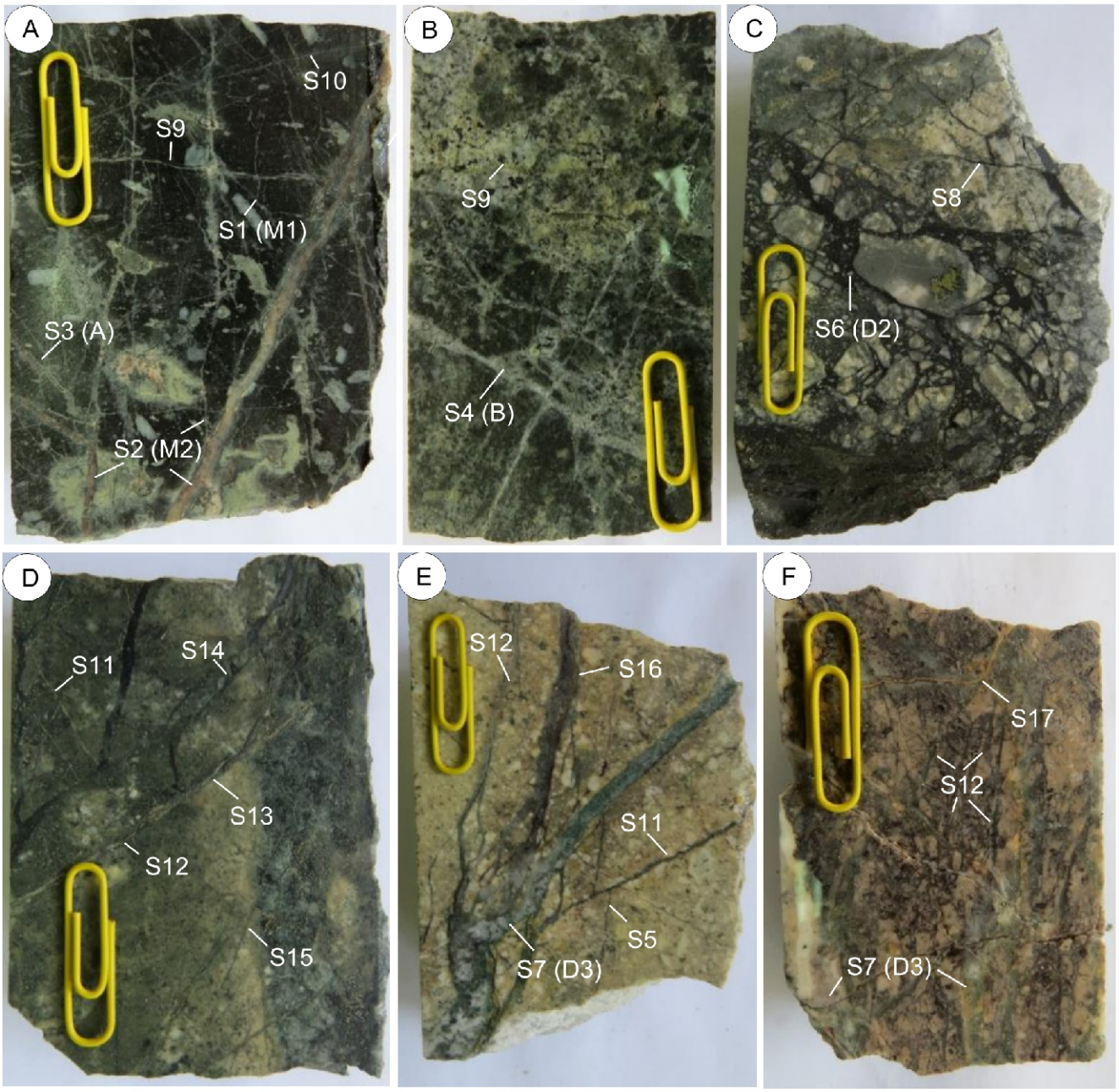

Fig. 9. Photographs of textures in the Sar-e-Yazd Cu (Mo) deposit porphyry system

A – veinlet from a drill core sample of the porphyritic quartzdiorite containing; M1-type sericite-pyrite-molybdenite veins (S1), M2-type weak quartz ± magnetite-pyrite veins (S2), A-type quartz-magnetite-pyrrhotite-bornite-pyrite, chlorite-epidote-rich veins (S9) and quartz-chlorite-rich veins (S10) in the potassic alteration; **B** – B-type sulphide-bearing, granular quartz-dominated veinlets (quartz-pyrite-molybdenite-chalcopyrite, S4 associated with potassic-propylitic boundary alteration; **C** – calcite and sometimes quartz breccia by infiltration D1-type pyrite-quartz vein (S5) within white propylitic-carbonate alteration, cross-cut by D2-type late carbonate-quartz vein with base-metal sulphides (pyrite-chalcopyrite-bornite; S6 or S8); **D** – pyrite veins (S11), quartz veins (S12), sericite-quartz veins (S13), pyrite-sericite veins (S14) and vesuvianite (Idocrase)-epidote veins (S15), in the propylitic-phyllic boundaries alteration; **E** – pyrite-quartz veins (S5), D1-type pyrite-quartz-sericite-calcite veins (S7), pyrite veins (S11), quartz veins (S12) and quartz-calcite veins (S16) in the phyllic alteration; **F** – Stockwork of quartz-sericite-calcite-pyrite vein (large; S7), a lot of quartz veins (S12) and calcite vein (they are younger; S17) associated sericitic alteration

ized, because fluids exsolved at low pressure are mostly low-density vapour (with only small volumes of high-density brine or even solid salt) that have little capacity to transport metals (Cline and Bodnar, 1991; Muntean and Einaudi, 2000). In contrast, most porphyry Cu deposits form at depths of 2 to 5 km, from supercritical saline fluids or liquids coexisting with higher density vapours that can efficiently transport Cu, Mo, Au, and other metals (Cline and Bodnar, 1991; Redmond et al., 2004; Landtwing et al., 2005; Rusk et al., 2008). These fluids in turn are derived from volatile-saturated magmas originating in the underlying source magma chamber at depths ranging from 5 to 10 km, as previously described. In the Sar-e-Yazd area, geological assessments reveal that the subsurface characteristics of the region play a significant role in influencing the extent of mineralization. At depths of less than 1 km, the geological composition appears to be less favourable for the accumulation

Table 1

Characteristics of various vein types from Sar-e-Yazd Cu (Mo) deposit, as documented by inspection of drill cores, and thin-polished sections

Vein type: mineralogy	Gustafson and Hunt (1975) equivalent	Wall rock alteration	Geometry	Cross-cutting relations and characteristic features
S1: Ser + Py + Mol	M1 type	Potassic	Discontinuous, non-planar veins-veinlets without internal symmetry	This vein system is cut by all other vein types
S2: Qtz + Mag + Py	M2 type	Potassic	Discontinuous, non-planar veins-veinlets without internal symmetry	This vein system is cut by all other vein types
S3: Qtz + Mag + Bn ± Py ± Ccp	A type	Potassic overprinte by phyllic and calcite	Discontinuous, non-planar veins-veinlets without internal symmetry; Qtz as anhedral, sugary aggregates, 1–10 mm thick	This vein system is cut by all other vein types
S4: Qtz + Py + Ccp ± Mol ± Mag	B type	Potassic-propylitic boundary, phyllic	Contiguous veins; sharp, parallel and accordance walls; with internal symmetry, mostly sulphide in central part; grey to transparent medium Qtz; 4 to 10 mm width	This vein type is most common, a represents the main stage of copper mineralization in the Sar-e-Yazd deposit (sulphide-bearing, granular quartz-dominated veinlets)
S5: Py ± Qtz	D1 type	Propylitic-carbonate	Planar veins mainly composed of Py and minor Qtz	Cross-cut by late carbonate-quartz vein with base-metal sulphide (pyrite- chalcopyrite - bornite (Py-Ccp-Bn)
S6: Py + Ccp ± Bn ± Qtz ± Cal	D2 type	Propylitic-carbonate	Planar veins mainly composed of Py and minor Ccp and Bn	This vein system commonly occurs in the marginal parts of the porphyritic granodiorite; Ccp and Bn is a minor to trace constituent; sericite locally occurs as thin rims, <1 mm thick. S6 veins cut all other vein types and are offset by S8 type veins
S7: Qtz + Ser + Py + Cal	D3 type	Phyllic	Planar veins mainly composed of Py	This vein system commonly occurs in the marginal parts of the porphyritic granodiorite; S7 veins cut all other vein types and are offset by S8 type veins
S8: Cal + Ccp ± Py ± Qtz ± Bn		Carbonate	Planar veins with significant continuity; occurring as fracture fillings. Py as euhedral grains, encompassed by Ccp. The veins grow thicker outwards	The calcite veins cut all other vein systems; they are distinguished by the common occurrence of Ccp as scattered patches in the veins. The wall rocks to the veins are intensely calcitized
S9: Chl + Ep **S10**: Qtz + Chl		Potassic, and propylitic	continuous, non-planar veins-veinlets without internal symmetry	These type of veins cut all other vein systems. lack of ore minerals
S11: Py, **S12**: Qtz **S13**: Ser + Qtz, **S14**: Py + Ser, **S15**: Ves + Ep **S16**: Cal + Qtz **S17**: Cal		Propylitic-phyllic boundaries, phyllic	Continuous, non-planar veins-veinlets without internal symmetry	S15 has secondary copper minerals vesuvianite (Idocrase) and others lack of ore minerals, S15, S16 and S17 veins cut all other vein systems

Abbreviations after Whitney and Evans (2010): Qtz – quartz, Mag – magnetite, Ccp – chalcopyrite, Py – pyrite, Bn – bornite, Mol – molybdenite, Cal – calcite, Ves – Vesuvianite, Ser – sericite, Ep – epidote, Chl – chlorite

of valuable minerals. This is further supported by variations in copper and molybdenum grades at different depths, as indicated by chemical analyses that will be elaborated upon in the subsequent sections.

HYPOGENE MINERALIZATION

The mineralization at the Sar-e-Yazd deposit is characterized by various forms, including disseminations, aggregates, veins, and veinlets, which play a critical role in elucidating the geological attributes of the region. Significantly, several vein types identified at this site exhibit marked similarities to those extensively documented in typical Porphyry Copper Deposits (PCDs), as outlined in key studies (e.g., Gustafson and Hunt, 1975; Muntean and Einaudi, 2001; Sillitoe, 2010).

The mineralogy and cross-cutting relations of the veins were investigated by inspection of drill cores and thin-polished sections. The various vein types at Sar-e-Yazd are shown in Figure 9 and their characteristics are described in Table. 1. In general, three main assemblages are present in Sar-e-Yazd: 1 – pyrite + chalcopyrite + molybdenite + magnetite associated with potassic and potassic-propylitic boundary alteration (Fig. 9A and B), 2 – pyrite + chalcopyrite + bornite related to propylitic and propylitic-phyllic boundary alteration (Fig. 9C and D) and 3 – pyrite + chalcopyrite associated with sericitic alteration (Fig. 9E and F).

Magnetite is associated with the potassic alteration, forming M-type veinlets that crosscut the potassic-altered dacite porphyry to porphyritic quartz diorite (Figs. 9A and10A, C). Additionally, chalcopyrite occurs within magnetite, typically found

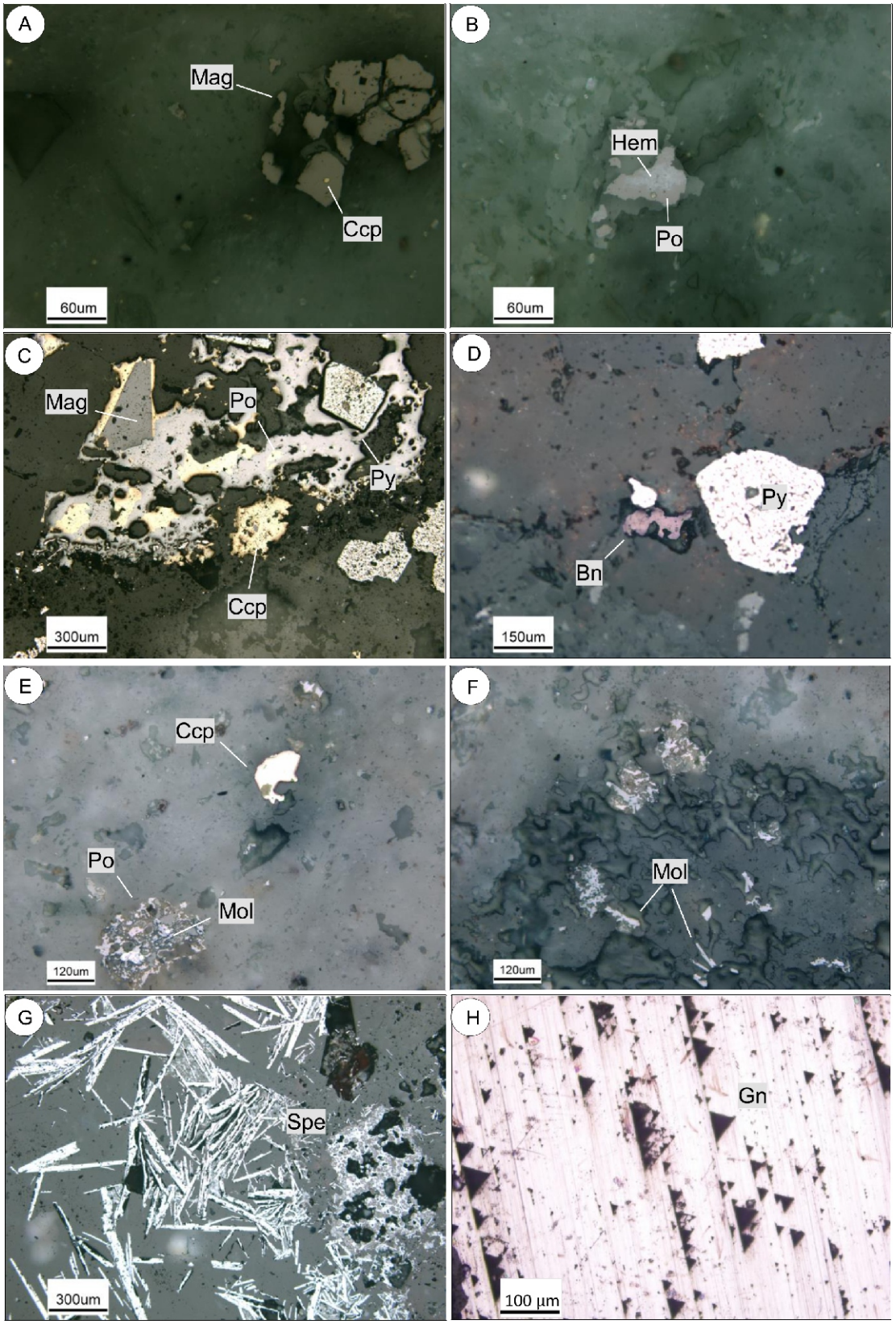

Fig. 10. Reflected light microscopy image of the minerals in the Sar-e-Yezp Cu (Mo) deposit porphyry system

A – chalcopyrite occurring within magnetite typically found in the deeper parts of porphyry system (potassic-propylitic boundary); **B** – hematite within pyrrhotite results from hydrothermal fluids rich in oxygen interacting with pyrrhotite, leading to the formation of hematite; **C** – magnetite in chalcopyrite with pyrrhotite and pyrite in the calcite and sometimes quartz breccia; **D** – occurrence of bornite and pyrite in potassic alteration; **E**, **F –** the formation of very small molybdenite inclusions in pyrrhotite typically occur in high temperature; **G** – tabular specularite crystals with open space filling primary texture, have filled pores between brecciated fragments of host rock in the hydrothermal veins around the centre of porphyry system in the Sar-e-Yazd deposit; **H** – galena in an apophyse located ~3 km from the centre of a porphyry system. Abbreviations after Whitney and Evans (2010): Mol – molybdenite, Ccp – chalcopyrite, Po – pyrrhotite, Hem – hematite, Mag – magnetite, Py – pyrite, Bn – bornite, Spe – specularite, Gn – galena

in the deeper parts of the porphyry system (Fig. 10A). It is also present in chalcopyrite as subhedral to euhedral inclusions (Fig. 10C).

Pyrrhotite a sulphide mineral, is commonly encountered in diverse geological settings, particularly within A- and B-type veins. Recent studies suggest that pyrrhotite is predominantly found at depths exceeding ~200 m in these vein systems (Fig. 9A and B). The formation of hematite within pyrrhotite is attributed to the interaction between oxygen-rich hydrothermal fluids and pyrrhotite, a common iron sulphide mineral. This interaction triggers a chemical reaction that transforms the iron sulphide into hematite, an iron oxide (Fig. 10B). The presence of hematite suggests an oxidizing environment. It is often found in the outer zones of porphyry systems where fluids have interacted with the surrounding rocks and become more oxidized. Pyrrhotite also is intergrown with pyrite, magnetite and chalcopyrite (Fig. 10C).

Pyrite is the most abundant sulphide mineral within the Sar-e-Yazd deposit porphyry system, occurring in intergrowths with chalcopyrite, pyrrhotite, bornite, and magnetite. Locally, it hosts rounded inclusions of chalcopyrite and euhedral inclusions of magnetite. It occurs as disseminations or intergrowths of anhedral to euhedral grains, with sizes varying from 25 to 300 μm and from 300 μm to 2 cm, respectively (Fig. 10C and D) and also pyrite forms veinlets (up to 3 mm in size) in many parts of the deposit.

Chalcopyrite is the second most abundant sulphide mineral and is predominantly associated with potassic alteration. It frequently occurs in conjunction with other sulphides, including pyrite, magnetite, and pyrrhotite (Fig. 10A, C and E). It occurs as disseminated grains (<200 μm in size), irregular aggregates (<300 μm in size), and rounded inclusions (<20 μm in diameter) in pyrite. Chalcopyrite also forms thin veinlets (<0.5 cm in width) along with pyrite inclusions (10–20 μm in size).

Bornite often forms through potassic alteration in the Sar-e-Yazd porphyry system. This process can lead to the development of rounded bornite inclusions within pyrite, with these inclusions ranging in size from 15 to 100 μm (Fig. 10D).

Molybdenite is frequently associated with chalcopyrite and pyrrhotite within potassic alteration zones. It typically occurs as small, disseminated lamellar grains, generally less than 30 μm in length. This association is commonly observed in potassically altered dacite porphyry and porphyritic quartz diorite, where the alteration process has led to notable textural and mineralogical modifications (Fig.10E and F). The formation of molybdenite inclusions in pyrrhotite typically occurs at high temperatures, often associated with the potassic and phyllic alteration zones of porphyry systems.

Specularite a variety of iron oxide commonly found in mineral deposits, plays a significant role in interpreting the geological conditions of epithermal veins. Its presence serves as an indicator of specific oxidation states and fluid flow dynamics within the mineralization system. Typically observed in the peripheral zones surrounding the central parts of these veins, specularite forms under conditions of elevated acidity and reduced temperature, reflecting the diverse environmental conditions during ore formation. At the Sar-e-Yazd deposit, specularite has been identified as veins within the peripheral areas encircling the central region of the porphyry system (Fig. 10E).

Galena is usually associated with late-stage mineralization events. It can be found in veins that form during the later stages of the hydrothermal system's evolution. In Sar-e-Yazd porphyry system galena in an apophyse located ~3 km from the centre of a porphyry system (Fig. 10F).

SUPERGENE MINERALIZATION

The supergene profile at Sar-e-Yazd is relatively thin, in common with those developed over most deposits in the Saveh-Naein-Jiroft belt. The leached capping is typically thickest over the core of the system, where it is hosted by the uppermost parts of the advanced argillic zone. All pyrite and other sulphide minerals, including any contained copper, have been completely removed from the oxidized rock. The acidic solutions generated by the pyrite oxidation produced an unquantified amount of supergene kaolinite, although most of this is impossible to distinguish from the preexisting hypogene component.

ENRICHED SUPERGENE SULPHIDE ZONES

Acid leaching by downward solutions plays a pivotal role in the formation of enriched supergene sulphide zones and the development of leached and oxide zones key outcomes of supergene processes in the Sar-e-Yazd area. However, the intensity of these processes is generally lower compared to similar deposits. Evidence of a well-developed supergene enrichment zone or significant accumulation of secondary minerals is limited in the Sar-e-Yazd field. It appears that most of the copper leached from the oxidized zone was lost to the palaeo-ground-water system. Nonetheless, chemical analyses reveal that the central area, situated just beneath the oxide leached zone, displays weak enrichment in several metallic elements, including Cu, Mo, Pb, Zn, and Ag, as detailed in subsequent sections.

LEACHED ZONE AND OXIDE ZONE

The fractured and crushed zones of quartz stockwork represent significant geological features that enhance the potential for acidic solution penetration. These zones exhibit increased porosity and permeability, facilitating the movement of acidic solutions through the rock. As these solutions percolate into the quartz stockwork, they promote chemical weathering processes, leading to the dissolution of minerals and alteration of the surrounding rock matrix. This interaction plays a crucial role in the development of supergene oxidized zones, where chemical weathering concentrates valuable metal oxides and secondary minerals.

At the Sar-e-Yazd deposit, supergene oxidized zones are identified by the presence of oxide- hydroxide aggregates and copper carbonate minerals. In surface outcrops and drill cores from depths of 1 to 47.65 m, quartz sulphide veins have been transformed into red-brown iron oxides (Fig. 8B, C and G). Overall, the products of the supergene processes in the oxidized zone include iron oxides and hydroxides, copper carbonates, and argillic minerals, such as kaolinite.

GEOCHEMISTRY OF ORE MINERALIZATION

In the central area of the porphyry system at the Sar-e-Yazd deposit, significant insights into the geochemical characteristics of the ore have been obtained through detailed studies. These investigations primarily rely on sampling from exploratory boreholes, which provide essential lithogeochemical data. In the study area, a total of 26 exploratory boreholes were drilled by Zarandishan Yazd Company, utilizing geological, alteration, and surface lithogeochemical data to evaluate the region's mineral potential (Fig. 11A). The drilling of these bore-

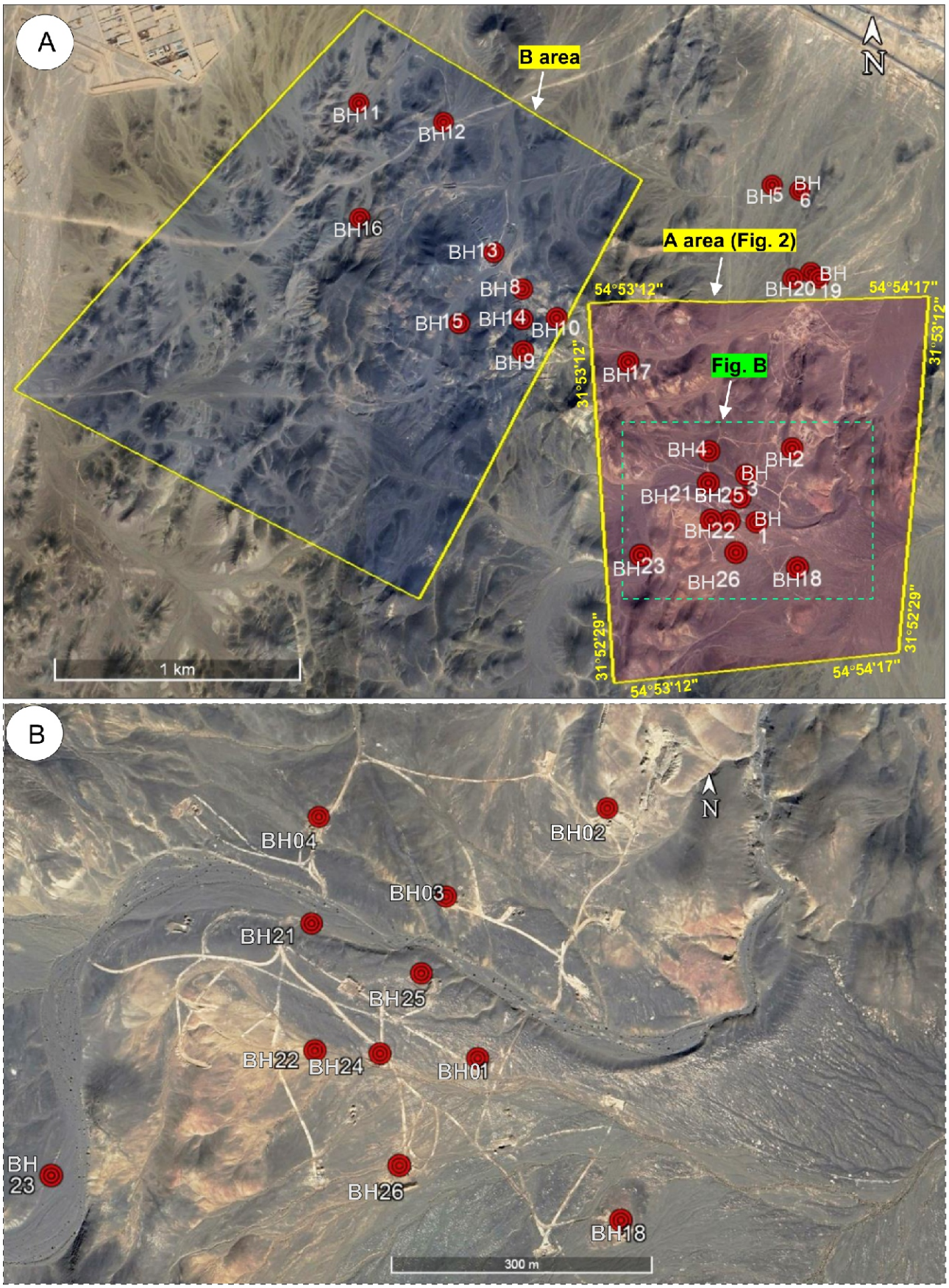

Fig. 11. Location of exploratory boreholes in the Sar-e-Yazd deposit

A – A area marked in red (as shown in Fig. 2), this area highlights the exploratory boreholes and B area marked in blue, this area also contains exploratory boreholes; **B** – close-up view focuses on the exploratory boreholes in the centre of the porphyry system within the A area

holes plays a critical role in understanding subsurface conditions and identifying valuable resources. It is noteworthy that the boreholes do not follow a regular drilling network; instead, they were drilled randomly and irregularly in locations where the likelihood of encountering mineralization was higher. Specifically, in the central area of the porphyry system (referred to as area A), 10 boreholes have been drilled (Fig. 11B). From these boreholes, only the geochemical data related to boreholes numbered BH_{01}, BH_{02}, BH_{03}, BH_{04}, BH_{05}, BH_{08}, BH_{09}, BH_{10}, BH_{13}, BH_{14}, BH_{18}, BH^{23}, and 8 samples from borehole BH_{26} are available, with one representative lithogeochemical sample taken per meter in each borehole. Geochemical analyses of boreholes BH_{01}, BH_{03}, BH_{04}, BH_{18}, BH_{23}, and 8 samples from borehole BH_{26} at depths of 701 to 708 m, which are located precisely in the central part of the deposit and have the highest signs of mineralization, were therefore examined in this study (Fig. 11B). These analyses were conducted using Inductively Coupled Plasma Optical Emission Spectroscopy (ICP-OES) by the Iranian Mining and Mineral Industries Development and Renovation Organization (IMIDRO). These analyses focused on elements such as copper, molybdenum, lead, zinc, and silver, as well as minor and some rare elements (Table 2). Detailed logging of exploratory borehole number 26, located at the center of the Sar-e-Yazd porphyry system, has provided valuable insights into alteration zoning and mineralogical characteristics. The findings from the borehole studies reveal that mineralization follows a zoned pattern, becoming progressively distinct with increasing depth. Along with leaching-oxidized zones, supergene enrichment and hypogene mineralization, the grade of metallic elements shows variations (Table 2). Subsequently, each metallic element is analysed and discussed in detail. Finally, the ore zoning from the surface to depth is thoroughly examined. A detailed account of the geochemical characteristics and grade variations of key elements, including copper, molybdenum, lead, zinc, and silver, within the exploratory boreholes is presented. This analysis is based on the chemical data from 6 drill cores from holes around the dacite porphyry to porphyritic quartzdiorite intrusive (BH_{01}, BH_{03}, BH_{04}, BH_{23}) and BH_{18} and BH_{26}, located on top of this intrusive body in the central part of the Sar-e-Yazd porphyry deposit. This area is locally under the oxide leached zone and is enriched in Cu, Mo, Pb, Zn, and Ag (Table 2). The highest metal concentrations at BH_{01} (a depth of 32 to 42 m) is 1620 ppm Cu and 1.9 ppm Ag at depth of 32 m, 74 ppm Mo at the depth of 33 m, 3017 ppm Pb and 6501 ppm Zn at the depth of 34 m, BH_{03} (3168 ppm Cu and 3416 ppm Pb at 49 m depth, BH_{04} (a depth of 55 to 58 m) is 4142 ppm Cu, 43.7 ppm Mo, >3% Pb and 2.6 ppm Ag at depth of 56 m, BH_{18} (a depth of 01 to 201 m) is 106 ppm Cu, 1.6 ppm Mo, 27ppm Pb and 0.4 ppm Ag, BH_{26} drilling core on top of the intrusive body show the highest metal concentrations in the hypogene mineralization zone at depth of 701 to 708m, 18962 ppm Cu, 29393 ppm Pb, >3% Zn and 58 ppm Ag at the depth of 705 m and 29.6 ppm Mo at the depth of 706 m and BH_{23}, 6597 ppm Cu, 13.4 ppm Mo, 17127 ppm Pb, >3% Zn and 15.7 ppm Ag at the depth of 25 m. The enrichment of base and precious metals within the Sar-e-Yazd porphyry system is strongly linked to hydrothermal alteration processes and the spatial distribution of metallic minerals formed through both supergene and hypogene mineralization. On the near surface (in the enriched supergene sulphide zones), the highest grades of Ag, Cu, Mo, Pb and Zn are mainly associated with the intense sericitic alteration and oxidized D-type veins on the northeastern side of the dacite porphyry to porphyritic quartzdiorite at Sar-e-Yazd. Strong anomalies of certain metals in zone BH_{26} highlight their notable presence in hypogene mineralization associated with porphyritic granodiorite stocks at depths of 701–708 m. Finally, based on the chemical analyses of 6 drill cores samples taken meter by meter (Table 3), the central area of the Sar-e-Yazd porphyry deposit is locally weakly enriched in Cu (avg: 529 ppm), Mo (avg: 8 ppm), Pb (avg: 926 ppm), Zn (avg: 698 ppm), and Ag (avg: 2.3 ppm).

STATISTICAL ANALYSIS OF CORRELATION COEFFICIENTS IN THE SAR-E-YAZD DEPOSIT

The data in Table 4 presents the correlation coefficients of the main metallic ores, calculated from the average values of all samples collected from each exploratory borehole. The results indicate a moderate positive correlation between copper and molybdenum, a characteristic feature of porphyry copper-molybdenum deposits. Additionally, copper exhibits a strong positive correlation with lead, zinc, and silver, which are known as trace and indicator elements in such systems. These elements also show strong positive correlations with one another, aligning with the expected geochemical associations in porphyry copper-molybdenum deposits. To further investigate element behaviour across different mineralization zones, samples from two closely spaced boreholes (BH_{01} and BH_{26}) in the centre of the Sar-e-Yazd porphyry system were analysed (Table 3). This analysis focused on the leached- oxidized, enriched sulphide (supergene), and hypogene mineralization zones, as well as their relationship with depth. A total of 135 samples were examined from borehole BH_{01}, covering depths from 1 to 35 m, corresponding to the leached-oxidized zone (1–31 m) and the enriched sulphide zone (32–35 m). Additionally, eight samples were analysed from borehole BH_{26} (701–708 m) for the hypogene zone. The results of the correlation analysis in these mineralization zones will be discussed in detail in the following sections.

OXIDE-LEACHING ZONE

The lowest copper grade in the oxide-leaching zone is a critical metric for evaluating the feasibility of mining operations in copper-rich regions. According to the data presented in Table 4, the average copper grade in this zone is ~190 ppm. This lower copper grade, compared to the hypogene zone, reflects the dissolution and downward mobility of copper into the lower part of the deposit (enriched zone). Notably, the correlation coefficient between copper and lead, as well as iron, in this zone is negative. With molybdenum, it should be at least negative to neutral, but it shows a very weak positive correlation, indicating the different geochemical behaviour of copper with these elements, especially lead and iron (Table 4). This is because, in this zone, anions with large ionic radii like molybdenum are immobile, and lead and iron exhibit the same behaviour. In contrast, copper and zinc are mobile and dissolve in this zone, so they should have at least a slight positive correlation, but they do not show a specific pattern and have a neutral correlation. In this zone, the relationships between molybdenum and other elements are characterized by varying correlation coefficients. Specifically, molybdenum exhibits a positive correlation coefficient with lead, indicating that higher concentrations of molybdenum tend to coincide with increased lead concentrations. This suggests a potentially linked presence or shared source for these two elements within the zone. In contrast, the correlation between molybdenum and iron is neutral, signifying the absence of a significant linear relationship; changes in molybdenum concentrations do not consistently correspond with variations in iron levels. Finally, the correlation between molybdenum and zinc is slightly positive, reflecting a weak tendency for zinc concentrations to increase alongside molybdenum, though

Table 2

Trace elements contents of analysed samples from central part of Sar-e-Yazd porphyry deposit

	Element	Cu (ppm)	Mo (ppm)	Pb (ppm)	Zn (ppm)	Ag (ppm)
	Detection limit	1	0.5	1	1	0.1
From 1 to 31 m of the leached-oxidized section BH_{01}	BH01-001	112	11.7	33	157	0.32
	BH01-002	166	9.4	113	305	0.45
	BH01-003	77	11.5	53	137	0.36
	BH01-004	293	13	273	778	0.26
	BH01-005	105	4.9	127	280	0.61
	BH01-006	130	29.1	202	218	0.81
	BH01-007	163	9.6	45	277	0.48
	BH01-008	176	3.9	75	221	0.44
	BH01-009	131	6.1	116	180	0.36
	BH01-010	201	25.7	47	136	0.34
	BH01-011	202	41.2	217	581	0.54
	BH01-012	263	12.4	32	183	0.45
	BH01-013	258	85.9	39	181	0.56
	BH01-014	262	61.8	126	253	0.79
	BH01-015	234	20.3	36	174	0.66
	BH01-016	352	11.8	27	155	0.44
	BH01-017		5.1	19	98	0.35
	BH01-018	131	25.1	56	183	0.39
	BH01-019	273	26	32	173	0.37
	BH01-020	224	29	108	289	0.47
	BH01-021	119	12.6	108	318	0.38
	BH01-022	160	34.9	207	664	0.61
	BH01-023	234	16	65	261	0.4
	BH01-024	223	19.8	75	260	0.55
	BH01-025	105	37.1	145	415	0.46
	BH01-026	112	22.2	65	179	0.36
	BH01-027	54	26.3	41	242	0.37
	BH01-028	84	9.4	79	299	0.32
	BH01-029	153	16.4	34	166	0.33
	BH01-030	417	22	64	133	0.61
	BH01-031	380	38.2	48	186	0.48
From 32 to 35 m of the supergene section of BH_{01}	BH01-032	1620	40	214	480	1.9
	BH01-033	500	74	83	183	0.48
	BH01-034	652	38.9	3017	6501	1.7
	BH01-035	104	71.6	704	1136	0.45
From 701 to 708 m of the hypogene section of BH_{26}	BH26-701	1567	24.7	>3%	2437	47
	BH26-702	29	1.01	345	418	0.32
	BH26-703	29	1.74	349	475	0.35
	BH26-704	18962	5.8	29393	>3%	58.2
	BH26-705	155	8.6	5242	3936	0.44
	BH26-706	263	29.6	3865	3426	0.36
	BH26-707	109	1.7	3170	4633	0.45
	BH26-708	3958	19.7	>3%	11296	20.6

Table 3

Trace elements contents of analysed samples from central part of Sar-e-Yazd porphyry deposit (Total average for each BH)

Element	Depth (m)	Cu (ppm)	Mo (ppm)	Pb (ppm)	Zn (ppm)	Ag (ppm)
Detection limit		1	0.5	1	1	0.1
BH01	001–135	220.58	19.36	130.66	319.54	0.44
BH03	001–086	154.51	4.63	100.34	282.15	0.43
BH03	001–140	142.49	6.66	68.96	152.41	0.50
BH04	001–061	372.20	14.45	22.18	56.77	0.39
BH04	001–190	269.62	13.01	37.67	125.34	0.39
BH18	001–071	36.23	1.15	27.30	38.03	0.38
BH18	072–201	177.53	2.06	28.31	108.30	0.43
BH23	001–076	261.21	4.52	971.26	1397.72	1.55
BH26	701–708	3134.00	11.61	7060.67	3803.00	15.97

Table 4

The correlation coefficients of elements using the Pearson method, based on the logarithm of lithogeochemical data in the centre of the Sar-e-Yazd porphyry system

		Ag	Cu	Mo	Fe	Pb	Zn
All exploratory borehole in the centre of the Sar-e-Yazd porphyry system (708 samples)	Ag	–					
	Cu	.95	–				
	Mo	.24	.28	–			
	Fe	.50	.66	.28	–		
	Pb	.95	.84	.25	.34	–	
	Zn	.91	.80	.24	.36	.96	–
Leached-oxidized zone (depth 1 to 31 m) of exploratory borehole BH_{01} in the centre of the Sar-e-Yazd porphyry system (31 samples)	Ag	–					
	Cu	.25	–				
	Mo	.46	.27	–			
	Fe	–.11	–.02	–.10	–		
	Pb	.27	–.05	.12	.23	–	
	Zn	.03	–.01	.10	.18	.85	–
Secondarily enriched zone (depth 31 to 35 m) of exploratory borehole BH_{01} in the centre of the Sar-e-Yazd porphyry system (5 samples)	Ag	–					
	Cu	.81	–				
	Mo	–.99	–.72	–			
	Fe	.85	.99	–.77	–		
	Pb	.42	–.17	–.54	–.09	–	
	Zn	.45	–.12	–.57	–.05	.99	–
Hypogene zone (depth 701 to 708 m) of exploratory borehole BH_{26} in the centre of the Sar-e-Yazd porphyry system (8 samples)	Ag	–					
	Cu	.78	–				
	Mo	.23	–.10	–			
	Fe	.10	.02	.63	–		
	Pb	.89	.62	.42	.19	–	
	Zn	.72	.97	–.07	.06	.63	–

this relationship is not strong enough to be considered definitive. In this zone, the correlation coefficient of lead with zinc is expected to be slightly negative to neutral; however, it is observed to be positive. Lead also shows a moderately positive correlation with iron (0.23). Similarly, zinc exhibits a moderately positive correlation with iron (0.18). The correlation coefficient between molybdenum and silver in the oxide-leaching zone is strongly positive (0.46). In the hypogene and supergene zones, lead and zinc demonstrate a moderately to strongly positive correlation (0.63). However, in the oxide-leaching zone, their correlation is anticipated to be at least slightly negative, but it is instead positive-possibly due to the very weak weathering processes affecting the deposit. Overall, in the oxide-leaching zone, which overlaps with the argillic alteration zone, the correlation between indicative elements such as copper and molybdenum decreases, while the correlation of elements typical of porphyry deposits, including lead, zinc, and silver, becomes more prominent. Based on the results obtained from this zone, the degree of weathering in the Sar-e-Yazd porphyry system appears to be minimal. This conclusion is supported by the observation that the underlying enriched zone is poorly developed, indicating a lack of significant weathering processes. The limited extent of weathering is further evidenced by the detection of only ~4 m of higher anomaly compared to the oxide-leaching zone, suggesting minimal alteration of the parent material.

SUPERGENE ZONE

The study of copper mineralization reveals significant variations in copper grades across different zones within the Sar-e-Yazd porphyry system. Notably, the secondary enriched sulphide zone displays a pronounced contrast in copper concentrations, with an average copper grade of 0.07%. In comparison, the hypogene zone, characterized by lower levels of secondary enrichment, exhibits the highest average copper grade of 0.31% (Table 4). Although 0.07% represents a very low sulphide enrichment, the higher copper grade in this zone compared to the leached-oxide zone (0.019%) suggests partial secondary sulphide enrichment and confirms the formation of secondary sulphide minerals, such as covellite and bornite. In this zone, molybdenum has an average grade of 56 ppm. Due to the limited data available for both the enriched and hypogene zones, it is not possible to determine the exact molybdenum grade. However, the secondary enriched zone demonstrates a higher molybdenum grade compared to the hypogene zone, which has an average grade of 11 ppm. The average grades of lead, zinc, and iron in this zone are 1000 ppm, 2000 ppm, and 3.4%, respectively.

In the secondary enriched sulphide zone, the correlation coefficient between copper and molybdenum, lead, and zinc is negative, while it is positive with iron. The correlation coefficient between copper and lead is weakly negative, which is not unexpected, as lead is immobile in the leached-oxide zone due to its geochemical behaviour. Therefore, the weakly negative correlation between copper and lead in the secondary enriched sulphide zone may reflect the relatively minor impact of weathering processes on the geochemical separation of these elements. Additionally, the correlation coefficients between molybdenum and lead, molybdenum and zinc, and molybdenum and iron are negative. A strongly positive correlation (0.99) is observed between lead and zinc, while the correlation of lead with iron is very weakly negative (–0.09; Table 4). Similarly, the correlation between zinc and iron is very weakly negative (–0.05). Interestingly, the correlation between molybdenum and silver in the secondary enriched sulphide zone is strongly negative (–0.99), in contrast to the positive correlation observed in the leached-oxide zone.

HYPOGENE ZONE

In the hypogene zone, the average grades of various metals exhibit notable values: copper averages 0.3%, molybdenum is found at 11.6 ppm, while lead, zinc, and iron show grades of >1.2%, >0.7%, and 4.4%, respectively. In this zone, copper has a positive correlation with lead, zinc, and silver, likely due to their association under reducing conditions. There is a weak negative correlation between copper and molybdenum. The correlation coefficient of molybdenum with lead is moderately positive, with zinc is very weakly negative, and with iron is positive. The strong positive correlation between molybdenum and iron is significant and can be explained by the association of molybdenite and magnetite in this area. In the hypogene zone, the correlation coefficient between lead and zinc is moderately positive (0.63), indicating that these two metals are likely found in minerals that formed simultaneously (McLemore et al., 1999). The correlation coefficients of iron with lead and zinc are weakly positive (Table 4).

Cu/Mo RATIO IN EACH OF THE ABOVE SECTIONS

The copper-to-molybdenum (Cu/Mo) ratio is a critical geochemical indicator in geology, used to distinguish between various mineralization zones within ore deposits. Variations in the Cu/Mo ratio reflect the processes and conditions under which mineralization occurred, as these two metals often coexist but may be distributed differently throughout a deposit. In porphyry copper deposits, higher Cu/Mo ratios typically signify proximity to the porphyry source, while lower ratios may indicate a more distal position in the system, where molybdenum becomes relatively concentrated. In the Sar-e-Yazd porphyry system, the Cu/Mo ratio shows a marked decline from the deeper hypogene zones to the shallower leached-oxide zones (Table 5). In the hypogene environment, characterized by high-temperature hydrothermal processes, copper and molybdenum are co-mingled in mineralization, resulting in relatively high Cu/Mo ratios. As geological processes progress toward the surface, a transition occurs to the leached-oxide zones, where weathering and oxidation processes significantly alter the mineral composition. This alteration typically leads to the depletion of molybdenum relative to copper, thereby lowering the Cu/Mo ratio.

ZONING OF METALIC ELEMENTS IN THE AREA

Copper serves as the primary ore-forming element in the central region of the Sar-e-Yazd porphyry system. This significant mineralization predominantly occurs in the form of chalcopyrite and bornite, which are economically valuable copper minerals. Additionally, copper is present in peripheral veins, where it occurs as malachite, azurite, and turquoise, further enriching the diversity of copper-bearing minerals within the geological system. To evaluate the distribution and concentration of copper deposits in the surveyed area, the statistical param of copper have been calculated separately for each of the exploratory boreholes. Lithogeochemical analysis of 708 samples collected from four exploratory boreholes in the central porphyry deposit provides valuable insights into the copper content of the region. The data reveal that the minimum copper concentration is <10 ppm, indicating low-grade mineralization. The average copper concentration ranges between 10 and 500 ppm, reflecting a moderate level of copper distribution in the analysed samples. Notably, the maximum copper content reaches up to 2%, highlighting localized areas of higher mineralization that may hold economic potential. A comparison of the variations in copper grades across four key exploratory boreholes shows that the average copper grades in boreholes BH_{01}, BH_{18}, and BH_{23} are 220 ppm, 127 ppm, and 261 ppm, respectively. Meanwhile, eight samples from borehole BH_{26}, at depths of 701 to 708 m, yield an average copper grade of 3134 ppm (0.3%; Table 3). The highest copper grades observed in boreholes 18 and 23 at various depths reveal significant geological features related to mineralization processes. At shallow depths of ~40–50 m, these anomalies are associated with porphyritic quartzdiorite rocks exhibiting argillic and phyllic alteration. They coincide with the boundary between the leached oxide zone and the supergene enrichment zone. At greater depths, around 700 m, the anomalies correspond to the hypogene zone, characterized by potassic alteration within the granodiorite intrusive. The geochemical variations in copper grade, similar to the boreholes in the centre of the porphyry system, were also conducted for all exploratory boreholes in the region from surface to depth and were used for the trace element distribution map across the entire area (Fig. 12A). Considering the averages obtained from the exploratory boreholes, if the economic cut-off grade for a porphyry deposit is considered to be around 0.4%, the high-grade copper mineralization in the centre of the Ser-e-Yazd porphyry system (especially borehole 26 at a depth of 701–708 m) with an average value of ~0.3% for 8 samples (with only one sample having a grade of 2%) indicates that mineralization in the Ser-e-Yazd deposit is non-economic and is classified as an enriched copper deposit. In some of the drilled boreholes (BH14) in the mesothermal veins on the north-west margin of the porphyry system, copper grades near the surface (depths of 10 to 15 m) averaged 0.78%, but again, these high-grade ores occurred in thin and limited thicknesses below the oxide zone.

Molybdenum is identified as an accessory element in the copper mineralization of the Sar-e-Yazd area. While molybdenum plays a crucial role in the geochemical processes associated with copper mineralization, it is rarely observed in its distinct form, molybdenite, during microscopic analysis of collected samples. The statistical param of molybdenum were calculated individually for each exploratory borehole in the central region of the porphyry system. These calculations provide valuable insights into the distribution and concentration of molybdenum, which serves as a significant indicator of mineralization within the geological framework. The results of these assessments are systematically detailed in Table 3. Based on lithogeochemical data from 708 samples from four exploratory boreholes in the centre of the porphyry system, the minimum, average, and maximum molybdenum values are <1, 1–2, and 74 ppm, respectively. The analysis of molybdenum grades across four exploratory boreholes – BH_{01}, BH_{18}, BH_{23}, and eight samples from borehole BH_{26} reveals significant variations in their average concentrations. The grades obtained from these boreholes highlight differing levels of mineralization, with recorded values of 19, 1.7, 4.5, and 11 ppm, respectively, as summarized in Table 3. Borehole 01 shows the highest molybdenum grades at various depths compared to other boreholes, and in borehole 26, at a depth of 701 to 708 m, molybdenum occurs at its highest level. These anomalies observed in borehole 1 (BH_{01}), in terms of lithology and alteration at shallow to moderate depths

Table 5

The Cu/ Mo ratio in each of the mineralization sections (leached-oxide, secondary enriched and hypogene) as an average from each of the zones of exploratory borehole BH_{01}

	ΣCu (ppm)	ΣMo (ppm)	ΣCu/ΣMo
Oxide-leaching zone	190.8	22.5	8.46
Supergene zone	719	56	12.8
Hypogene zone	3134	11.6	270

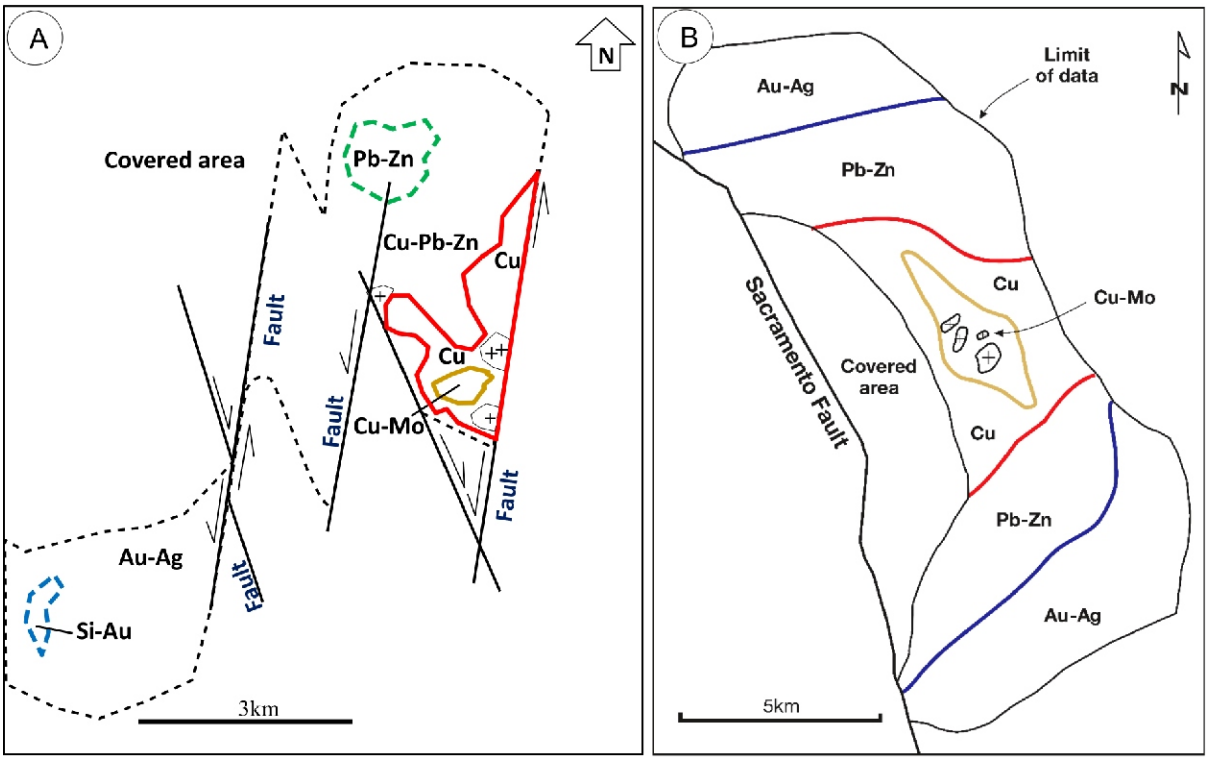

Fig. 12. Similarity of metal zoning in the Sar-e-Yazd deposit with other porphyry deposits: A – Sar-e-Yazd deposit area (based on the geological structures identified in Fig. 4) and B – the Mineral Park copper-molybdenum deposit in Arizona (after Lang and Eastoe, 1988)

(~5–100 m), are associated with porphyritic quartzdiorite rock exhibiting argillic and phyllic alteration. These features largely correspond to the leached oxide zone and supergene enrichment. In contrast, borehole BH_{26}, situated within the hypogene mineralization zone characterized by potassic alteration of the granodiorite intrusive, reveals significant geological findings, particularly regarding molybdenum and copper concentrations. The analysis indicates that borehole BH_{26} contains higher grades of these minerals compared to other boreholes in the vicinity. The geochemical variations in molybdenum grade, similar to the boreholes in the centre of the porphyry system, were also conducted for all exploratory boreholes in the region from surface to depth and were used for the trace element distribution map across the entire area (Fig. 12A). The molybdenum grade in global porphyry copper deposits varies in the range of 50 to 300 grams per ton, with an average of 175 grams per ton (Sillitoe, 2010). Additionally, in the veins on the edge of the porphyry system, according to Harati (2016), the molybdenum grade reaches 29 grams per ton. Therefore, considering the averages obtained from the exploratory boreholes, as well as the molybdenum grade in the mesothermal veins on the edge of the system, molybdenum mineralization in the Ser-e-Yazd porphyry deposit is very weak and minimal.

Silver serves as an important byproduct in porphyry copper deposits. The statistical analysis of silver concentrations in the Sar-e-Yazd area, derived from exploratory boreholes, provides valuable insights into the spatial distribution of this element within the porphyry structure. The data indicate that silver grades in the central region of the porphyry system are relatively low, with averages ranging from 0.4 to 4 ppm. However, in the peripheral mesothermal veins associated with borehole BH_{13}, the grade of this element shows a relatively higher concentration. Analysis of the borehole reveals that the highest recorded grade occurs at a depth of 11 m, where the concentration reaches 88 ppm. Additionally, in the peripheral veins of the porphyry system, as reported by Harati (2016), the silver grade is observed to reach 14 grams per ton. In the mesothermal veins on the periphery of the porphyry system, the *lead* and zinc grades are so high that they are being mined and extracted as galena and sphalerite, along with secondary carbonate minerals of lead and zinc. According to Harati (2016), the lead grade in the peripheral veins of the porphyry system reaches >3%. However, in the centre of the porphyry system, the average total grade of this element is ~500 ppm, with only two samples having the highest lead grades at depths of 701 and 708 m in borehole number 26, containing more than 3 percent lead (Table 3). The average concentration of *zinc* across all lithogeochemical section samples is notably low, resembling the distribution pattern of lead in the core of the porphyry system. The overall average grade of zinc is ~500 ppm. However, the highest recorded concentrations, exceeding 3%, are found at a depth of 25 m in borehole 23 and at a depth of 704 m in borehole 26 (Table 3). In contrast, similar to lead, the veins located on the periphery of the porphyry system exhibit higher zinc grades. As reported by Harati (2016), the average zinc grade in these peripheral veins reaches up to 1.5%, which is significantly higher than the average grade in the system's core. In the Sar-e-Yazd region, the spatial distribution of lead and zinc displays a zoning pattern consistent with the typical characteristics observed in porphyry deposits worldwide. The highest amount of *arsenie* in the lithogeochemical section is related to exploratory borehole number 05, which is located on the periphery of the porphyry system (Fig. 12). Many samples from this borehole exhibit arsenic concentrations exceeding 100 ppm, although the overall average arsenic concentration is 33 ppm. Among all boreholes, the highest average arsenic grades are observed in boreholes 01, 02, and 05, as well as at a depth of 700 m in borehole 26. Overall, the data suggests that arsenic

concentrations increase progressively from the centre of the porphyry system toward its periphery and with greater depth from the surface. Based on Sillitoe (2010), well-developed metal zoning is observed in porphyry copper deposits from the centre of the system outward. Overall, metal zoning in these porphyry systems shows that from the centre outward, the Cu ± Mo ± Au zone is categorized in the central cores of the system along with potassic, chlorite-sericite, and sericitic alterations. This central zone usually has kilometre-scale halos of Zn, Pb, and Ag anomalies, reflecting low-temperature hydrothermal fluid conditions. In some systems, the outermost part of the halo is distinctly enriched in Mn (±Ag), as seen in the Butte deposit (Meyer et al., 1967). Zn-Pb-Ag ± Mn halos typically have spatial coincidence with propylitic alteration zones but are invariably best characterized in distal skarn environments (e.g., Meinert, 1987; Meinert et al., 2005). Veins cutting through propylitic halos may be rich in Au, and in the Mineral Park deposit in Arizona, an outer zone of Pb-Zn and Au- Ag is observed (Eidel et al., 1968; Lang and Eastoe, 1988). Despite this, in some porphyry copper deposits, these metal halos, especially Zn, occur as late-stage veins overlapping with the copper- dominant core, as seen in the Chuquicamata deposit (Ossandón et al., 2001).

Exploratory borehole analyses conducted at the centre of the Sar-e-Yazd porphyry system have identified significant copper anomalies alongside minor occurrences of molybdenum, consistent with the characteristics of other porphyry systems. An analysis of all exploratory borehole samples, as presented in Table 3, indicates that the average copper content in the studied samples is relatively low compared to porphyry deposits within the Naein-Jiroft magmatic belt and the Kerman copper porphyry belt. However, the concentrations of arsenic (18.5 grams per ton), antimony (1.9 grams per ton), and lead (497 grams per ton) are comparatively high. Notably, arsenic and lead are recognized as supergene elements in porphyry copper deposits (Gergorian, 2003).

The distribution of copper and molybdenum in the central region of the Sar-e-Yazd porphyry system and its peripheral boreholes has been thoroughly studied to better understand the mineral composition of this area. Borehole data reveals significant variations in the concentrations of these elements, extending from surface levels to depths of up to 780 m. The distribution patterns for these elements were mapped for all sampled boreholes, similar to those located in the central part of the system. Furthermore, the concentrations of other key metal elements were analysed, and the average grade of each element was calculated for each exploratory borehole.

The results indicate that the spatial distribution of metal elements in the studied area follows a zoning pattern consistent with those observed in porphyry deposits worldwide. Individual zoning maps were prepared for each examined element in the deposit (Fig. 12). Based on the distribution and zoning of the primary metal ores, the porphyry mineralization at Sar-e-Yazd shows a remarkable similarity to the copper-molybdenum mineralization observed in the Mineral Park deposit in Arizona.

COMPARISON OF SAR-E-YAZD DEPOSIT WITH PCD DEPOSITS

Comprehensive studies and examinations of the Sar-e-Yazd porphyry Cu (Mo) mineralization, incorporating field investigations, geological surveys of the mining area, mineralization-controlling structures, alteration processes, petrography, mineralogy, geochemistry, and fluid inclusion analyses, facilitated a comparison between the Sar-e-Yazd deposit and various types of mineralization and deposits both within Iran and globally. Based on geological and ore-related characteristics, the porphyry mineralization features of Sar-e-Yazd were compared with prominent porphyry copper deposits in Iran, including the Sungun porphyry Cu (Mo) deposit (Arasbaran zone, northwestern Iran), the Dalli porphyry Cu-Au deposit (Saveh-Naein magmatic belt), the Sarcheshmeh porphyry Cu-Mo (Au) deposit, the Sara or Perkam deposit (Naein-Jiroft magmatic belt or Kerman copper belt), and the Takht-e-Gonbad porphyry Cu-Mo deposit (Kerman copper belt; Table. 6). The Sar-e-Yazd Cu (Mo) deposit demonstrates several geological and mineralogical characteristics that closely align with those of the renowned Sungun and Sarcheshmeh copper deposits. However, the Sar-e-Yazd deposit shares the highest degree of similarity with the Takht-e-Gonbad and Dalli porphyry copper deposits, particularly with respect to their geological settings and mineral compositions.

FLUID INCLUSION STUDY

A comprehensive fluid inclusion study was conducted to classify various inclusions based on their origins and the phases present at room temperature. This analysis focused on quartz-chalcopyrite veins and hydrothermal quartz grains associated with phyllic (sericitic) alteration, which is linked to porphyry mineralization. Samples of veins intersecting altered porphyritic quartzdiorite were collected from several drill cores, including BH_{08}, BH_{18}, BH_{24}, BH_{25} and BH_{26}. Detailed descriptions of the samples and corresponding measurements are provided in Table 3. Most measured inclusions were primary, following the criteria of Roedder (1979; 1984) and Shepherd et al. (1985). Sometimes in the moderate depth of deposit, quartz in the veins and sericite alteration is mainly equigranular, anhedral, and it possesses a polygonal shape. The contacts among quartz grains form triple junctions with angles at 120° (Fig. 13A). This implies that the quartz maybe recrystallized so that the fluid inclusion migrated to grain boundaries (Tarantola et al., 2012). As a result, the fluid inclusions in sample 2 from Sar-e-Yazd were sparse however this sample contained usable inclusions. These fluid inclusions were clustered together (Fig. 13B) and were considered to be primary. The fluid inclusions that occur in planes along healed fractures (Fig. 13C) are considered to be secondary and possibly reflect fluid circulation associated with a late stage of fluid entrapment. The inclusions vary in size, generally between 5 and 25 μm, and sizes of 25–100 μm are rarely observed. They occur in ovoid, rounded, spindle, and irregular shapes, as wells as negative crystal forms. On the basis of phase ratios observed at room temperature and phase transition during homogenization, five types of fluid inclusions are present in the early-stage veins and the phyllic alteration of the host rock: one-phase liquid only (L) or two-phase liquid-rich aqueous (L+V, V < 50%; Type 1; F1; Fig. 13D and E), multiphase halite- bearing fluids (L+V+H; L+V+Op; L+V+H+Op; Type 2; F2; Fig. 13F and H), two-phase vapour-rich aqueous (V+L, L < 10%; Type 3; F3; Fig. 13I and K), and one- phase vapour only (V; Type 4; F4; Fig. 13K) inclusions. The Sar-e-Yazd porphyry system does not exhibit any inclusions containing visible liquid carbon dioxide (CO_2), indicating a distinct geochemical environment during their formation. Detailed analyses confirmed that none of the inclusions fulfilled the criteria for containing liquid CO_2, and clathrate formation was not observed during freezing experiments (Type 5; F5; Fig. 13L). Halite crystals were identified by their colourless, isotropic cubic morphology (Fig. 13F, H and K). The opaque phases (Fig. 13G and H) were found to be either cubic or triangular in shape, likely representing pyrite or chalcopyrite, respectively, as well as he-

Table 6

Comparison of the characteristics of the Sar-e-Yazd deposit with porphyry copper deposits in Iran [Sungun, Sarcheshmeh, Sara (Perkam), Dalli and Takht-e-Gonbad]

Deposit name	Sungun	Dali	Sarcheshmeh	Takht-e Gonbad	Sara (Perkam)	Sar-e-Yazd
Tectonic setting	Continental Margin	Continental Margin	Continental Margin	Island Arc	Continental Margin	Island Arc
Intrusive body	Quartz Diorite, Granodiorite, Granite	Granodiorite, Basaltic Dike	Granodiorite	Porphyritic Granodiorite	Diorite, Quartzdiorite	Porphyritic Granodiorite to Quartzdiorite, Diabase Dike
Mineralization type	Monzonitic	Monzonitic	Monzonitic	–	–	Monzonitic
Alteration zoning differentiation	Distinct	Distinct	Distinct	Indistinct and Overlapping	Distinct	Indistinct and Overlapping
Stockwork texture	Common	Common	Common	Common		Common
Breccia texture	Common	Common	Common	Rare	Present	Rare
Disseminated texture	Common	Common	Common	Common	Common	Common
Endogenous ore	Pyrite, Chalcopyrite, Molybdenite	Chalcopyrite, Bornite, Magnetite, Pure Gold	Chalcopyrite, Pyrite, Bornite, Magnetite	Pyrite, Chalcopyrite, Magnetite, Molybdenite, Bornite	Pyrite, Chalcopyrite, Magnetite	Chalcopyrite, Pyrite, Bornite, Magnetite
Enriched zone ore	Hematite, Malachite	Malachite, Azurite, Cuprite, Hematite, Digenite	Chalcocite, Covellite, Digenite	Chalcocite, Covellite, Neotocite	Covellite, Bornite	Malachite, Azurite, Hematite, Turquoise
Copper grade	0.76%	0.50%	0.69%	0.56%	0.16%	>0.3%
Molybdenum grade	0.01%	–	0.03%	80 ppm	0.00%	1.9%
Salinity of ore-forming fluid (equivalent to NaCl)	69%	75%	61.90%	55–68%	–	4–64%
Homogenization temperature of ore-forming fluid (isotopic temperature results)	100–620°C	140–620°C	520.2°C	340–600°C	263–441°C	130–542°C
References	Asghari and Hezarkhani (2008)	Daneshjou et al. (2016)	Shahabpour and Doorandish (2008)	Hosseini et al. (2017)	Mohammadilaghab et al. (2011)	Taghipour and Dorani (2013)

matite. The F1 and F3 type inclusions underwent homogenization through the disappearance of vapor and liquid, respectively, while the F2 type inclusions homogenized through the dissolution of solid phases (halite) and the disappearance of vapor. The F2 inclusions are characterized by high salinity and high Th values; the F3 inclusions display low salinity but high Th values; and the F1 inclusions exhibit both low Th and low salinity values (Fig. 14).

FLUID INCLUSION MICROTHERMOMETRY

The microthermometric data obtained from 136 fluid inclusions in quartz associated with phyllic alteration and quartz-ore-bearing veins in the Sar-e-Yazd porphyry system provide critical insights into the thermal and compositional characteristics of the fluid systems involved in the mineralization process. These measurements, summarized in Table 7, detail the homogenization temperatures and salinities of the fluid inclusions. The heating and freezing method was employed to determine the homogenization temperatures.

The homogenization temperatures of the studied fluid inclusions fall into three distinct ranges: low to medium temperatures (130–280°C), medium temperatures (280–480°C), and high to very high temperatures (480–550°C; Fig. 14). The highest average homogenization temperature was observed in three-phase fluid inclusions containing daughter halite ± opaque minerals. These inclusions frequently homogenized through the disappearance of the vapour phase into the liquid phase (Table 7). In some samples, salt solved into liquid phase. Halite solution temperature is higher than homogenization temperature and indicates entrapment in higher pressure (Bodnar, 1994). In general, the minimum salinity is recorded at 4 wt.% NaCl with a maximum of 62 wt.% NaCl equivalent, and the homogenization temperature ranges between 136 and 542°C (Fig. 14).

An average homogenization temperature and salinity range for fluid inclusions are as follows: ~346°C and ~14 wt.% NaCl equivalent for type 1 (F1) ~353°C and ~47 wt.% NaCl equivalent for type 2 (F2) and ~410°C and ~12.5 wt.% NaCl equivalent for type 3 (F3; Table 7). Two-phase fluid inclusions rich in liquid (F1) and two-phase fluid inclusions rich in vapour (F3), the most common (85 inclusions of L+V types and 25 inclusions of V+L type). The homogenization temperatures for liquid and vapour phases (L+V) range from 136 to 490°C, whereas the homogenization temperatures for vapour and liquid phases (V+L) range from 320 to 541 °C. The frequency of homogenization temperatures in three-phase fluid inclusions, specifically those classified as F2 (comprising liquid, vapour, and either hydrocarbon or another liquid phase) and F5 (comprising two liquid phases and a vapour phase), predominantly indicates a trend toward homogenization into the liquid phase. The maximum temperatures were in the ranges of 280 to 369°C, 327 to 370°C, and 456 to 542°C, respectively. The homogenization temperature

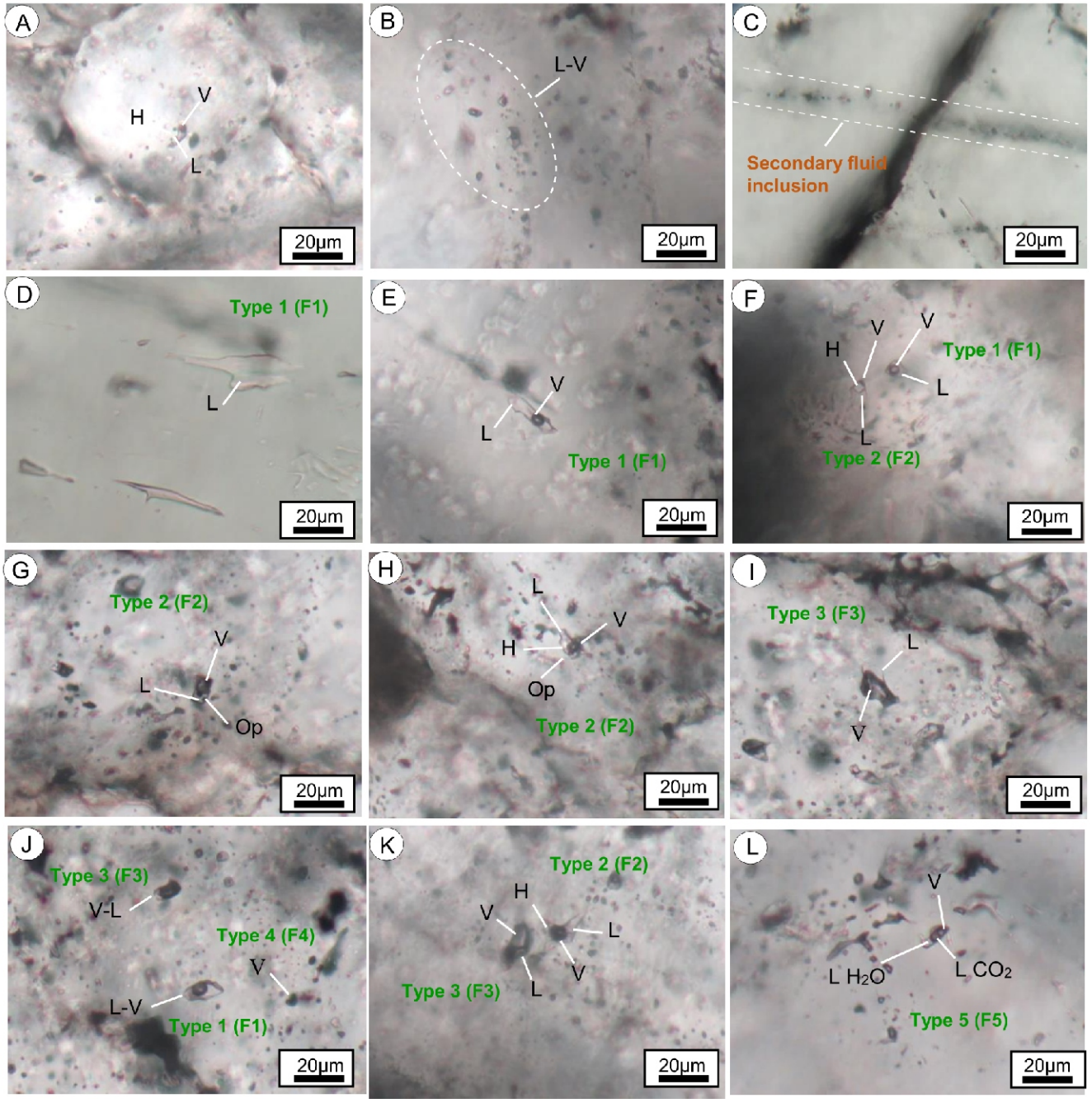

Fig. 13. Photomicrographs of fluid inclusions in quartz-chalcopyrite veins from the Sar-e-Yazd deposit

A – equigranular quartz grains in association with the ore minerals, forming triple junctions with angles of 120°; **B** – a cluster of primary two-phase liquid-vapour fluid inclusions; **C** – vapour-only secondary inclusions in planes along healed fractures; **D** – type 1 fluid inclusions in hydrothermal quartz grains in the sericitic alteration; **E** – type 1 two phase liquid-vapour fluid inclusions; **F** – type 2 three phase liquid-vapour-halite fluid inclusions; **G** – type 2 three phase liquid-vapour-opaque (possibly chalcopyrite or pyrite) fluid inclusions; **H** – type 2 multiphase fluid inclusions containing liquid, vapour, halite and opaque minerals; **I** – type 3 vapour-rich inclusions; **J** – type 1 and 3 inclusions with type 4 inclusion; **K** – typical fluid inclusion assemblage in porphyry-style mineralization showing co-existing type 2 and 3 inclusions and **L** – type 5 fluid inclusions contain two phase liquid LH_2O and LCO_2. FI – fluid inclusion, L – liquid, V – vapour; H – halite, Op – opaque

of fluid inclusions containing halite ± opaque phases was generally recorded at 365°C, occurring prior to the dissolution of halite. In deeper samples (e.g., BH_{24}), halite daughter minerals were identifiable, and opaque daughter minerals, particularly hematite, were observed with higher frequency. The rare occurrence of halite daughter minerals in other examined fluid inclusions may suggest low sodium (Na) and chloride (Cl) content in the magmatic hydrothermal fluids that evolved within the mineralizing system. The salinity and homogenization temperature results for each sample are illustrated in Figure 14.

Additionally, eutectic ice-melting temperatures (Te) for all type 1 inclusions were recorded below –21.1°C (Fig. 14). This indicates that NaCl is not the dominant salt species in these inclusions, and other salts, such as $CaCl_2$, $MgCl_2$, or KCl, may be present in the solution (Shepherd et al., 1985). The eutectic temperatures of type 3 inclusions were found to be similar to those of type 1 inclusions, suggesting a potential similarity in their thermal properties and phase behaviours.

Table 7

Microthermometric data of the fluid inclusions wall rock quartz- sericite alteration and quartz- ore bearing veins from Sar-e-Yazd

Sample no.	Borehole/ depth (m)	Alteration assemblage/host rock	FI type	FI * phases	n	Th (°C)	Tm (ice) (°C)	Salinity (wt.% NaCl equiv*)
SYZ-1	BH_{08}/50.40	Ore-bearing quartz crystals veins	F2	(L-V-H→L)	(n=3)	323.66	–	43
			F3	(V-L→V)	(n=5)	410.20	–9.38	12.78
			F1	(L-V→L)	(n=16)	398.12	–11.36	17.85
SYZ-2	BH_{18}/283.30	Phyllic/porphyritic quartzdiorite	F2	(L-V-H→L)	(n=4)	368.75	–	45.95
			F3	(V-L→V)	(n=4)	364.25	–12.07	14.95
			F1	(L-V→L)	(n=17)	368.75	–9.39	19.79
SYZ-3	BH_{24}/639.50	Phyllic/porphyritic quartzdiorite	F2	(L-V-H→L)	(n=2)	338	–	48.00
			F2	(L-V-H-Op)	(n=2)	366	–	49.40
			F2	(L-V-Op)	(n=2)	514	–12.70	15.46
			F3	(V-L→V)	(n=5)	502.20	–10.22	13.36
			F1	(L-V→L)	(n=14)	347.71	–9.71	14.33
SYZ-4	BH_{24}/701.70	Ore-bearing quartz crystals veins	F2	(L-V-H→L)	(n=3)	337	–	47.93
			F2	(L-V-Op)	(n=2)	464	–11.8	14.71
			F3	(V-L→V)	(n=3)	418.33	–8.23	11.42
			F1	(L-V→L)	(n=11)	380.81	–7.57	10.72
SYZ-5	BH_{25}/49.25	Quartz veins; phyllic/porphyritic quartzdiorite	F1	(L-V→L)	(n=1)	225	–5.29	8.61
SYZ-6	BH_{25}/172.80	Ore-bearing quartz crystals veins	F1	(L-L-V)	(n=4)	350.25	–	2.30
			F3	(V-L→V)	(n=4)	410.75	–10	12.97
			F1	(L-V→L)	(n=11)	396	–8.57	11.71
SYZ-7	BH_{26}/429.50	Phyllic/porphyritic quartzdiorite	F2	(L-V-H→L)	(n=4)	399.75	–	50
			F3	(V-L→V)	(n=4)	403.50	–7.85	10.85
			F1	(L-V→L)	(n=10)	359	–8.9	9.72

DISCUSSION

GEOTECTONIC SETTING AND MAGMA EMPLACEMENT

The Sar-e-Yazd Cu (Mo) deposit represents a significant geological site, where mineralization processes are strongly associated with the Oligocene porphyritic granodiorite intrusion into Eocene volcanoclastic units. This geological relationship highlights the critical role of the thermal and chemical conditions provided by the granodiorite in the mobilization and deposition of Cu and Mo minerals (Harati and Moayyed, 2020). Mineralization occurs both in quartz-sulphide stockwork and as disseminations within the hydrothermally altered volcanoclastic rocks and porphyritic intrusions. These intrusions exhibit variable alteration types, including potassic, sericite, chlorite, and epidote alterations. The ore mineralogy, as well as the textures and structures of the ores at the Sar-e-Yazd deposit, bear similarities to those reported in other porphyry copper deposits (PCDs) within the NJB or KB regions, as documented by Shahabpour (1982), Hassanzadeh (1993) and Alirezaei and Hassanpour (2011). Studies show that porphyry mineralization is related to the subduction of the Arabian plate under the Iranian plate and occurred in the back-arc setting (Hassanzadeh, 1993; Shahabpour, 2005, 2007; Hezarkhani, 2006). The magmatic complex at Sar-e-Yazd was emplaced during this post-subduction tectonic extension During the Oligocene, several deep to shallow late subvolcanic stocks, plugs, and dikes, which vary from intermediate to felsic in composition, intruded the volcanic and volcanoclastic rocks in the Sar-e-Yazd area (Harati and Moayyed, 2020). The Sar-e-Yazd porphyritic granodiorite has been dated to the Oligocene (Harati and Moayyed, 2020), rendering it significantly older than similar formations reported from the northern Kerman belt (KB). This age notably contrasts with that of the world-class Sarcheshmeh and

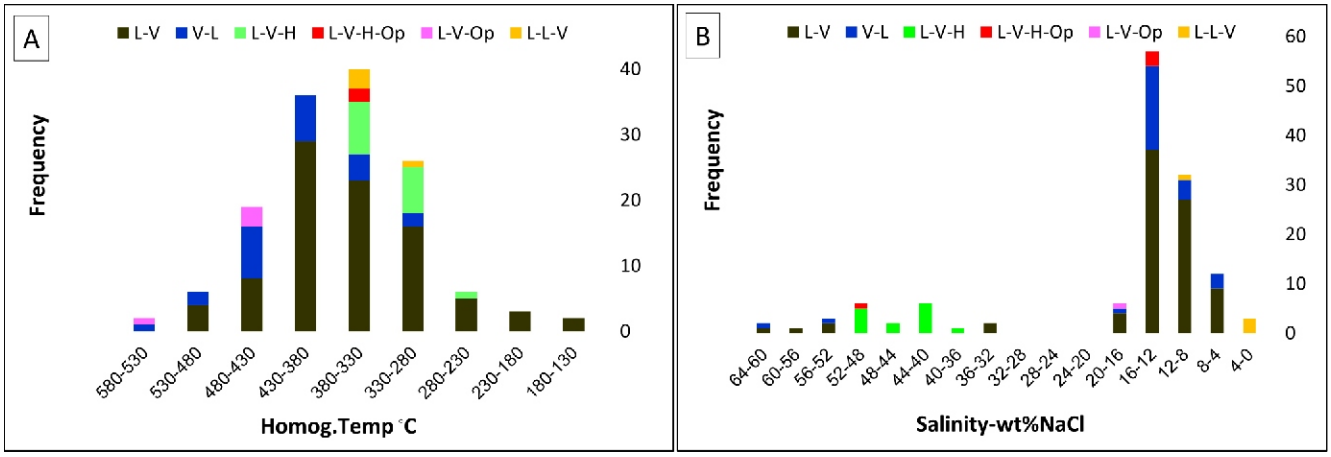

Fig. 14A – homogenization temperature *versus* frequency in samples from the study area; B – salinity diagram *versus* frequency in samples from the study area

Miduk deposits, which have been dated to the mid to late Miocene (16–9 Ma) according to various studies (Ghorashizadeh, 1978; Shahabpour, 1982; Hassanzadeh, 1993; McInnes et al., 2005; Taghipour et al., 2008). Similar late Oligocene age is recently reported for the Bondar-e-Hanza porphyry in the southern section of the KB (Mohebi, 2015) and Takht-e-Gonbad copper deposit (Hosseini et al., 2017). The Sar-e-Yazd deposit, along with two other deposits, is located toward the southern margin of the Kerman belt (KB) and suggests a discrete episode of copper mineralization, likely occurring prior to the collision (pre-collisional). The Jebal Barez-type granitoids in the KB, within the southern section of the NJMB arc (Dimitrijevic, 1973), are generally considered to date from the early-middle Oligocene to the middle Miocene (e.g., Conrad et al., 1977; Hassanzadeh, 1993; Chiu et al., 2013). The Takht-e-Baneh batholith, extending from the north to the south of the Takht-e-Gonbad deposit and exhibiting characteristics of Jebal Barez-type granitoids, has yielded a zircon U-Pb age of 25.0 ±0.7 Ma. This result aligns with previously proposed ages for these granitoids (e.g., Dimitrijevic, 1973; Conrad et al., 1977; Hassanzadeh, 1993; Chiu et al., 2013). Similar to findings from the Takht-e-Gonbad deposit, this study highlights a confirmed potential for porphyry copper deposits contemporaneous with the so-called barren Jebal Barez-type granitoids.

STRUCTURAL CONTROL ON MINERALIZATION

Deformations related to high tectonic forces in the crust are characterized by shearing processes (Ramsay and Huber, 1987; Brown and Solar, 1998; Peacock et al., 2002; Montest and Hirth, 2003; Wang and Ludman, 2004; Brogi, 2006). Identification of structural factors related to cutting (especially faults) and their relationship with intrusive, in the areas affected by magmatic activities, is of great interest in the identification and discovery of mineral deposits. In general, the meeting point of main faults can be a suitable place for magma infiltration and mineralization (Forster, 1978). The Sar-e-Yazd porphyry Cu (Mo) deposit is significantly influenced by the regional structural framework. Geological studies reveal that the emplacement of mineralization within the deposit is closely associated with a network of faults, primarily trending in NNW, NNE, WNW, and N–S orientations. These structural features are critical as they provide pathways for hydrothermal fluids, facilitating the formation of porphyry-style mineralization by localizing magmatic-hydrothermal fluid circulation (Fig. 3, inset map).

In general, the connection between magmatic activity, ore-forming processes, and dykes with the regional structural setting can be understood through three main stages:

The first stage of tension is characterized by a compressional system involving large-scale folding and the formation of middle Eocene fractures. This system is comparable to the regional structures observed in porphyry copper deposits northeast of Shahr-e-Babak (Dimitrijevic, 1973; Ebadi et al., 2011) and in the Mehriz region (north-west of the Sar-e-Yazd area), where the Sani Abad syncline developed during this phase.

During this stage, dacite porphyry to porphyritic quartzdiorite intrusions, as well as the first group of diabasic dykes, were emplaced into longitudinal fractures resulting from folding. These dykes, extending in a WNW direction, are linked to the older T_2 fractures within the shear system described by Storti et al. (2006). In contrast, a second group of later diabasic dykes, which commonly intruded in a north-south orientation, is attributed to tensile fractures associated with the T_1 shear system. These dykes and faults were subsequently displaced by younger northeast-southwest trending faults.

In ***the second stage,*** as with dykes, the pattern of hydrothermal veins is directly influenced by regional tension and exhibits two main trends: (1) tension splits related to T_1 (north-south) and tensile fractures, which play a crucial role in the late-stage mineralization system, and (2) the pennant vein pattern associated with R/R' diagonal fractures. Fractures trending NNW (R), which are predominantly filled with iron oxides, are relatively younger and do not play a significant role in mineralization. In contrast, fractures associated with the (R') shear system appear to have been instrumental in the emplacement of porphyritic granodiorite within the region. This observation aligns with Saric's (1973) theory regarding the emplacement of porphyry intrusives. Overall, the anti-Riedel (R') fractures, in conjunction with the fractures formed during the first stage, provided a conducive framework for the intrusion and alteration of igneous rocks, as well as the development of porphyry-style mineralization.

In ***the third stage,*** with the change in the tension regime and the development of shear stress, fractures formed in an approxymately north-south direction (Azimuth of 20 ; aligned with the T_1 fractures). These fractures created pathways for the migration of hydrothermal fluids (remnants of porphyry copper-producing fluids) and magma, resulting in the formation of polymetallic veins (the first group of veins) and dykes (the second group of dykes). The mineralization at Sar-e-Yazd is primarily hosted in dacite porphyry to porphyritic quartzdiorite but is genetically related to porphyritic granodiorite. This granodiorite intruded the older dacite porphyry to porphyritic quartzdiorite and the tuffs of the volcanoclastic unit. The microgranular and porphyritic textures, as well as the elongated shape of the ore-related dacite porphyry to porphyritic quartzdiorite, are attributed to rapid magma ascent and subsequent crystallization at shallow depths in an extensional tectonic regime. Melfos et al. (2002) described a similar mechanism for the origin of microgranite porphyry associated with the Maronia Cu-Mo deposit, NE Greece. The presence of the microdiorite xenolith fragments in the porphyritic granodiorite at Sar-e-Yazd, suggest that porphyritic granodiorite intruded the porphyritic quartzdiorite (Harati and Moayyed, 2020).

PHYSICOCHEMICAL PARAM OF THE HYDROTHERMAL FLUIDS

The fluid inclusion systematics at the Sar-e-Yazd deposit is comparable to those reported from several other PCDs in the Kerman belt (KB; Etminan, 1978; Hezarkhani, 2009), and elsewhere (Bodnar et al., 2014; Hosseini et al., 2017).

The results of fluid inclusion analyses from the study area were plotted on a diagram comparing homogenization temperatures and salinities typical of porphyry, skarn, and epithermal deposits (Fig. 15A). The diagram reveals that the final homogenization temperatures and salinities of the fluid inclusions fall within the range characteristic of porphyry deposits (Wilkinson, 2011). Moreover, the fluid inclusions in quartz veins at Sar-e-Yazd suggest that quartz and associated metallic mineralization formed as a result of phase separation from an initial high-temperature (>540°C), moderate-salinity supercritical magmatic fluid (Fig. 15B). This process occurred under boiling conditions during the ascent and cooling of the fluids. The rapid decrease in temperature and pressure promoted fluid immiscibility in these veins, leading to the formation of a saline brine (40–62 wt% NaCl equiv; F2) alongside a coexisting low-salinity (7.5–15 wt% NaCl equiv; F3), vapour-rich fluid. These phases were stable under lithostatic pressures and homogenized over a temperature range predominantly between 300 and 542°C. This evidence, combined with the presence of vapour-type sin-

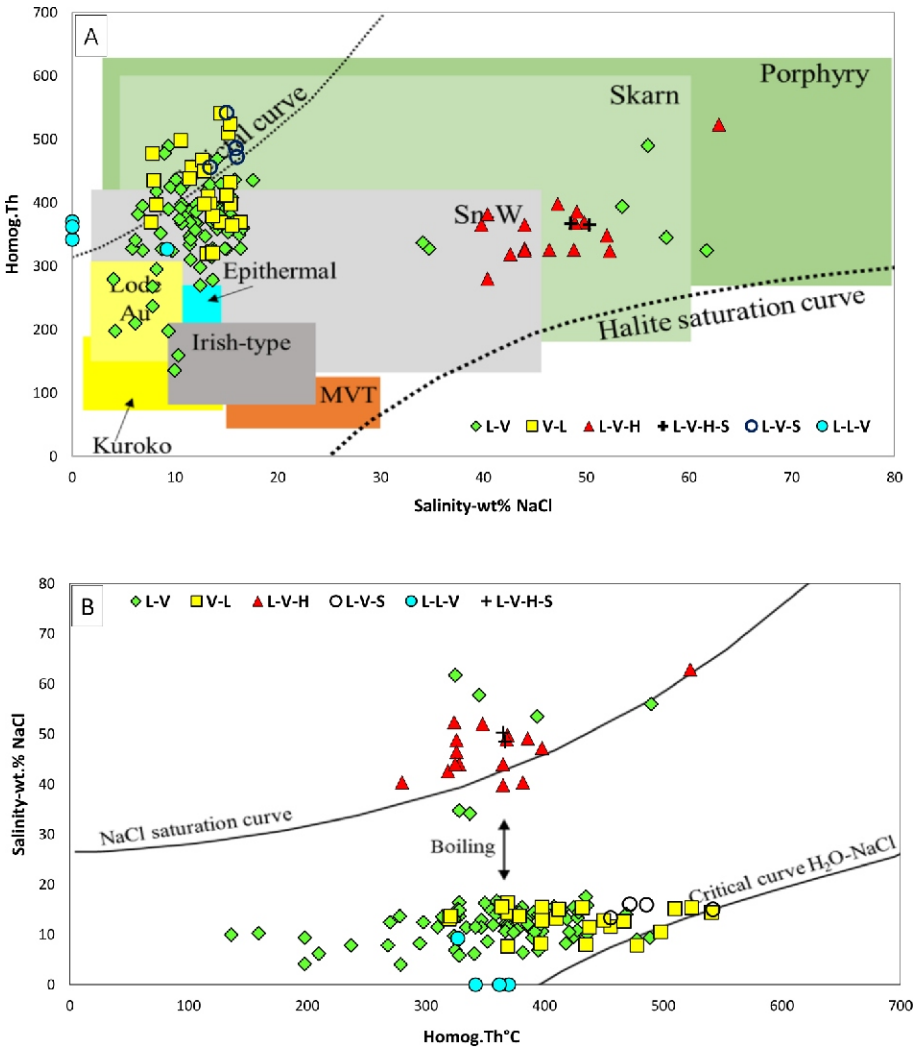

Fig. 15A – salinity *versus* final homogenization temperature of fluid inclusions in the Sar-e-Yazd deposit within the range of common fluid inclusions of the ore deposits (based on Wilkinson, 2011); B – salinity *versus* homogenization temperature plot of the fluid inclusions from the Sar-e-Yazd deposit

gle-phase fluid inclusions (F4), supports the occurrence of boiling in the ore-forming fluids (Ronacher et al., 2000; Moncada et al., 2017). Consequently, at the Sar-e-Yazd deposit, the boundaries of potassic-sericitic alteration are inferred to be associated with fluid boiling (Fig. 15B). A portion of the copper content within the solution may have been deposited as chalcopyrite due to boiling processes. Chalcopyrite, the dominant mineral at the Sar-e-Yazd deposit, formed through mechanisms analogous to those observed in porphyry copper deposits. Evidence suggests that boiling played a significant role in the mineralization process, indicating a spatial-temporal relationship between fluid boiling and deposit formation (Samson et al., 2003). The simultaneous occurrence of V, V-L, and L-V type fluid inclusions within quartz veins supports the hypothesis that mineralization at the Sar-e-Yazd deposit likely resulted from a boiling fluid. Microthermometric analyses of V-L type fluid inclusions from the Sar-e-Yazd field reveal homogenization temperature ranges for samples 1, 3, 4, 6, and 7 as 320 to 467°C, 321 to 398°C, 379 to 478°C, 364 to 450°C, and 369 to 435°C, respectively. These temperatures are consistent with those observed for L-V type fluid inclusions, which range from 328 to 489°C, 324 to 425°C, 319 to 472°C, 326 to 478°C, and 278 to 415°C. This alignment of temperature ranges confirms the occurrence of fluid boiling during the formation of mineralized quartz veins at the Sar-e-Yazd deposit. In general, F2-type fluid inclusions are considered to best represent the characteristics of mineralizing hydrothermal fluids. V-L (F3-type) inclusions are interpreted as products of boiling, while the L-V and V-L (F1 and F3 types) inclusions can be attributed to fluid mixing processes. This mixing likely occurred between high-salinity magmatic fluids (F2) and low-salinity meteoric water. Such fluid mixing is a well-documented phenomenon in porphyry copper deposit (PCD) systems, as these systems typically develop in shallow environments (<6 km; e.g., Carten, 1986; Valencia et al., 2008; Sillitoe, 2010). The physico-chemical characteristics of fluids, responsible for copper mineralization at Sar-e-Yazd, are comparable to those in PCDs worldwide, as reported by Bodnar et al., (2014). New physico-chemical conditions, changes in pH and temperature transitioning lithostatic to hydrostatic conditions, associated with boiling led to quartz and sulphide deposition (Bodnar et al., 2014). Abundant stockwork and silica veins in the area, associated with chalcopyrite, magnetite, molybdenite, quartz, and pyrite as both dissemination and vein-type occurrences, provide strong evidence of mineralization. Fluid boil-

ing can lead to extensive hydraulic fracturing of the wall rocks, facilitating the mixing of ascending boiling magmatic fluids with meteoric water at the ductile-to-brittle transition under hydrostatic pressures (Zhong et al., 2014). The lower-temperature (225–398°C) and lower-salinity (8–19 wt.% NaCl equivalent) type 1 liquid- rich fluid inclusions in the hydrothermal quartz of porphyritic quartzdiorite at Sar-e-Yazd (Fig. 13) likely represent a late-stage fluid associated with decompression under hydrostatic pressures. This decompression, caused by extensive hydrofracturing, generated fractures that are closely linked to the metallic mineralization at Sar-e-Yazd. These fractures are associated with sericitic alteration.

The presence of hydrothermal shears and ore-rich shear veins in the Sar-e-Yazd deposit, combined with evidence of a boiling event, indicates the involvement of compatible fluids. Shearing is typically indicative of decreasing pressure, which can trigger boiling in hydrothermal systems (Jobson et al., 1994; Jebrak, 1997). The ore veins in the Sar-e-Yazd deposit exhibit sharp boundaries with their host units, suggesting that the veins were formed by fluid filling spaces under hydrostatic pressure (Liu et al., 2014; Ouyang et al., 2014). This process ultimately contributed to the development of hydrothermal fractures.

INTRUSION ALTERATION AND MINERALIZATION

The emplacement of multiple phases of late Oligocene porphyritic granodiorite intrusions is intricately linked to the influx of mineralized hydrothermal fluids, which played a crucial role in the deposition of ore at Sar-e-Yazd. These intrusions were emplaced as structurally localized, overlapping pre-, syn-, and post-mineralization dykes, as well as tabular to upwardly tapering wedge-shaped bodies. The earliest magmatic pulse comprised a set of porphyritic dykes, known as mineralized dykes (Harati and Moayyed, 2020). These dykes were juxtaposed against younger and larger mineralized granodiorite bodies due to intra-mineral faulting at Sar-e-Yazd (Figs. 3 and 4). Mineralization at Sar-e-Yazd is associated with multiple, telescoped stages of intrusion and alteration. The alteration is dominated by an extensive phyllic assemblage, accompanied by irregular zones of propylitic and minor potassic assemblages at depth. However, no consistent patterns in alteration assemblages and silicate zoning, as observed in most porphyry copper deposits (PCDs) in the NJMB or KB (e.g., Shahabpour, 1982; Alirezaei and Hassanpour, 2011) and other regions (e.g., Lowell and Guilbert, 1970; Cannell et al., 2005; Sillitoe, 2010), can be discerned at Sar-e-Yazd. This can be attributed to repeated magma intrusions and the superposition or overprinting of alteration assemblages, along with the branching and dyke-like nature of the porphyritic intrusion at shallow depths. Potassic alteration, as reported from many other PCDs in the NJMB or KB (e.g., Waterman and Hamilton, 1975; Shahabpour, 1982; Alirezaei and Mohammadzadeh, 2009) and elsewhere (e.g., Lowell and Guilbert, 1970; Sillitoe, 2010) might also be present at Sar-e-Yazd. This alteration is characterized by the presence of quartz, hydrothermal biotite, K-feldspar, magnetite, chalcopyrite, molybdenite, and pyrite. This might be due to an extensive phyllic overprint that masks earlier potassic assemblages. Such pervasive phyllic alteration and the near-total destruction of earlier potassic assemblages have been reported in Seridun, Iju, and Kader (Alirezaei and Hassanpour, 2011) within the NJMB or KB, as well as in other locations (Richards et al., 1999; Ossandón et al., 2001). Phyllic alteration is characterized by abundant sericite and quartz, along with subordinate amounts of chlorite, pyrite, and chalcopyrite. Sericitic alteration is characterized by the nearly complete replacement of magmatic K-feldspar, clinopyroxene, hornblende, and biotite, as well as the extensive presence of sericite and quartz in the groundmass. Kaolinite constitutes a minor phase. Propylitic alteration, characterized by varying amounts of chlorite, calcite, epidote, and actinolite, is widespread in the dacite porphyry to porphyritic quartz diorite and volcanoclastic rocks, occurring peripherally to the ore zone. Trace amounts of pyrite and chalcopyrite within the propylitic alteration zone indicate a slight increase in the sulphur fugacity of the hydrothermal fluids and/or an elevation in fluid temperature (Hemley et al., 1992). Carbonate alteration, a subtype of propylitic alteration enriched in sulphides, is predominantly characterized by calcite. It is locally observed as scattered patches of calcite + pyrite ± quartz ± chalcopyrite, as well as sulphide- bearing calcite veinlets, occurring both in the porphyritic granodiorite bodies and the surrounding volcaniclastic rocks. Argillic alteration is extensively developed at shallower depths, transitioning into phyllic alteration zones. Sericitic alteration overprints earlier potassic and propylitic alteration. The magmatic fluid activity responsible for forming these alteration zones during the late stages of the porphyry system was predominantly controlled by a major N-S trending fault at Sar-e-Yazd. Researchers have explored various sources for the fluids involved in phyllic alteration within porphyry copper deposits (PCDs). Evidence points to the involvement of external fluid influx into the magmatic-hydrothermal system during the late stages of sericite and clay formation (e.g., Sheets et al., 1996; Taylor, 1997; Cooke et al., 2011). However, other workers have demonstrated a magmatic origin for late-stage sericite and illite alteration in PCDs (e.g., Kusakabe et al., 1984,1990; Hedenquist et al., 1998; Watanabe and Hedenquist, 2001; Harris and Golding, 2002; Calagary, 2003). According to Cooke et al. (2014), a magmatic-hydrothermal origin for late-stage phyllic alteration aligns with the substantial copper (Cu) endowment observed in veins associated with this alteration stage. Conversely, a meteoric origin may be applicable to other deposits where phyllic-stage veins are barren or only weakly mineralized. At Sar-e-Yazd, the weakly mineralized nature of phyllic-stage veins and their limited association with mineralization provide evidence that supports the involvement of an external fluid source in late-stage sericite and clay formation. The presence of kaolinite, along with smaller quantities of montmorillonite and iron oxides/hydroxides, suggests a supergene origin for this alteration (cf. John, 2010; Taylor, 2011). Supergene argillic alteration is a widespread characteristic and has been documented in numerous porphyry copper deposits (PCDs) within the KB, as reported by Tangestani and Moore, (2001, 2002), Ranjbar et al., (2004), Alirezaei and Hassanpour, (2011).

ORIGIN OF THE SAR-E-YAZD Cu (Mo) DEPOSIT

The Nain-Jiroft Magmatic Belt (NJMB), also referred to as the Kerman Cenozoic Magmatic Arc (KCMA), constitutes the southern segment of the Southern Nain-Jiroft Magmatic Belt (SNJMB). This region is predominantly composed of calc-alkaline volcanic and plutonic rocks (Zarasvandi et al., 2007). The KCMA hosts several deposits ranging from world-class to moderate- and small-scale, including Sarcheshmeh, Meiduk, Chahfiruzeh, Keder and Reagan (Shafiei et al., 2009; Asadi et al., 2014). As highlighted by Zarasvandi et al. (2005), Taghipour et al. (2008), Shafiei et al. (2009), Hou et al. (2011), Richards et al. (2012) and Asadi et al. (2014), the continental collision stage during the Miocene was the primary driver behind the formation of numerous porphyry copper deposits (PCDs) within the KCMA. According to Shafiei et al. (2009) and Asadi et al. (2014), the majority of economic and sub-economic porphyry

intrusions in the NJMB or KCMA are associated with mid-late Miocene-Pliocene post-subduction and/or collisional stages, such as the Chahfiruzeh and Keder porphyry systems (Zarasvandi et al., 2019). In contrast, Eocene-Oligocene intrusions are predominantly associated with subduction and/or pre-collisional processes. Notable examples include the late Oligocene Bondar-e-Hanza and Takht-e-Gonbad intrusions (Mohebi, 2015; Hosseini et al., 2017), as well as the Reagan and Daralou copper porphyry deposits (Zarasvandi et al., 2019). The Sar-e-Yazd Cu (Mo) deposit, as previously noted, is situated within the NJMB, also referred to as the KCMA belt. The prevalence of calc-alkaline volcano-plutonic rocks in this belt (Aghanabati, 2005) enhances the likelihood of porphyry-style mineralization in the Sar-e-Yazd area. Mineralization at Sar-e-Yazd is associated with Oligocene porphyritic granodiorite intrusions that cut through Eocene volcaniclastic units (Harati and Moayyed, 2020). Ore mineralization is observed in quartz-sulphide stockwork and disseminations within hydrothermally altered volcaniclastic rocks and porphyritic intrusions. These mineralized zones exhibit varying degrees of potassic, sericitic, chloritic, and epidotic alterations. The ore mineralogy and textural/structural characteristics at the Sar-e-Yazd deposit are comparable to those reported in numerous porphyry copper deposits (PCDs) within the NJMB or KB, as documented by Shahabpour (1982), Hassanzadeh (1993) and Alirezaei and Hassanpour (2011). Studies show that porphyry mineralization is related to the subduction of the Arabian plate under the Iranian plate and occurred in the back-arc setting (Hassanzadeh, 1993; Shahabpour, 2005, 2007; Hezarkhani, 2006). The magmatic complex at Sar-e-Yazd was emplaced during this post-subduction tectonic extension during the Oligocene, several deep to shallow late subvolcanic stocks, plugs, and dikes, which vary from intermediate to felsic in composition, intruded the volcanic and volcanoclastic rocks in the Sar-e-Yazd area (Harati and Moayyed, 2020). The Oligocene age of the main Sar-e-Yazd porphyritic granodiorite (Harati and Moayyed, 2020) is notably older than the ages reported for porphyry deposits in the northern KB, such as the world-class Sarcheshmeh and Miduk deposits (16–9 Ma, mid to late Miocene; Ghorashizadeh, 1978; Shahabpour, 1982; Hassanzadeh, 1993; McInnes et al., 2005; Taghipour et al., 2008). A comparable late Oligocene age has been recently identified for the Bondar-e-Hanza porphyry in the southern KB (Mohebi, 2015) and the Takht-e-Gonbad copper deposit (Hosseini et al., 2017). The Sar-e-Yazd deposit, along with Bondar-e-Hanza and Takht-e-Gonbad, is situated near the southern margin of the KB, indicating a distinct episode of copper mineralization, likely predating the continental collision (pre-collisional). At Sar-e-Yazd, the ore-forming magma concentrated at the intersection of major regional structural features in the upper crust, at depths exceeding 3 km. Here, it crystallized to form stocks, plugs, and dikes with compositions ranging from intermediate to felsic (refer to Fig. 3, inset map). The major and minor structural features provided a vertically extensive dilatant network, which favored the evolution of the magmatic-hydrothermal porphyry system at Sar-e-Yazd (Fig. 4A). Based on the findings of Zarasvandi et al. (2019), we conducted a comparative analysis of the silicate chemistry (plagioclase, biotite, and amphibole) in Miocene collisional porphyries (e.g., Chahfiruzeh and Keder) and Eocene-Oligocene pre-collisional porphyry systems (e.g., Reagan and Daralou) within the KCMA. Pre-collisional porphyry systems, which exhibit the lowest degree of copper (Cu) mineralization, also demonstrate the lowest An% and Al* values compared to their collisional counterparts. Plagioclase chemistry suggests that the magmatic systems in collisional deposits are relatively closed, with lower rates of magmatic mixing compared to pre-collisional deposits. Biotite chemistry indicates a progressive decrease in temperature from Keder to Reagan, Daralou, and Chahfiruzeh. The absence of a consistent temperature gradient in pre-collisional porphyry systems may contribute to their lower-grade mineralization. High biotite halogen fugacity ratios (fH_2O/fHF and $fH_2O/fHCl$ >1) reflect the water-rich nature of the studied porphyry systems. Additionally, the relative enrichment in fluorine (F) in collisional porphyry deposits (e.g., Keder) appears to correlate with magnesium (Mg) enrichment in these systems. Pre-collisional porphyry systems, characterized by low Cu mineralization, display distinctive features such as the lowest An% and Al* values, higher rates of magmatic mixing, and depletion in both F and Mg compared to collisional porphyries. These attributes are evident in the Sar-e-Yazd pre-collisional porphyry systems, which share similarities with the Reagan and Daralou deposits.

CONCLUSIONS

1. Mineralization at the Sar-e-Yazd copper (molybdenum) deposit occurred in relation to porphyritic granodiorite bodies within a pre-collision back-arc setting during the Oligomiocene. This age is considerably older than those reported for porphyry copper deposits in the northern Kerman Belt, including the world-class Sarcheshmeh and Meiduk deposits.

2. Unlike most porphyry copper deposits in the Kerman Belt and other regions, where economic ore is primarily associated with potassic alteration and the potassic-phyllic boundary, the majority of copper mineralization at Sar-e-Yazd is linked to supergene processes under argillic kaolinite alteration. A smaller proportion of mineralization is associated with potassic alteration and the potassic-phyllic boundary at depth in borehole BH_{26} (701–708 m).

3. Analysis of average samples from each exploratory borehole reveals a positive, moderate correlation between copper and molybdenum, suggesting the presence of porphyry copper-molybdenum deposits at Sar-e-Yazd. Furthermore, copper exhibits strong positive correlations with lead, zinc, and silver, which are recognized as trace and indicator elements of such deposits.

4. In contrast to earlier perspectives, geochronological data indicate the potential existence of a porphyry copper deposit coeval with the so-called barren Jebal Barez-type granitoids in the Kerman Belt or Naein-Jiroft Magmatic Belt.

5. Three major fault groups trending E–W, NW–SE, and NE-SW define the regional structural framework. These faults controlled the emplacement of intrusions, late-stage dykes, and mineralized veins within the crystalline basement of the volcanic-volcanoclastic unit.

6. Potassic alteration is associated with an ore assemblage comprising pyrite + chalcopyrite + bornite + molybdenite + magnetite, primarily occurring in M- and A-type veins. Propylitic alteration corresponds to an assemblage of pyrite + chalcopyrite, while late sericitic alteration is linked to pyrite + chalcopyrite in D-type veins. The assemblage sphalerite + galena + specularite + pyrite is associated with a subsequent epithermal overprinting event.

7. Metallic mineralization, particularly abundant in boreholes BH_{01}, BH_{03}, BH_{04} and BH_{23}, is attributed to secondary supergene processes. The total average of the highest metallic mineralization is significantly enriched (3881 ppm Cu, 43.7 ppm Mo, 13,390 ppm Pb, 18,250 ppm Zn, 6.7 ppm Ag) in the 25–58 m depth interval.

8. The coexistence of vapour-rich inclusions (F3 type) with high salinity and liquid-rich inclusions (F2 type) of similar homogenization temperatures provides compelling evidence for boiling. The physicochemical characteristics of fluids responsible for copper mineralization at Sar-e-Yazd are comparable to those reported for porphyry copper deposits (PCDs) worldwide (Bodnar et al., 2014).

9. The distribution and zoning of the principal metal ores at Sar-e-Yazd exhibit a strong resemblance to the copper-molybdenum mineralization observed in the Mineral Park deposit in Arizona.

10. Based on geological and ore characteristics, the porphyry mineralization features of Sar-e-Yazd have been compared with several porphyry copper deposits in Iran, including the Sungun porphyry copper (molybdenum) deposit, the Dalli porphyry copper-gold deposit, the Sarcheshmeh porphyry copper-molybdenum (gold) deposit, the Sara or Perkam deposit, and the Takht-e-Gonbad porphyry copper-molybdenum deposit. While Sar-e-Yazd shares numerous features with the Sungun and Sarcheshmeh deposits, it demonstrates the closest similarity to the Takht-e-Gonbad and Dalli porphyry copper deposits.

Acknowledgements. The authors would like to express the gratitude to Zar-Andishan Yazd Co. for generously providing field survey facilities, accommodation, and access to drill cores and exploration data.

REFERENCES

Agard, P., Omrani, J., Jolivet, L., Mouthereau, F., 2005. Convergence history across Zagros (Iran): constraints from collisional and earlier deformation. International Journal of Earth Sciences, **94**: 401–419; https://doi.org/10.1007/s00531-005-0481-4

Agard, P., Omrani, J., Jolivet, L., Whitechurch, H., Vrielynck, B., Spakman, W., Monié, P., Meyer, B., Wortel, R., 2011. Zagros orogeny: a subduction-dominated process. Geological Magazine, **148**: 692–725; https://doi.org/10.1017/S001675681100046X

Aghanabati, 2005. Geology of Iran. Geological Survey of Iran. https://www.gisoom.com/book/11083834/

Aghazadeh, M., Hou, Z., Badrzadeh, Z., Zhou, L., 2015. Temporal-spatial distribution and tectonic setting of porphyry copper deposits in Iran: Constraints from zircon U–Pb and molybdenite Re–Os geochronology. Ore Geology Reviews, **70**: 385–406; https://doi.org/10.1016/j.oregeorev.2015.03.003

Alavi, M., 1994. Tectonics of the Zagros orogenic belt of Iran: new data and interpretations. Tectonophysics, **229**: 211–238; https://doi.org/10.1016/0040-1951(94)90030-2

Alavi, M, 2007. Structures of the Zagros fold-thrust belt in Iran. American Journal of Science, **307**: 1064–1095; https://doi.org/10.2475/09.2007.02

Alimohammadi, M., Alirezaei, S., Kontak, D.J., 2015. Application of ASTER data for exploration of porphyry copper deposits: a case study of Daraloo–Sarmeshk area, southern part of the Kerman copper belt, Iran. Ore Geology Reviews, **70**: 290–304; https://doi.org/10.1016/j.oregeorev.2015.04.010

Alirezaei, S., Borhanzadeh, F., Sabouri, M., 2013. Alteration-mineralization in the Miduk porphyry Cu-Au deposit; Cenozoic Urumieh-Dokhtar magmatic belt, Iran. Geological Association of Canada-Mineralogical Association of Canada, New Brunswick, Canada.

Alirezaei, S., Hassanpour, S., 2011. An overview of porphyry copper deposits in Iran. In: Proceedings with abstracts. The 1st World Copper Congress, Iran: 49–62; https://www.researchgate.net/publication/284264180_An_overview_of_porphyry_copper_deposits_in_Iran

Alirezaei, S., Mohammadzadeh, Z., 2009. Hydrothermal alteration-mineralization at Chahfiroozeh porphyry copper deposit, Kerman province, southern Iran. Geological Association of Canada-Mineralogical Association of Canada-American Geophysical Union Joint Assembly, Toronto, Abstract GA71A-15; https://www.researchgate.net/publication/308795544_Hydrothermal_Alteration-Mineralization_in_Chahfiroozeh_Porphyry_Copper_Deposit_Kerman_Province_Southern_Iran

Asadi, S., Moore, F., Zarasvandi, A., 2014. Discriminating productive and barren porphyry copper deposits in the southeastern part of the central Iranian volcano-plutonic belt, Kerman region, Iran: a review. Earth-Science Reviews, **138**: 25–46; https://doi.org/10.1016/j.earscirev.2014.08.001

Asghari, O., Hezarkhani, A., 2008. Appling discriminant analysis to separate the alteration zones within the Sungun porphyry copper deposit. Journal of Applied Sciences, **24**: 4472–4486; https://doi.org/10.3923/jas.2008.4472.4486

Berberian, F., Muir, I.D., Pankhurst, R.J., Berberian, M., 1982. Late Cretaceous and early Miocene Andean-type plutonic activity in northern Makran and Central Iran. Journal of the Geological Society, **139**: 605–614; https://doi.org/10.1144/gsjgs.139.5.0605

Bodnar, R.J., 1994. Synthetic fluid inclusions. XII. Experimental determination of the liquidus and isochores for a 40 wt.% H_2O-NaCl solution. Geochimica et Cosmochimica Acta, **58**: 1053–1063; https://doi.org/10.1016/0016-7037(94)90571-1

Bodnar, R.J., Lecumberri-Sanchez, P., Moncada, D., Steele-MacInnis, M., 2014. Fluid inclusions in hydrothermal ore deposits, Chapter 13.5. In: Treatise on Geochemistry. 2nd Ed; https://doi.org/10.1016/b978-0-08-095975-7.01105-0

Brogi, A., 2006. Evolution, formation mechanism and kinematics of a contractional shallow shear zone within sedimentary rocks of the Northern Apennines (Italy). Eclogae Geologicae Helvetiae, **99**: 29–47; https://doi.org/10.1007/s00015-006-1174-0

Brown, L.J., Solar, M., 1998. Model of the copper and polymetallic vein family of deposits- applications in Slovakia, Hungary and Romania. International Geology Review, **45**: 12–19; https://doi.org/10.2747/0020-6814.45.2.143

Calagary, A., 2003. Stable isotope (S, O, H and C) studies of the phyllic and potassic-phyllic alteration zones of the porphyry copper deposit at Sungun, East Azarbaidjan, and Iran. Journal of Asian Earth Sciences, **21**: 767–780; http://dx.doi.org/10.1016/S1367-9120(02)00083-4

Cannell, J., Cooke, D.R., Walshe, J.L., Stein, H., 2005. Geology, mineralization, alteration, and structural evolution of the El Teniente porphyry Cu-Mo deposit. Economic Geology, **100**: 979–1003; https://doi.org/10.2113/100.5.979

Carten, R.B., 1986. Sodium-calcium metasomatism; chemical, temporal, and spatial relationships at the Yerington, Nevada, and porphyry copper deposit. Economic Geology, **81**: 1495–1519; https://doi.org/10.2113/gsecongeo.81.6.1495

Chang, Z., Hedenquist, J.W., White, N.C., Cooke, D.R., Roach, M., Deyell, C.L., Garcia Jr, J., Gemmell, J.B., McKnight, S., Cuison, A.L., 2011. Exploration tools for linked porphyry and epithermal deposits: Example from the Mankayan intrusion-cen-

tered Cu-Au district, Luzon, Philippines. Economic Geology, **106**: 1365–1398; https://doi.org/10.2113/econgeo.106.8.1365

Chiu, H.-Y., Chung, S.-L., Zarinkoub, M.H., Mohammadi, S.S., Khatib, M.M., Iizuka, Y., 2013. Zircon U-Pb age constraints from Iran on the magmatic evolution related to Neotethyan subduction and Zagros orogeny. Lithos, **162**: 70–87; https://doi.org/10.1016/j.lithos.2013.01.006

Cline, J.S., Bodnar, R.J., 1991. Can economic porphyry copper mineralization be generated by a typical calc-alkaline melt? Journal of Geophysical Research: Solid Earth, **96**: 8113–8126; https://doi.org/10.1029/91JB00053

Conrad, G., Conrad, J., Girod, M., 1977. Les formations continentales tertiaires et quaternaires du Lout (Iran). Importance du plutonisme et du volcanisme. (Livre à la Mémoire de A. F. de Lapparent). Mémoires H. S. Société géologique de France, fascicule **8**: 53–75; https://doi.org/10.3406/geolm.1982.1169

Cooke, D.R., Deyell, C.L., Waters, P.J., Gonzales, R.I., Zaw, K., 2011. Evidence for magmatic–hydrothermal fluids and ore-forming processes in epithermal and porphyry deposits of the Baguio district, Philippines. Economic Geology, **106**: 1399–1424; https://doi.org/10.2113/econgeo.106.8.1399

Cooke, D.R., Hollings, P., Wilkinson, J.J., Tosdal, R.M., 2014. Geochemistry of porphyry deposits, Chapter 13.14. In: Treatise on Geochemistry. 2nd ed.: 357–381; https://doi.org/10.1016/B978-0-08-095975-7.01116-5

Cox, L.J., Chaffee, M.A., Cox, D.P., Klein, D.P., 1986. Porphyry Cu deposits. Model 17. United States Geological Survey.

Damian, F., 2003. The mineralogical characteristics of the hydrothermal types alteration from Nistru ore deposit, Baia Mare metallogenetic district. Studia UBB Geologia, **48**: 101–112; https://doi.org/10.5038/1937-8602.48.1.9

Daneshjou, M., Zarasvandi, A., Pourkaseb, H., Rezaei, M. and Asadi Harooni, H., 2016. Investigation of effective factors in mineralization at Dalli porphyry Cu-Au deposit, Markazi province: base on geological, mineralogical and geochemical evidences. Petrological Journal, **7:** 73–94; https://doi.org/10.22108/ijp.2016.21231

Dimitrijevic, M.D., 1973. Geology of Kerman region. Institute for Geological and Mining Exploration and Investigation of Nuclear and Other Mineral Raw Materials, Report no. **52**; https://books.google.com/books/about/Geology_of_Kerman_Region.html?id=b3LmOgAACAAJ

Ebadi, L., Alavi, S., A., Shafii-Bafti, Sh., 2011. The development of tensional structures in a transgressional regime and their relationship with the formation of vein-type and porphyry copper deposits in the northeast of Babak city (in Persian with English summary). Earth Sciences, Tehran, Iran. **21**: 101–114; https://sid.ir/paper/32033/fa

Eidel, J.J., Frost, J.E., Clippinger, D.M., 1968. Copper-molybdenum mineralization at Mineral Park, Mohave County, Arizona. In: Ore Deposits of the United States, 1933–67 (ed. J.D. Ridge). New York, American Institute of Mining, Metallurgical and Petroleum Engineers, **2**: 1258–1281.

Etminan, H., 1978. Fluid inclusion studies of the porphyry copper ore bodies at Sar-Cheshmeh, Darreh Zar and Mieduk (Kerman region, southeastern Iran) and porphyry copper discoveries at Sar-Cheshmeh, Gozan, and Kighal, Azarbaijan region (northwestern Iran). International Association, Genesis of Ore Deposits Fifth Symposium, Snowbird, Utah, Abstract 88.

Fazeli, B., Khalili, M., Köksal, F.T., Esfahani, M.M., Beavers, R., 2017. Petrological constraints on the origin of the plutonic massif of the Ghaleh Yaghmesh area, Urumieh-Dokhtar magmatic arc, Iran. Journal of African Earth Sciences, **129**: 233–247; https://doi.org/10.1016/j.jafrearsci.2016.12.014

Förster, H., 1978. Mesozoic–cenozoic metallogenesis in Iran. Journal of the Geological society, **135**: 443–455; https://doi.org/10.1144/gsjgs.135.4.0443

Ghorashizadeh, M., 1978. Development of hypogene and supergene alteration and copper mineralization patterns, Sar-Cheshmeh porphyry copper deposit, Iran. M.Sc. thesis, Brock University, Canada; http://hdl.handle.net/10464/1573

Ghorbani, M., 2013. Geology of Iran, Arin Zemin (in Persian); https://doi.org/10.1007/978-94-007-5625-0

Gergorian, S., 2003. Assessment of geochemical anomalies (Sonajil area). National Iranian Copper Company, NICICO report.

Gustafson, L.B., Hunt, J.P., 1975. The porphyry copper deposit at El Salvador, Chile. Economic Geology. **70**: 857–912; https://doi.org/10.2113/gsecongeo.70.5.857

Harati, H., 2016. Introduction of the Ser-e-Yazd polymetallic deposit in the central part of the Urmia-Dokhtar magmatic belt (southeast of Yazd). Iranian Geological Society Conference; https://elmnet.ir/doc/20757875-51142

Harati, H., Moayyed, M., 2020. Introducing Mehriz porphyry copper deposit in the southeast of Yazd. The 40th National Science Conference. Tehran, Iran; https://civilica.com/doc/1471858/

Harris, A.C., Golding, S.D., 2002. New evidence of magmatic-fluid-related phyllic alteration: implications for the genesis of porphyry Cu deposits. Geology **30**: 335–338; http://dx.doi.org/10.2113/gsecongeo.70.5.857

Hassanzadeh, J., 1993. Metallogenic and tectono-magmatic events in the SE sector of the Cenozoic active continental margin of Iran (Shahr e Babak area, Kerman province). Ph.D. thesis, University of California, Los Angeles, U.S.A.; https://scholar.google.com/citations?view_op=view_citation&hl=en&user=kze419gAAAAJ&citation_for_view=kze419gAAAAJ:Y0pCki6q_DkC

Hedenquist, J.W., Arribas Jr., A., Reynolds, T.J., 1998. Evolution of an intrusioncentred hydrothermal system: far Southeast-Lepanto Porphyry and Epithermal Cu-Au deposits, Philippines. Economic Geology, **93**: 373–404; https://doi.org/10.2113/gsecongeo.93.4.373

Hemley, J.J., Cygan, G.L., Fein, J.B., Robinson, G.R., d'Angelo, W.M., 1992. Hydrothermal ore-forming processes in the light of studies in rock-buffered systems; I, Iron-copper-zinc-lead sulphide solubility relations. Economic Geology, **87**: 1–22; https://doi.org/10.2113/gsecongeo.87.1.1

Hezarkhani, A., 2006. Hydrothermal evolution of Sarcheshmeh porphyry Cu-Mo deposit, Iran: evidence from fluid inclusion. Journal of Asian Earth Sciences, **28**: 409–422; https://doi.org/10.1016/j.jseaes.2005.11.003

Hezarkhani, A., 2009. Hydrothermal fluid geochemistry at the Chah-Firuzeh porphyry copper deposit, Iran: evidence from fluid inclusions. Geochemical Exploration, **101**: 254–264; https://doi.org/10.1016/j.gexplo.2008.09.002

Holliday, J.R., Cooke, D.R., 2007. Advances in Geological Models and Exploration Methods for Copper ± Gold Porphyry Deposits. Ore Deposits and Exploration Technology, **53**: 791–809; https://static1.squarespace.com/static/5f10604a2eb3d3179de51001/t/63f3f8fd2764b604666b18bf/1676933375365/53.pdf

Hosseini, M.R., Ghaderi, M., Alirezaei, S., Sun, W., 2017. Geological characteristics and geochronology of the Takht-e-Gonbad copper deposit, SE Iran: a variant of porphyry type deposits. Ore Geology Reviews, **86**: 440–458; https://doi.org/10.1016/j.oregeorev.2017.03.003

Hosseini, M.R., Hassanzadeh, J., Alirezaei, S., Sun, W., Li, C.Y., 2017. Age revision of the Neotethyan arc migration into the southeast Urumieh-Dokhtar belt of Iran: geochemistry and U-Pb zircon geochronology. Lithos, **284**: 296–309; https://doi.org/10.1016/j.lithos.2017.03.012

Hou, Z.Q., Zhang, H.R., Pan, X.F., Yang, Z.M., 2011. Porphyry Cu (-Mo-Au) deposits related to melting of thickened mafic lower crust: examples from the eastern Tethyan metallogenic domain. Ore Geology Reviews, **39**: 21–45; https://doi.org/10.1016/j.oregeorev.2010.09.002

Jébrak, M., 1997. Hydrothermal breccias in vein-type ore deposits: a review of mechanisms, morphology and size distribution. Ore Geology Reviews, **12**: 111–134; https://doi.org/10.1016/S0169-1368 (97)00009-7

Jobson, D.H., Boulter, C.A., Foster, R.P., 1994. Structural controls and genesis of epithermal gold-bearing breccias at the Lebong Tandai mine, Western Sumatra, Indonesia. Journal of Geochemical Exploration, **50**: 409–428; https://doi.org/10.1016/0375-6742(94)90034-5

John, D.A., Ayuso, R.A., Barton, M.D., Bodnar, R.J., Dilles, J.H., Gray, F., Graybeal, F.T., Mars, J.C., McPhee, D.K., Seal, R.R., Taylor, R.D., Vikre, P.G., 2010. Porphyry copper deposit model, Chapter B of Mineral deposit models for resource assessment. U.S. Geological Survey Scientific Investigations Report, 2010–5070–B; https://pubs.usgs.gov/sir/2010/5070/b/

Karimpour, M.H., Rezaei, M., Zarasvandi, A., Malekzadeh Shafaroudi, A., 2021. Saveh-Nain-Jiroft Magmatic Belt replaces Urumieh-Dokhtar Magmatic Belt: investigation of genetic relationship between porphyry copper deposits and adakitic and non-adakitic granitoids. Journal of Economic Geology, **13**: 465–506; https://doi.org/10.22067/econg.v13i3.1034

Kusakabe, M., Nakagawa, S., Hori, M., Matsuhisa, Y., Ojeda, J.M., Serrano, L., 1984. Oxygen and sulphur isotopic compositions of quartz, anhydrite and sulphide minerals from the El Teniente and Rio Blanco porphyry copper deposits, Chile. Bulletin of the Geological Survey of Japan, **35**: 583–614; https://www.researchgate.net/publication/292639355_Oxygen_and_sulfur_isotopic_compositions_of_quartz_anhydrite_and_sulfide_minerals_from_the_El_Teniente_and_Rio_Blanco_porphyry_copper_deposits_Chile

Kusakabe, M., Hori, M., Yukihhiro, M., 1990. Primary mineralization-alteration of the El Teniente and Rio Blanco porphyry copper deposits, Chile. Stable isotopes, fluid inclusions and $Mg^{2+}/Fe^{2+}/Fe^{2+}$ ratios in hydrothermal biotite, **2**: 244–259. University of Western Australia Publication; https://pascal-francis.inist.fr/vibad/index.php?action=getRecordDetail&idt=6530858

Lagat, J., 2009. Hydrothermal alteration mineralogy in geothermal fields with case examples from Olkaria domes geothermal field, Kenya. Short course IV on exploration for geothermal resources; https://rafhladan.is/bitstream/handle/10802/13871/UNU-GTP-SC-23-0104.pdf

Landtwing, M.R., Pettke, T., Halter, W.E., Heinrich, C.A., Redmond, P.B., Einaudi, M.T., Kunze, K., 2005. Copper deposition during quartz dissolution by cooling magmatic-hydrothermal fluids: the Bingham porphyry. Earth and Planetary Science Letters, **235**: 229–243; https://doi.org/10.1016/j.epsl.2005.02.046

Lang, J.R., Eastoe, C.J., 1988. Relationships between a porphyry Cu-Mo deposit, base and precious metal veins and Laramide intrusions, Mineral Park, Arizona. Economic Geology, **83**: 551–567; https://doi.org/10.2113/gsecongeo.83.3.551

Liu, J., Mao, J.W., Wu, G., Wang, F., Luo, D.F., Hu, Y.Q., Li, T.G., 2014. Fluid inclusions and H-O-S-Pb isotope systematics of the Chalukou giant porphyry Mo deposit, Heilongjiang Province, China. Ore Geology Reviews, **59**: 83–96; https://doi.org/10.1016/j.oregeorev.2013.12.006

Lowell, J.D., Guilbert, J.M., 1970. Lateral and vertical alteration-mineralization zoning in porphyry ore deposits. Economic Geology, **65**: 373–408; https://doi.org/10.2113/gsecongeo.65.4.373

McInnes, B.I.A., Evans, N.J., Fu, F.Q., Garwin, S., Belousova, E., Griffin, W.L., Bertens, A., Sukama, D., Permanadewi, S., Andrew, R.L., Deckart, K., 2005. Thermal history analysis of selected Chilean, Indonesian, and Iranian porphyry Cu-Mo-Au deposits. In: Super Porphyry Copper and Gold Deposits: A Global Perspective (ed. T.M. Porter): 27–42. Porter Geoconsultancy Publishing, de Adelaide, Australia; https://researchers.mq.edu.au/en/publications/thermal-history-analysis-of-selected-chilean-indonesian-and-irani

Melfos, V., Vavelidis, M., Christofides, G., Seidel, E., 2002. Origin and evolution of the Tertiary Maronia porphyry copper-molybdenum deposit, Thrace, Greece. Mineralium Deposita, **37**: 648–668; https://doi.org/10.1007/s00126-002-0277-4

Meinert, L.D., 1987. Skarn zonation and fluid evolution in the Groundhog mine, Central mining district, New Mexico. Economic Geology, **82**: 523–545; https://www.elaiet.com/IronGlen/MeinertGroundHogNM523.pdf

Meinert, L.D., Dipple, G.M., Nicolescu, S., 2005. World skarn deposits. Economic Geology, **100**: Anniversary Volume: 299–336; https://www.researchgate.net/publication/232751265_World_Skarn_Deposits

Meyer, C., Hemley, J.J., 1967. Wall rock alteration. In: Geochemistry of hydrothermal ore deposits (ed. H.L. Barnes): 166–235. New York, Holt, Rinehart and Winston; https://books.google.com/books?hl=en&lr=&id=vy2_QnyojPYC&oi=fnd&pg=PR11&dq=Meyer,+C.,+and+Hemley,+J.J.,+1967,+Wall+rock+alteration,+in+Barnes,+H.L.,+ed.,+Geochemistry+of+hydrothermal+ore+deposits:+New+York,+Holt,+Rinehart+and+Winston,+p.+166-235.&ots=uUxwhli2AL&sig=dlkBPIr09Qe5_BYyJoGm7uh8Pig#v=onepage&q&f=false

McLemore, V.T., Munroe, E.A., Heizler, M.T. McKee, C., 1999. Geochemistry of the Copper Flat porphyry and associated deposits in the Hillsboro mining district, Sierra Country, New Mexico, USA. Geochemical Exploration, **67**: 167–189; https://scholar.google.com/citations?view_op=view_citation&hl=en&user=ypDkQLYAAAAJ&citation_for_view=ypDkQLYAAAAJ:Tiz5es2fbqcC

Moayyed, M., 2019. Report on the completion of exploration of Mehriz mining area, Yazd Province. Industry, Mining and Trade Organization.

Mohammadilaghab, H., Taghipour, N., Iranmanesh, M., 2011. Distribution Pattern of Copper, Molybdenum, Lead, Zinc, and Iron Elements in the Sara (Perkam) Porphyry Copper Deposit, Shahr Babak, Kerman Province. Geology of Iran, **5:** 17–28. https://sid.ir/paper/129371/fa

Mohebi, A., 2015. Economic geology of Bondar Hanza porphyry copper deposit in eastern Rabor (Baft), with special attention to understanding the origin of intrusive bodies and hydrothermal fluids (in Persian with English abstract). Ph.D. thesis, Shahid Beheshti University, Tehran, Iran; https://ganj.irandoc.ac.ir

Moncada, D., Baker, D., Bodnar, R.J., 2017. Mineralogical, petrographic, and fluid inclusion evidence for the link between boiling and epithermal Ag–Au mineralization in the La Luz area, Guanajuato Mining District, México. Ore Geology Reviews, **89**: 143–170; https://doi.org/10.1016/j.oregeorev.2017.05.024

Montest, L.G.J., Hirth, G., 2003. Grain size evolution and the rheology of ductile shear zone: from laboratory experiments to postseismic creep. Earth and Planetary Science Letters, **211**: 97–110; https://doi.org/10.1016/S0012-821X(03)00196-1

Muntean, J.L., Einaudi, M.T., 2000. Porphyry gold deposits of the Refugio district, Maricunga belt, northern Chile. Economic Geology, **95**: 1445–1472; https://doi.org/10.2113/gsecongeo.95.7.1445

Muntean, J.L., Einaudi, M.T., 2001. Porphyry-epithermal transition: Maricunga belt, northern Chile. Economic Geology, **96**: 743–772; https://doi.org/10.2113/gsecongeo.96.4.743

Nabavi, M.H., 1972. Geologic map of Yazd quadrangle, Scale 1:250,000. Geological survey of Iran, Tehran, Iran; https://shop.geospatial.com/publication/5KD5BEB1109G4GAXVQGCDMTN94/Iran-1-to-250000-Scale-Geological-Maps

Omrani, J., Agard, P., Whitechurch, H., Benoit, M., Prouteau, G., Jolivet, L., 2008. Arc-magmatism and subduction history beneath the Zagros Mountains, Iran: a new report of adakites and geodynamic consequences. Lithos, **106**: 380–398; https://doi.org/10.1016/j.lithos.2008.09.008

Ossandón, G., Freraut, R., Gustafson, L.B., Lindsay, D.D., Zentilli, M., 2001. Geology of the Chuquicamata Mine: a progress report. Economic Geology. **96**: 249–270; https://doi.org/10.2113/gsecongeo.96.2.249

Ouyang, H., Wu, X., Mao, J.W., Su, H., Santosh, M., Zhou, Z., Li, C., 2014. The nature and timing of ore formation in the Budunhua copper deposit, southern Great Xing'an Range:

evidence from geology, fluid inclusions, and U-Pb and Re-Os geochronology. Ore Geology Reviews, **63**: 238–251; https://doi.org/10.1016/j.oregeorev.2014.05.016

Peacock, S.M., 2002. Blueschist-facies metamorphism, shear heating and P-T- t paths in subduction shear zones. Journal of Geophysical Research, **97**: 17693–17707; https://doi.org/10.1029/92JB01768

Ramsay, J.G., Huber, M.I., 1987. The Techniques of Modern Structural Geology. Folds and Fractures. **2**: 309–700; https://doi:10.1017/S0016756800010384

Ranjbar, H., Honarmand, M., Moezifar, Z., 2004. Application of the Crosta technique for porphyry copper alteration mapping, using ETM+ data in the southern part of the Iranian volcanic sedimentary belt. Journal of Asian Earth Sciences, **24**: 237–243; https://doi.org/10.1016/j.jseaes.2003.11.001

Redmond, P.B., Einaudi, M.T., Inan, E.E., Landtwing, M.R., Heinrich, C.A., 2004. Copper deposition by fluid cooling in intrusion-centered systems – new insights from the Bingham porphyry ore deposit, Utah. Geology, **32**: 217–220; https://doi.org/10.1130/G19986.1

Richards, J.P., 2009. Postsubduction porphyry Cu-Au and epithermal Au deposits: Products of remelting of subduction-modified lithosphere. Geology, **37:** 247–250; https://doi.org/10.1130/G25451A.1

Richards, J.P., Noble, S.R., Pringle, M.S., 1999. A revised late Eocene age for porphyry Cu magmatism in the Escondida area, northern Chile. Economic Geology, **94**: 1231–1247; https://doi.org/10.2113/gsecongeo.94.8.1231

Richards, J.P., Spell, T., Rameh, E., Razique, A., Fletcher, T., 2012. High Sr/Y magmas reflect arc maturity, high magmatic water content, and porphyry Cu ± Mo ± Au potential: examples from the Tethyan arcs of Central and Eastern Iran and Western Pakistan. Economic Geology, **107**: 295–332; https://doi.org/10.2113/econgeo.107.2.295

Roedder, E., 1979. Origin and significance of magmatic inclusions. Bulletin de Minéralogie, **102**: 487–510; https://www.persee.fr/doc/bulmi_0180-9210_1979_act_102_5_7299

Roedder, E., 1984. Fluid inclusions. Reviews in Mineralogy and Geochemistry, **12**: 644; https://doi.org/10.1515/9781501508271

Ronacher, E., Richards, J.P., Johnston, M.D., 2000. Evidence for fluid phase separation in high-grade ore zones at the Porgera gold deposit, Papua New Guinea. Mineralium Deposita, **35**: 683–688; https://doi.org/10.1007/s001260050271

Rusk, B.G., Reed, M.H., Dilles, J.H., 2008. Fluid inclusion evidence for magmatic-hydrothermal fluid evolution in the porphyry copper-molybdenum deposit at Butte, Montana. Economic Geology, **103**: 307–334; https://doi.org/10.2113/gsecongeo.103.2.307

Samson, I., Anderson, A., Marshall, D.D., 2003. Fluid Inclusions: analysis and interpretation. SEPM Short Course, **32**; https://doi.org/10.3749/9780921294672.fm02

Saric, B., 1973. Report on exploration at Darrehzar copper mineral deposit. Geological Survey of Iran, Report No Yu. 51.

Sarjoughian, F., Kananian, A., 2017. Zircon UPb geochronology and emplacement history of intrusive rocks in the Ardestan section, central Iran. Geologica Acta, **15**: 25–36; https://doi.org/10.1344/GeologicaActa2017.15.1.3

Shafiei, B., 2010. Lead isotope signatures of the igneous rocks and porphyry copper deposits from the Kerman Cenozoic magmatic arc (SE Iran), and their magmatic-metallogenetic implications. Ore Geology Reviews, **38**: 27–36; https://doi.org/10.1016/j.oregeorev.2010.05.004

Shafiei, B., Haschke, M., Shahabpour, J., 2009. Recycling of orogenic arc crust triggers porphyry Cu mineralization in Kerman Cenozoic arc rocks, southeastern Iran. Mineralium Deposita, **44**: 265–283; https://doi.org/10.1007/s00126-008-0216-0

Shahabpour, J., 1982. Aspects of alteration and mineralization at the SarCheshmeh copper-molybdenum deposit, Kerman, Iran. Ph.D. thesis, University of Leeds, England.

Shahabpour, J., 2005. Tectonic evolution of the orogenic belt in the region located between Kerman and Neyriz. Journal of Asian Earth Sciences, **24**: 405–417; https://doi.org/10.1016/j.jseaes.2003.11.007

Shahabpour, J., 2007. Island-arc affinity of the Central Iranian Volcanic Belt, Journal of Asian Earth Sciences, **30**: 652–665; https://doi.org/10.1016/j.jseaes.2007.02.004

Shahabpour, J. Doorandish, M., 2008. Mine drainage water from the Sar Cheshmeh porphyry copper mine, Kerman, IR Iran. Environmental Monitoring and Assessment, **141:** 105–120; https://link.springer.com/article/10.1007/s10661-007-9861-5

Shanks III, W.P., Koski, R.A., Mosier, D.L., Schulz, K.J., Morgan, L.A., Slack, J.F., Ridley, W.I., Dusel-Bacon, C., Seal II, R.R., Piatak, N.M., 2012. Volcanogenic massive sulphide occurrence model. Chapter C in Mineral deposit models for resource assessment (No. 2010-5070-C). US Geological Survey.

Sheets, R.W., Nesbitt, B., Muehlenbachs, K., 1996. Meteoric water component in magmatic fluids from porphyry copper mineralization, Babine Lake area, British Columbia. Geology, **24**: 1091–1094; https://doi.org/10.1130/0091-7613(1996)024%3C1091:MWCIMF%3E2.3.CO;2

Shepherd, T.J., Rankin, A.H., Alderton, D.H., M., 1985. A practical guide to fluid inclusion studies. Blackie, Chapman and Hall; https://doi:10.1180/minmag.1986.050.356.32

Sillitoe, R.H., 1995. Exploration for porphyry copper lithocaps. In: PACRIM Congress 1995: 527–532, Melbourne. Australia Institute Mining Metal; https://www.ausimm.com/publications/conference-proceedings/pacrim-95-congress-auckland-new-zealand-november-1995/exploration-of-porphyry-copper-lithocaps/

Sillitoe, R.H., 2010. Porphyry copper systems. Economic geology, **105**: 3–41; https://doi.org/10.2113/gsecongeo.105.1.3

Simmons, S.F., Browne, P.R.L., 2000. Hydrothermal minerals and precious metals in the Broadlands-Ohaaki geothermal system: implications for understanding low-sulphidation epithermal environments. Economic Geology, **95**: 971–1000; https://doi.org/10.2113/gsecongeo.95.5.971

Sinclair, W.D, 2007. Porphyry Deposits. In: Mineral Deposits of Canada: A Synthesis of Major Deposit-Types, District Metallogeny, the Evolution of Geological Provinces, and Exploration Methods (ed. W.D. Goodfellow): 223–243. Geological Association of Canada, Mineral Deposits Division, Canada, Newfoundland; https://www.researchgate.net/publication/228668686_Porphyry_deposits

Singer, D.A., 1995. World class base and precious metal deposits; a quantitative analysis. Economic Geology, **90:** 88–104; http://dx.doi.org/10.2113/gsecongeo.90.1.88

Stöcklin, J., 1968. Structural history and tectonics of Iran: a review. AAPG Bulletin, **52**: 1229–1258; https://doi.org/10.1306/5D25C4A5-16C1-11D7-8645000102C1865D

Storti, F., Rossetti, F., Läufer, A.L., Salvini, F., 2006. Consistent kinematic architecture in the damage zones of intraplate strike-slip fault systems in North Victoria Land, Antarctica and implications for fault zone evolution. Journal of Structural Geology, **28**: 50–63; https://doi.org/10.1016/j.jsg.2005.09.004

Taghipour, N., Aftabi, A., Mathur, R., 2008. Geology and Re-Os geochronology of mineralization of the Miduk porphyry copper deposit, Iran. Resour. Geol., **58**: 143–160; https://doi.org/10.1111/j.1751-3928.2008.00054.x

Taghipour, N., Dorani, M., 2013. Stable isotope geochemistry of sulphur and oxygen in sulphide and sulphate minerals of the Perkam Porphyry Copper Deposit, Shahr Babak, Kerman Province. Advanced Applied Geology, **3:** 61–70; https://journals.scu.ac.ir/article_10860.html

Tangestani, M.H., Moore, F., 2001. Comparison of three principal component analysis techniques to porphyry copper alteration mapping: a case study, Meiduk area, Kerman, Iran. Canadian Journal of Remote Sensing, **27**: 176–181; https://doi.org/10.1080/07038992.2001.10854931

Tangestani, M.H., Moore, F., 2002. Porphyry copper alteration mapping at the Meiduk area, Iran. International Journal of Remote Sensing, **23**: 4815–4825; https://doi.org/10.1080/01431160110115564

Tarantola, A., Diamond, L.W., Stünitz, H., Thust, A., Pec, M., 2012. Modification of fluid inclusions in quartz by deviatoric stress. III: Influence of principal stresses on inclusion density and orientation. Contributions to Mineralogy and Petrology, **164**: 537–550; http://dx.doi.org/10.1007/s00410-012-0749-1

Taylor, Jr., H.P., 1997. Oxygen and hydrogen isotope relationships in hydrothermal mineral deposits. Geochemistry of Hydrothermal Ore Deposits, **3**: 229–302; https://typeset.io/papers/oxygen-and-hydrogen-isotope-relationships-in-hydrothermal-2n992x2502

Taylor, R., Taylor, R., 2011. Leached cappings in porphyry copper systems. Gossans and Leached Cappings, Field Assessment: 107–138; https://doi.org/10.1007/978-3-642-22051-7_8

Tosdal, R.M., Richards, J.P., 2018. Magmatic and tectonic settings of Porphyry Copper Deposits. Economic Geology, **113:** 587–602.

Valencia, V.A., Eastoe, C., Ruiz, J., Ochoa-Landin, L., Gehrels, G., Gonzàlez-Leon, C., Barra, F., Espinoza, E., 2008. Hydrothermal evolution of the porphyry copper deposit at La Caridad, Sonora, Mexico, and the relationship with a neighboring high-sulphidation epithermal deposit. Economic Geology, **103**: 473–491; https://doi.org/10.2113/gsecongeo.103.3.473

Wang, C., Ludman A., 2004. Deformation conditions, kinematics and dis-placement history of shallow crustal ductile shearing in the Norumberga fault system in the Northern Appalachians, eastern Maine. Tectonophysics, **384**: 129–148; https://doi.org/10.1016/j.tecto.2004.03.013

Watanabe, Y., Hedenquist, J.W., 2001. Mineralogic and stable isotope zonation at the surface over the El Salvador porphyry copper deposit, Chile. Economic Geology, **96**: 1775–1797; https://doi.org/10.2113/gsecongeo.96.8.1775

Waterman, G.C., Hamilton, R.L. 1975. The Sar Cheshmeh porphyry copper deposit. Economic Geology, **70**: 568–576; https://doi.org/10.2113/gsecongeo.70.3.568

Whitney, D.L., Evans, B.W., 2010. Abbreviations for names of rock-forming minerals. American Mineralogist, **95**: 185–187; http://dx.doi.org/10.2138/am.2010.3371

Wilkinson, J. J. 2011. Fluid inclusions in hydrothermal ore deposits. Lithos, **55**: 229–272; https://doi.org/10.1016/S0024-4937(00)00047-5

Zarasvandi, A., Liaghat, S., Zentilli, M., 2005. Geology of the Darreh-Zerreshk and Ali- Abad porphyry copper deposits, Central Iran. International Geology Review, **47**: 620–646; https://doi.org/10.2747/0020-6814.47.6.620

Zarasvandi, A., Liaghat, S., Zentilli, M., Reynolds, P.H., 2007. $^{40}Ar/^{39}Ar$ geochronology of alteration and petrogenesis of porphyry copper-related granitoids in the Darreh-Zerreshk and Ali-Abad area, central Iran. Exploration and Mining Geology, **16**: 11–24; https://doi.org/10.2113/gsemg.16.1-2.11

Zarasvandi, A., Heidari, M., Raith, J., Rezaei, M., Saki, A., 2019. Geochemical characteristics of collisional and pre-collisional porphyry copper systems in Kerman Cenozoic Magmatic Arc, Iran: using plagioclase, biotite and amphibole chemistry. Lithos, **326**: 279–297; https://doi.org/10.1016/j.lithos.2018.12.029

Zhong, J. Chen, Y.J., Pirajno, F., Chen, J., Li, J., Qi, J.P., Li, N., 2014. Geology, geochronology, fluid inclusion and H-O isotope geochemistry of the Luoboling porphyry Cu-Mo deposit, Zijinshan Orefield, Fujian Province, China. Ore Geology Reviews, **57**: 61–77; https://doi.org/10.1016/j.oregeorev.2013.09.004